

REPORT  
FLOOD PROTECTION AT BRIDGE CROSSINGS  
by  
D.B. Simons and G.L. Lewis

*Redone*

Prepared for  
Wyoming State Highway Department  
Planning and Research Division  
in cooperation with the  
U.S. Department of Transportation  
Federal Highway Administration  
Bureau of Public Roads  
1970

CER70-71DBS-GLL31

REPORT  
FLOOD PROTECTION AT BRIDGE CROSSINGS  
by  
D.B. Simons and G.L. Lewis

Prepared for  
Wyoming State Highway Department  
Planning and Research Division  
in cooperation with the  
U.S. Department of Transportation  
Federal Highway Administration  
Bureau of Public Roads

1970

CER70-71DBS-GLL31

#### AUTHORIZATION OF PROJECT

The problems to be investigated were formulated by the staff of the State Highway Commission of Wyoming in consultation with personnel of Colorado State University and the Bureau of Public Roads. The project was initiated by the signing of the agreement "Engineering Investigation Pertaining to Flood Protection of Bridges and Culverts," dated February 16, 1966. This agreement was modified in an addendum to the agreement dated October 8, 1969.

#### DISCLAIMER

The opinions, findings, and conclusions in this publication are those of the authors and not necessarily those of the State Highway Commission of Wyoming or the Bureau of Public Roads.

## ABSTRACT

### FLOOD PROTECTION AT BRIDGE CROSSINGS

Techniques for the design of stable rock-riprap protection in the vicinity of bridge crossings are presented. Hydraulic properties of the crossings are computed from methods derived in other sources, and the properties are related to particle sizes for riprap protection of abutments and piers.

Design steps for prototype bridge crossings are enumerated so that the hydraulic engineer may use this report as a design manual. An example of the design of protection for a prototype bridge crossing is included to clarify the suggested design procedures.

Riprap-protected spill-through abutments were constructed in the hydraulic facilities at Colorado State University in order to test the validity of the suggested design procedures.



# TABLE OF CONTENTS

<u>Chapter</u>		<u>Page</u>
	AUTHORIZATION OF PROJECT . . . . .	i
	DISCLAIMER . . . . .	i
	ABSTRACT . . . . .	ii
	NOTATION . . . . .	v
	LIST OF FIGURES . . . . .	x
	LIST OF TABLES . . . . .	xiii
I	INTRODUCTION . . . . .	1
	Scope . . . . .	1
	Application . . . . .	2
	Protection of Bridge Crossings . . . . .	2
	Regions of Required Protection . . . . .	3
	Types of Protection . . . . .	3
	Flow Conditions . . . . .	6
	Channel Shapes . . . . .	6
	Abutment Types . . . . .	7
	Geometric Properties . . . . .	7
II	DERIVATION OF DESIGN CRITERIA . . . . .	9
	Backwater Equations . . . . .	9
	Design Velocities . . . . .	15
	Velocity Field . . . . .	17
	Design of Riprap . . . . .	18
	Particle Stability . . . . .	20
	Lift Forces . . . . .	23
	Wave Forces . . . . .	25
	Freeboard . . . . .	27
	Scour at Abutments . . . . .	28
	Scour at Piers . . . . .	31
	Lateral Extent of Scour . . . . .	32
III	PROPOSED DESIGN PROCEDURES . . . . .	34
	Computed Parameters . . . . .	35
	Backwater . . . . .	37
	Design Velocity . . . . .	38
	Toe Protection . . . . .	39
	Riprap Sizing . . . . .	42
	Abutment Spill-Slope Protection . . . . .	45
	Downstream Side Slope Protection . . . . .	47
	Upstream Side Slope Protection . . . . .	48

# TABLE OF CONTENTS (Continued)

<u>Chapter</u>		<u>Page</u>
	Pier Protection . . . . .	51
	Protection of Special Cases . . . . .	52
IV	LABORATORY VERIFICATION OF DESIGN PROCEDURE . . .	54
	Facilities . . . . .	54
	Models . . . . .	55
	Testing Procedure . . . . .	58
	Velocity Data . . . . .	59
	Depth Data . . . . .	60
	Photographic Data . . . . .	61
	Data Analysis . . . . .	62
	Backwater and Design Velocities . . . . .	62
	Upstream Velocities . . . . .	65
	Riprap Stability . . . . .	66
	Summary . . . . .	70
V	DESIGN EXAMPLE . . . . .	72
	BIBLIOGRAPHY . . . . .	88
	APPENDIX A - FIGURES . . . . .	95
	APPENDIX B - BACKWATER AND TOTAL WATER SURFACE DROP THROUGH THE ABUTMENTS . . . . .	127
	APPENDIX C - COMPUTATION OF STABILITY COEFFICIENT . . . . .	156

# NOTATION

<u>SYMBOL</u>	<u>DEFINITION</u>	<u>UNITS</u>
a	Half width or radius of a pier	ft
A	Cross-sectional area	sq ft
$A_{2c}$	Critical flow area at section 2	sq ft
$A_c$	Area at critical flow	sq ft
$A_i$	Flow area at section i	sq ft
$A_n$	Unconstricted flow area	sq ft
$A_{ni}$	Flow area at section i below normal stage	sq ft
$A_s$	Area of scour in the constriction	sq ft
b	Width of constriction	ft
b'	Top-width between spill-through abutments	ft
$b_n$	Net width of waterway excluding piers	ft
$b_p$	Width of pier on a normal to the flow	ft
$b_r$	Base width of trapezoid	ft
$b_s$	Distance between skewed abutments	ft
$b_{tc}$	Top width of flow between abutments at $h_{2c}$	ft
B	Top width of unconstricted channel	ft
C	Correction factor for backwater with scour	--
$C_b$	Critical flow base backwater coefficient	--
$C_d$	Coefficient of discharge	--
$d_i$	Sieve size for which i(%) passes	ft-in
$d_m$	Effective diameter of rock mixture	ft-in
$d_{se}$	Equilibrium scour depth below bed	ft
D	Depth of flow in flow Reynolds number	ft
$D_b$	Differential level ratio	--

NOTATION (Continued)

<u>SYMBOL</u>	<u>DEFINITION</u>	<u>UNITS</u>
$\Delta D_e$	Differential level ratio increment-eccentricity	--
$\Delta D_s$	Differential level ratio increment-skew	--
$D_s$	Mean bed particle diameter	ft
$e$	Eccentricity of a bridge crossing	--
$F$	Fetch length	ft
$F_B$	Buoyant weight	lb
$F_D$	Drag force	lb
$F_e$	Effective fetch length	ft
$g$	Acceleration of gravity	ft/sec <sup>2</sup>
$h$	Height of model above flood plain	ft
$\Delta h$	Total water surface drop through bridge	ft
$h_A$	Depth of flow at the abutment at section 2	ft
$h_b^*$	Backwater at normal crossing with no piers	ft
$h_{bA}^*$	Backwater for abnormal flow excluding piers	ft
$h_d^*$	Backwater for dual bridges	ft
$h_i$	Flow depth at section i	ft
$h_{ic}$	Critical depth at section i	ft
$h_{L1-3}$	Energy losses between section 1 and 3	ft
$\Delta h_m$	Measured value of $\Delta h$	ft
$h_n$	Normal stage at design discharge	ft
$h_{nc}$	Critical depth in unconstricted channel	ft
$\bar{h}_{n2}$	Depth in constriction below normal stage	ft
$h_s$	Safety factor for freeboard	ft
$\Delta h_s$	Value of $\Delta h$ with scour	ft
$\Delta h_t$	Theoretical value of $\Delta h$	ft

# NOTATION (Continued)

<u>SYMBOL</u>	<u>DEFINITION</u>	<u>UNITS</u>
$h_u$	Flow depth at section 1 for girders in flow	ft
$h_u^*$	Backwater for girders in the flow	ft
$h_1^*$	Backwater at normal crossing including piers	ft
$h_{1A}^*$	Backwater for abnormal stage-discharge	ft
$h_{1s}^*$	Backwater with scour	ft
$h_3^*$	Normal depth less the depth at section 3	ft
$h_{3A}^*$	Difference of abnormal stage and depth at section 3	ft
$h_{3B}^*$	Difference of normal and section 3 depths for dual bridges	ft
$h_{3s}^*$	Difference of normal and section 3 depth with scour	ft
H	Wave height	ft
K	Conveyance	--
$K^*$	Total backwater coefficient	--
$K_b$	Backwater coefficient for normal crossing	--
$\Delta K_e$	Incremental backwater coefficient-eccentricity	--
$\Delta K_p$	Incremental backwater coefficient-piers	--
$\Delta K_s$	Incremental backwater coefficient-skew	--
$K_i$	Functions of $\eta$	--
$K_i'$	Derivatives of $K_i$ with respect to $\eta$	--
L	Length of embankment	ft
$L_{1-3}$	Distance between section 1 and section 3	ft
$L_D$	Distance between dual bridges	ft
$L_e$	Effective approach embankment length	ft
$L^*$	Distance to maximum backwater	ft

# NOTATION (Continued)

<u>SYMBOL</u>	<u>DEFINITION</u>	<u>UNITS</u>
$L_w$	Wave length	ft
$m$	Side-slope run for a unit rise	--
$M$	Discharge opening ratio	--
$M'$	Geometric opening ratio	--
$n$	Manning's roughness coefficient	--
$Q$	Discharge	cfs
$Q_b$	Discharge in the width $b$	cfs
$Q_f$	Failure discharge	cfs
$r$	Abutment nose radius	ft
$R$	Hydraulic radius	ft
$\bar{R}$	Pier Reynolds Number	--
$IR$	Flow Reynolds Number	--
$R_e$	Resultant force	lb
$R_p$	Particle Reynolds Number	--
$S_s$	Specific gravity of sediment	--
$S_o$	Slope of channel bed	--
$t$	Riprap layer thickness	ft-in
$V$	Velocity	fps
$V_b$	Bed Velocity	fps
$\bar{V}$	Average velocity	fps
$V_d$	Design velocity	fps
$V_n$	Average unconfined velocity	fps
$V_{n2}$	Average velocity in area $A_{n2}$	fps
$V_w$	Wind velocity	fps



# NOTATION (Continued)

<u>SYMBOL</u>	<u>DEFINITION</u>	<u>UNITS</u>
$V_{wm}$	Additional bottom velocity due to waves	fps
$V_i$	Average velocity at section i	fps
$V_{2c}$	Critical velocity at section 2	fps
$W$	Roadway width at top of abutment	ft
$W_F$	Fetch width	ft
$W_s$	Stone weight resistant to waves	lb
$\alpha$	Side slope angle with horizontal	deg
$\alpha_i$	Velocity head correction coefficient	--
$\gamma$	Specific weight	lb/ft <sup>3</sup>
$\eta$	Stability coefficient	--
$\theta$	Abutment skew angle	deg
$\lambda_1$	Drag force angle with horizontal	deg
$\nu$	Kinematic fluid viscosity	ft <sup>2</sup> /sec
$\rho$	Mass density	lb-sec <sup>2</sup> /ft <sup>4</sup>
$\tau$	Shear stress	lb/ft <sup>2</sup>
$\phi$	Angle of repose of riprap	deg
$1/\psi$	Lift force factor	--

# LIST OF FIGURES

<u>FIGURE</u>		<u>PAGE</u>
1	Classification of Flow Conditions . . . . .	96
2	Classification of Abutment Types . . . . .	97
3	Classification of Geometry . . . . .	98
4	Variation of Velocity Along Embankments . . . . .	99
5	Flow Around a Spill-through Abutment . . . . .	100
6	Stability of a Particle on the Bank of a Bend . . .	100
7	Stability Coefficient and Particle Reynolds Number . . . . .	101
8	Relation for Mean Velocity and Particle Diameter . . . . .	102
9	Angle of Repose of Non-cohesive Material . . . . .	103
10	Lift Force Factor Versus Flow Reynolds Number . . .	104
11	Average Shear Stress Versus $d_{85}$ Size of Bed Material . . . . .	105
12	Definition Sketch for Scour . . . . .	106
13	Clear-water Scour at an Abutment . . . . .	106
14	Scour Length Along Embankment Sides . . . . .	107
15	Factor for Piers not Aligned with the Flow . . . .	108
16	Model Geometry Variables . . . . .	109
17	Measured Velocities for Wide Channel Flow . . . . .	110
18	Measured Velocities for Overbank Flow . . . . .	111
19	Water Surface Contours for Wide Channel Flow . . .	112
20	Water Surface Contours for Overbank Flow . . . . .	113
21	Photograph of the 20-ft Wide Flume . . . . .	114
22	Photograph of Water Surface at $Q = 11.1$ cfs . . .	114
23	Photograph of Water Surface at $Q = 11.1$ cfs . . .	115

# LIST OF FIGURES (Continued)

<u>FIGURE</u>		<u>PAGE</u>
24	Photograph of Scour on an Abutment at Q = 11.1 cfs . . . . .	115
25	Photograph of Scour on an Abutment at Q = 12.7 cfs . . . . .	116
26	Photograph of Water Surface at Q = 16.0 cfs . . . .	116
27	Photograph of Scour on the Opposite Abutment . . . .	117
28	Photograph of Final Scour After Shutdown . . . . .	117
29	Photograph of the 6-ft Wide Flume . . . . .	118
30	Photograph of an Overbank Model . . . . .	118
31	Photograph of Water Surface Characteristics . . . .	119
32	Photograph of Scour Occurring . . . . .	119
33	Photograph of Scoured Abutment after Shutdown . . .	120
34	Photograph of Scour and Deposition After Shutdown .	120
35	Variation of Velocity Along Approach Embankments . .	121
36	Stability of Model Abutment Riprap . . . . .	122
37	Lift Stability of Model Abutment Riprap . . . . .	123
38	Design Example Plan and Cross-section . . . . .	124
39	Determination of $d_{85}$ for Nose Riprap in Example 1 . . . . .	125
40	Determination of $d_{85}$ for Embankment Riprap in Example 1 . . . . .	125
41	Summary of Design Example 1 . . . . .	126
B.1	Aid for Estimating $\alpha_2$ . . . . .	138
B.2	Backwater Coefficient Base Curves . . . . .	139
B.3	Normal Crossings: Spill-through Abutments . . . . .	140
B.4	Skewed Crossings . . . . .	141

# LIST OF FIGURES (Continued)

<u>FIGURE</u>		<u>PAGE</u>
B.5	Incremental Backwater Coefficient for Piers . . . .	142
B.6	Incremental Backwater Coefficient for Eccentricity.	143
B.7	Incremental Backwater Coefficient for Skew . . . .	144
B.8	Tentative Backwater Coefficient for Type II Flow .	145
B.9	Backwater with Abnormal Stage-discharge . . . . .	146
B.10	Differential Water Level Ratio Base Curves . . . .	147
B.11	Incremental Differential Level Ratio for Eccentricity . . . . .	148
B.12	Incremental Differential Level Ratio for Skew . . .	149
B.13	Distance to Maximum Backwater . . . . .	150
B.14	Effect of Scour on Bridge Backwater . . . . .	151
B.15	Correction Factor for Backwater with Scour . . . .	152
B.16	Differential Level Multiplication Factor for Dual Bridges . . . . .	152
B.17	Backwater Multiplication Factor for Dual Bridges .	153
B.18	Discharge Coefficients for Upstream Girder in the Flow . . . . .	154
B.19	Discharge Coefficient for all Girders in the Flow .	155

# LIST OF TABLES

<u>TABLE</u>		<u>PAGE</u>
1	Summary of Model Geometry Values . . . . .	56
2	Comparisons of Measured and Theoretical Values . . .	63
3	Computed Model Parameters at Failure Conditions . .	68
C1	Computational Example for the Solution of the Stability Coefficient $\eta$ on a Spill-Through Abutment Spill-Slope . . . . .	160

## Chapter I

### INTRODUCTION

In order to supplement the current knowledge of protection from scour at bridge crossings and other hydraulic structures, the State Highway Commission of Wyoming, in conjunction with the U.S. Bureau of Public Roads, initiated a program of research involving the design and performance of channel stabilization techniques. The original agreement for "Engineering Investigation Pertaining to Flood Protection of Bridges and Culverts" was accepted by personnel of Colorado State University on February 16, 1966.

The agreement specified three phases of investigation including the stabilization of culvert outlets, the stabilization of bridge crossings, and the study of alternative methods and techniques of stabilization when gravel or rock-riprap are not available, or where special problems arise.

Due to a later need for more extensive studies of the first two phases, the third phase was cancelled in an addendum to the original agreement on October 8, 1969, and the funds allocated for this phase were re-allocated to the first two phases. This report finalizes the second phase of the Colorado State University study.

#### Scope

Channel stabilization in the vicinity of bridge crossings must be designed from a knowledge of the relationships between stability of protection forms and the hydraulic properties of the crossings. Most of the research for this phase of the study involved the development of design methods for the stabilization of bridge crossings with known



or predictable hydraulic properties. A survey of the pertinent literature revealed that other investigators have defined the expected hydraulic and scour characteristics of bridge crossings. This report supplements the work of others with design techniques for protection from increased backwater and extreme flow velocities at bridge constrictions.

### Application

The proposed design procedure was developed using backwater and scour information obtained from a review of the literature. Hydraulic data from model and prototype bridge crossings were found for most common bridge crossings, and the design techniques should be applicable for all these cases.

The laboratory portion of this study was comprised of tests of the proposed design methods. Verification of the design for the tested models does not imply verification for prototype crossings, and the design may be used only with engineering judgment to produce theoretically stable bridge crossings.

### Protection of Bridge Crossings

Flood protection requirements vary from one bridge to another. Some bridges may need to allow the passage beneath the deck of livestock and farm equipment during periods of low flow. Others may require low embankments due to aesthetic considerations, especially in populated areas. Still other bridges may require short spans with long approaches and numerous piers for economic reasons. Labor costs and availability of protection materials vary from region to region.

All of these factors and many more contribute to the difficulty in generalizing stabilization techniques for all bridge crossings.

A classification of bridge crossings based on prominent features would help to alleviate this difficulty. Classifying the regions requiring protection of each crossing, the possible types of protection, the possible flow conditions, the possible channel shapes, the possible abutment types, and the various geometric conditions for crossings will aid the engineer in selecting the correct design for the conditions he has encountered.

#### Regions of Required Protection

Bridge crossings generally include earth-fill embankments and piers or pier bents. These structures reduce the initial cost of the bridge by shortening the reinforced concrete or steel superstructure that must span the low-flow channel between the abutments. Regions of required protection for this type of crossing not only include pier footings and the embankment and abutment slopes and toes, but also the downstream channel which is subjected to the high velocity jet from the crossing. Downstream slopes of embankments for perennial streams must also be protected from wave forces due to wind. In semi-arid regions, wave protection is required only if winds are expected during the design flood.

#### Types of Protection

The region near and including the abutments may be protected in several ways. One method is to armor the possible scour surfaces with a more resistant material. Protection may also be accomplished by diverting the attacking water away from the abutment, or by reducing

flow velocities with retards, jetties, vegetation, or any other means of slowing or diverting the flood waters.

Another protection consideration includes "fuse-plug" designs which allow the loss of a section of the approach embankment during floods. The replacement of the plug takes only a few days, and the expenditures are minor compared to the cost of replacing the bridge superstructure. Relief bridges, or secondary bridges spanning portions of the flood plains, accomplish this same purpose.

Another protection possibility is the "sagged-roadway design" which uses the construction of approach roadways at grade on the flood plains, with the bridge spanning the low water channel. This allows the flood waters to pass over the roadway, but the roadway will occasionally be inundated leaving the bridge standing in the flow with interruptions in traffic. Hazardous vertical curves may also be present with this design.

These alternative designs are only mentioned herein, and more thorough discussions are given by Posey (60), Bradley (12), Laursen (47), and the State of California (15).

Armoring a surface with more resistant materials involves several possible types of protection which must also be classified and considered in each design. The designs herein are based only on the use of loose rock riprap placed by conventional means. Other forms such as sacked concrete, pneumatically applied concrete mortar, grouted rock, asphalt paving, concrete slabs, broken concrete, precast concrete blocks, rock and wire mattresses, rock and wire sausages, willow mattresses, tetrapods, sheet piles, or even sea-shells, have been successfully used and should not be excluded from economic

consideration, especially in areas where rock riprap is scarce. Design methods and construction techniques for all of these forms of protection have been published by private and governmental agencies such as "Shore Protection Planning and Design," by the Corps of Engineers (77), "Bank and Shore Protection in California Highway Practice," by the State of California (15), and "Use of Riprap For Bank Protection," by the Bureau of Public Roads (68).

Rock riprap for channel stabilization has several advantages over other forms whenever it is available. The State of California lists the advantages as:

1. It is flexible and is therefore not weakened by slight movements of the settling embankments.
2. Local damage is easily repaired.
3. Construction involving its use is not complicated by special equipment.
4. The appearance is natural and adds to the aesthetics of the design.
5. Vegetation will grow through the voids and increase the structural strength with time.
6. The thickness can be varied to provide more protection in critical zones.
7. Wave runup on sloping surfaces is less (as much as 70 percent) than the runup on smooth surfaces.
8. It may be stockpiled and re-used.
9. It is usually the most economical whenever stones of sufficient size and quantity are available.

### Flow Conditions

Five possible types of flow conditions at bridge crossings based on non-scouring or equilibrium scour conditions are shown in Figure 1.

They include:

- (a) Subcritical - the flow depth remains above critical depth upstream, through, and downstream of the crossing.
- (b) Critical flow in the gap - the flow depth passes from subcritical to supercritical depth in the gap and returns to subcritical flow downstream. Critical depth in the gap is greater than critical depth for the downstream reach.
- (c) Critical - the flow depth passes from subcritical to supercritical depth in the gap and continues below critical depth downstream of the crossing. A hydraulic jump then forms downstream if the resistance or some control in that reach returns the depth to normal, subcritical flow conditions.
- (d) Supercritical - the flow upstream, through, and downstream of the crossing remains below critical depth at every section. The slope is classified as steep because normal depth is below critical. This condition may occur in mountain streams.
- (e) Abnormal - due to some downstream control, the flow must return to a depth greater than normal.

### Channel Shapes

Classification by channel shape includes the two categories shown in Figure 3. These are as follows:

- (a) Wide-channel flow - the flow channel is relatively wide with no flood plain, and the flow depth remains relatively constant across the channel.

(b) Overbank flow - the channel has a wide flood plain with a central low-flow channel.

### Abutment Types

Types of abutments common in prototype crossings are shown in Figure 2 and include:

(a) Vertical wall - the embankment sides and abutment nose are vertical retaining walls.

(b) Vertical wall with sloping embankments - the embankment sides are sloped, and the abutment nose is a vertical retaining wall.

(c) Spill-through - the embankment sides and abutment nose are sloped with circular or other sloping transitions between them.

(d) Wing-wall - the embankment sides are sloped, and the abutment nose is vertical with vertical wing-walls forming the transition between the sides and the nose.

### Geometric Properties

Geometric properties of bridge crossings are more difficult to classify than the flow conditions, channel shapes, and abutment types. Any of the geometric properties illustrated in Figure 3 may be used depending on the conditions at the proposed site. The approaches may be skewed or normal (perpendicular) to the direction of flow, or one approach may be longer than the other, producing an eccentric crossing. Abutments used for the overbank-flow case may be set back from the low-flow channel banks to allow passage of livestock and machinery, or the abutments may extend up to the banks or even protrude over the banks, constricting the low-flow channel. Piers, dual bridges for



multi-lane freeways, channel bed conditions, and spur dikes add to the list of geometric classifications.

In the past, geometric factors have been treated with solutions for some basic or standard crossing, with additive or multiplicative coefficients for geometric variations. The coefficients have been derived from laboratory and field observations of bridge crossings, and corrections are made for the effects of skewness, eccentricity, scour, abutment setback, channel shape, submergence of the superstructure, debris, spur dikes, windwaves, ice, piers, abutment types, and flow conditions. The design procedures presented herein take advantage of the large volume of work, using the above technique, that has been done by others in describing the scour characteristics and hydraulics of bridge crossings.

## Chapter II

## DERIVATION OF DESIGN CRITERIA

The design presented in this chapter is derived from predictable hydraulic and scour properties of bridge crossings. The crossing geometric variables and flow conditions before the bridge constriction are used to predict the backwater produced by the crossing at design discharge. A maximum expected design velocity is derived from the knowledge of the backwater and the turbulent fluctuations in the flow field. Values of the velocity at critical points in the flow field are related to the design velocity, and a technique for relating velocity to stable rock size and gradation is presented.

Verification of the design of rock riprap for the protection of spill-slopes on spill-through abutments is presented in Chapter IV. The research for this investigation, as stated in Chapter I, was concerned mainly with the verification of the design procedures. The development of the design procedures is based on engineering fundamentals and data presented by other investigators.

A team of investigators was involved with the research for this report. Contributions made by Simons, Field, and Callander are mentioned at various points in this chapter to show where each individual contributed. Additional work with the analytical and experimental results of the research is being conducted by Lewis and will be presented in a dissertation and supplemental report in 1971.

Backwater Equations

Various methods of predicting backwater at flow constrictions are found in the literature. The most recent publication, "Hydraulics of

Bridge Waterways" (14), utilizes both model and recent prototype data for predicting backwater at bridge crossings. Effects of most of the variations shown in Figures 1, 2, and 3 are presented in the publication, and the whole procedure has been programmed for the computer in another publication (79). The methods presented below are based on the backwater predicted (Appendix B) from these publications. Other methods of predicting backwater should be equally applicable as long as the definitions are consistent.

Bradley (14) presents two backwater equations for bridge crossings. The first applies to subcritical flow conditions, and the second is used for each of the critical flow conditions shown in Figure 1.

By applying the energy equation from the point of maximum backwater upstream of the bridge to the downstream point at which the flow returns to normal conditions (Figure 1a), Bradley derives the subcritical flow equation

$$h_1^* = K^* \alpha_2 \frac{V_{n2}^2}{2g} + \alpha_1 \left[ \left( \frac{A_{n2}}{A_4} \right)^2 - \left( \frac{A_{n2}}{A_1} \right)^2 \right] \frac{V_{n2}^2}{2g} .$$

The equation is applicable to models and prototypes, and the terms are defined as

$h_1^*$  = total backwater (Figure 1a), or  $h_1 - h_n$  (ft),

$K^*$  = total backwater head loss coefficient,

$\alpha_1$  = velocity head correction coefficient at the upstream section of maximum backwater,

$\alpha_2$  = velocity head correction coefficient in the constriction,

$A_{n2}$  = cross-sectional area in the constriction, measured below the unconfined design stage (sq ft),

$V_{n2}$  = average velocity in the constriction for flow at the design discharge, or  $Q/A_{n2}$  (fps),

$A_4$  = cross-sectional area at the downstream point where normal stage has been re-established (sq ft), and

$A_1$  = cross-sectional area at the upstream section of maximum backwater measured below the water surface (including  $h_1^*$ ).

For the critical flow conditions in Figure 1b and 1c the critical section controls the backwater. For this case

$$h_1^* = \frac{\alpha_2 V_{2c}^2}{2g} (C_b + 1) + h_{2c} - h_n - \frac{\alpha_1 V_1^2}{2g},$$

where  $h_1^*$ ,  $\alpha_2$ , and  $h_n$  were previously defined, and

$V_{2c}$  = critical velocity (fps) in the constriction satisfying the relationship

$$V_{2c}^2 b_{tc} = gA_{2c},$$

$b_{tc}$  = top width between the abutments measured at critical depth (ft),

$A_{2c}$  = the cross-sectional area in the constriction measured below critical depth (ft<sup>2</sup>),

$C_b$  = backwater coefficient for critical flow, similar to  $K^*$  for the subcritical case,

$V_1$  = average velocity at the section of maximum backwater, or  $Q/A_1$  (fps), and

$h_{2c}$  = critical depth in the constriction (ft).

Normal stage for the subcritical and critical equations is defined as the stage at which the unconfined river would flow for the design

discharge. The backwater,  $h_1^*$ , is simply the maximum rise of the flow above normal stage.

Bradley's solutions for  $C_b$  and  $K^*$  in these equations require values of the opening ratio,  $M$ , for the bridge crossing. Different investigators (10, 19, 23, 40, 43, 73, 75, 78) have used several definitions of  $M$  which are based either on the geometric or the flow conditions for the constriction. The geometric definition is the average distance between the abutments,  $b$ , divided by the top water surface width of the channel at normal flow,  $B$ . This is a gap-width to channel-width ratio. Flow definitions incorporate the possibility of different values of flow resistance for the flood plains and low-flow channel. For this case,

$$M = Q_b/Q ,$$

where

$M$  = bridge opening ratio,

$Q$  = design discharge, and

$Q_b$  = the portion of the unconfined flow that can pass unimpeded through the bridge constriction.

If the wide channel flow case of Figure 3 is encountered, the resistance across the channel is constant, and the flow definition of  $M$  becomes

$$M = \frac{Q_b}{Q} = \frac{b h_n V_n}{B h_n V_n} = \frac{b}{B} ,$$

where

$b/B$  = the geometric definition of the opening ratio,

$b$  = the average width between the abutments measured below  $h_n$ (ft),

$B$  = the top width of the unconfined channel measured at  $h_n$  (ft),

$h_n$  = the stage in the unconfined channel flowing at design discharge (ft), and

$V_n$  = the velocity (fps) in the unconfined channel flowing at design discharge.

The average width between the abutments,  $b$ , is well defined for the vertical abutments in Figure 2. For the spill-through abutment,

$$b = A_{n2} / \bar{h}_{n2} ,$$

where  $A_{n2}$  has previously been defined, and  $\bar{h}_{n2}$  is the depth shown in Figure 2 after the irregular section has been converted to a trapezoid of area  $A_{n2}$ .

For the overbank flow case of Figure 3, the resistance to flow is generally greater on the flood plains. If the abutments are set back from the low-water channel banks, then the value for  $Q_b$  is comprised of the high-velocity flow in the center of the channel and the low-velocity flow on the flood plains. For this case, the differences in velocities and depths do not allow a reduction of  $Q_b/Q$  to the geometric definition of the opening ratio.

The flow definition of  $M$  therefore applies to both types of channels and is more amenable to prototype conditions. Whenever wide channel conditions are encountered, the flow definition reduces to the geometric definition.

If the distribution of normal unconfined flow across the channel is known, a central section of width,  $b$ , may be selected, and the flow,  $Q_b$ , may be determined. The discharge,  $Q$ , is the design discharge, and a value of  $M$  may be found from these values.



The opening ratio,  $M$ , may also be determined from conveyance curves, if available, for the bridge site cross-section. The conveyance for a cross-section is defined as

$$K = Q/S^{1/2} ,$$

where

$K$  = conveyance of the cross section,

$Q$  = discharge (cfs) of the section, and

$S$  = slope of the energy grade-line at the section.

For uniform flow, the bed slope and friction slope are equal, and if Manning's equation is substituted for  $Q$ , then

$$K = \frac{Q}{S_o^{1/2}} = \frac{1.486}{n} AR^{2/3} .$$

Assuming that the bed slopes for the flood plains and the low-flow channel are equal results in

$$M = \frac{Q_b}{Q} = \frac{K_b S_o^{1/2}}{K S_o^{1/2}} = \frac{K_b}{K} ,$$

where  $K_b$  is the conveyance of the opening width,  $b$ , and  $K$  is the total conveyance for the cross section.

Having a value for the flow opening ratio provides a solution for the backwater equations. Values for  $K^*$  and  $C_b$  may be obtained from Bradley's curves relating  $K^*$  and  $C_b$  to  $M$  for the various flow and geometric conditions depicted in Figures 1, 2, and 3. Appendix B contains most of Bradley's experimental curves.

### Design Velocities

Energy considerations were successfully used to predict backwater, and this implied that this concept can be used to define the velocity field at a bridge crossing. The energy equation applied between the point of maximum backwater and the downstream point of return to normal depth was utilized in predicting backwater. For this research, the energy equation applied between the point of maximum backwater and the point of minimum depth in Figure 1a yields the relationship

$$\alpha_1 \frac{V_1^2}{2g} + h_1 + S_o L_{1-3} = h_3 + \alpha_3 \frac{V_3^2}{2g} + h_{L\ 1-3} ,$$

where  $\alpha_1$ ,  $V_1$ ,  $h_1$ , and  $S_o$  have been defined, and

$L_{1-3}$  = length along the channel between the points of maximum backwater and minimum jet depth (ft),

$h_3$  = the minimum depth in the jet (ft),

$\alpha_3$  = velocity head correction coefficient at the point of minimum depth,

$V_3$  = the velocity at the point of minimum depth (fps), and

$h_{L\ 1-3}$  = the energy losses between the two sections (ft).

Solving this equation for  $V_3$  produces the equation

$$V_3 = \sqrt{\frac{2g}{\alpha_3} \left[ \alpha_1 \frac{V_1^2}{2g} + S_o L_{1-3} + (h_1 - h_3) - h_{L\ 1-3} \right]} .$$

By defining  $\Delta h$  as  $h_1 - h_3 + S_o L_{1-3}$ , then

$$V_3 = \sqrt{\frac{2g}{\alpha_3} \left[ \alpha_1 \frac{V_1^2}{2g} + \Delta h - h_{L\ 1-3} \right]} .$$

A conservative estimate of  $V_3$  is obtained by neglecting the energy losses, so that

$$V_3' = \sqrt{\frac{2g}{\alpha_3} \left( \alpha_1 \frac{V_1^2}{2g} + \Delta h \right)} > V_3 .$$

Because  $\alpha_3$  is greater than or equal to 1.0, assuming a value of unity increases  $V_3'$  to

$$V_d = \sqrt{2g \left( \alpha_1 \frac{V_1^2}{2g} + \Delta h \right)} > V_3' > V_3 .$$

This velocity represents a conservative estimate of the maximum velocity expected in the jet. The inclusion of  $\alpha_3$  and  $h_{L\ 1-3}$  serve to reduce  $V_d$  to  $V_3$ . If  $V_d$  is used as a riprap design velocity, then the riprap will be oversized whenever either the head loss,  $h_{L\ 1-3}$ , or the value of  $\alpha_3$  is large. Large values of  $\alpha_3$  and  $h_{L\ 1-3}$  are indicative of extreme constrictions and highly turbulent flow, and riprap for these cases should be oversized to account for the turbulent fluctuations of the velocity about its mean value.

Turbulent flow cannot be described accurately by an average velocity because the actual velocity fluctuates above and below some mean value. Most continual records of turbulent velocity reveal an oscillating trace, with recorded velocities both greater and less than the time-averaged mean. Even through the deviations from the mean occur for short periods of time, the maximum fluctuation must be considered in selecting design velocities.

Velocities greater than 150 percent of the mean exist for very short periods, and may be neglected (17). The design velocity deduced from the above energy equation is already conservative, but design

techniques demand factors for safety, and the use of  $1.5 V_d$  (derived from the 150 percent value) is recommended as a design velocity in this report. Care should be exercised in applying this safety factor, and other values may be used in the event that experience or prototype data produce larger or smaller values.

### Velocity Field

The design velocity derived in the last section theoretically applies near the outlet of the constriction at the vena contracta of the jet. Design velocities for other zones of the crossing may be desired if stable stone sizes determined from a value of  $1.5 V_d$  are not sufficient for placement at all the critical zones of protection.

Field (23) participated in this study and presents Figure 4 as a solution for the velocities on the upstream side of the approach embankments. The figure is based on ideal flow conditions through a two-dimensional nozzle, and the geometric definition of  $M = b/B$  is used. The curves apply to half-embankments placed at various angles to the flow, and may be used as guides in determining stable riprap sizes on the upstream side-slopes of embankments.

Velocities at other regions of the flow are difficult to predict analytically. Two-dimensional approaches similar to Field's are possible, but effects of free water surfaces and separation are difficult to incorporate into these analyses. Callander and Lewis are attempting to extend Field's work with two-dimensional solutions for the entire velocity field in the vicinity of bridge crossings. The findings from these analyses will be included in a supplemental report in 1971. For the present, reliance must be placed on experimental approaches based on data from laboratory and field bridge constrictions.

### Design of Riprap

The stability of graded gravel and rock riprap is closely related to the riprap characteristics and the hydraulic and geometric properties of the bridge crossing. All of these factors are important to the stability of a proposed riprap.

Methods of choosing stable rock sizes are usually based on riprap properties and the hydraulic and geometric characteristics of the fluid flow. Velocities, pressures, depths, and shearing stresses have all been related individually and collectively to the stability of riprap.

The method chosen for use in this report was originally presented in a dissertation by Bhowmik (8), and has recently been presented by Bhowmik and Simons (9) at the Institute of River Mechanics held at Colorado State University in June, 1970, and at a meeting of the American Society of Civil Engineers held at New Orleans, Louisiana, in February, 1969.

The report presents a design method for riprap stabilization of the beds and banks of straight reaches and bends in alluvial channels. Step-by-step design procedures for each of these conditions are outlined in the publication, along with the theoretical and experimental relationships required for the design procedures.

Bhowmik's methods were not developed explicitly for bridge crossings, and modifications were needed to relate the design method to the flow near bridge abutments and piers.

If the flow along the upstream slope of a bridge embankment may be equated to flow near the sloping bank of a straight reach in a channel, then Bhowmik's methods could be used to predict stable riprap for the side-slope and toe of the embankment.

Stabilization of the bed and banks downstream of the crossing could be accomplished by using the straight-reach methods, developed by Bhowmik, if the jet characteristics were known for the particular design.

Stabilization of the channel or flood plain between the abutments may be accomplished by using Bhowmik's technique for side slopes and beds of straight reaches. The maximum velocity in this region may be approximated by the design velocity,  $1.5 V_d$ . The velocities in the constriction are somewhat less than the vena-contracta velocities, and  $1.5 V_d$  is therefore a conservative design velocity. Laboratory measurements (Chapter IV) reveal magnitudes of the depth-averaged abutment toe velocity between 60 and 100 percent of the vena-contracta velocity.

The sloping nose of a spill-through abutment may be protected with riprap if the design size is based on the component of particle weight acting downslope and the force of the plunging flow at the upstream corner of the abutment. For the same flow conditions, particles resting on this slope are less stable than particles on the bed. Riprap sizes required for the spill-slopes of spill-through abutments are therefore larger than the sizes required for the low-flow channel and the flood plain.

Figure 5 represents a spill-through abutment spill-slope showing the water surface drop around the upstream shoulder. The research for this report and other experiments (53, 54, 73) have shown that the flow through spill-through abutments separates near the tangent with the central slope (point A in Figure 5) and submerges beneath the downstream water surface. The angle of the flow down the slope is approximated by the angle,  $\lambda_1$ , in the figure. Scour of the spill-slope riprap generally

begins slightly downstream of point C, and the angle,  $\lambda_1$ , is conservatively large.

The vertical distance of point A above the channel bed at the abutment very closely approximates the unconstricted normal stage (52). Defining  $h_A$  as this depth, then  $h_A = h_n$ , and

$$\tan \lambda_1 = \frac{\overline{BC}}{\overline{AB}} = \frac{h_n / \sin \alpha}{W/2} .$$

Figure 6 illustrates the relationship between this equation and Bhowmik's sizing procedure for riprap on the concave bank of a channel bend. Due to transverse circulation in a bend, the resultant drag force,  $F_D$ , is not parallel to the flow as it would be in a straight reach. Figure 6 shows the drag force deflected at an angle,  $\lambda_1$ , to the direction of flow. This drag force is a resultant of the parallel drag force and the downslope force due to the transverse circulation in the bend. The analogy between the drag forces in Figures 5 and 6 results in identical treatment of the particle stability for each case.

#### Particle Stability

Figure 7 represents Bhowmik's relationship between particle stability and the particle Reynold's number. The values of  $V_b$  and  $d_m$  represent the bottom velocity and mean diameter of the riprap. The bottom velocity is computed as 0.8 times the mean velocity, and the mean or effective diameter,  $d_m$ , was derived by Simons, Stevens, and Watts (74) as

$$d_m = \left[ \frac{\sum_{i=1}^{10} d_i^3}{10} \right]^{1/3} ,$$

where

$$\begin{aligned} d_i (i=1) &= \frac{d_0 + d_{10}}{2} , \\ d_i (i=2) &= \frac{d_{10} + d_{20}}{2} , \\ &\vdots \\ d_i (i=10) &= \frac{d_{90} + d_{100}}{2} . \end{aligned}$$

The terms  $d_0, d_{10}, \dots, d_{100}$  are the sieve diameters of the riprap for which 0, 10, ..., 100 percent, respectively, of the material (by weight) is finer.

Bhowmik originally used the  $d_{50}$  size of the riprap in Figures 7, 8, and 10, and the use of  $d_m$  simply produces a slight margin of safety because  $d_m$  is always larger than the  $d_{50}$  size. The mean diameter was also used in the culvert report and its use here provides consistency between the two reports. Better riprap gradation curves and better scaling results from model to prototype are both present when using  $d_m$  instead of  $d_{50}$ .

The stability coefficient,  $\eta$ , is found from a consideration of the forces acting on particles resting on the banks and beds of channel bends and straight reaches. For the concave bank of the bend shown in Figure 6, Bhowmik derives the equation

$$K_1 = [K_2 + 1.74 V_b^2 \eta (\gamma_s - \gamma_f) \sin \alpha \sin \lambda_1]^{1/2} ,$$

where

$\eta$  = the stability coefficient,

$V_b$  = the bottom velocity (fps), or 0.8 times the mean velocity,

$\gamma_s$  = the specific weight of the riprap (lb/ft<sup>3</sup>),



$\gamma_f$  = the specific weight of the fluid,

$\alpha$  = the bank side slope,

$\lambda_1$  = the deflection angle of the drag force with the flow direction,

$$K_1 = [(\gamma_s - \gamma_f) \cos \alpha - 0.743 V_b^2 \eta] \tan \phi,$$

$$K_2 = [0.76 (V_b^2 \eta)^2 + \{(\gamma_s - \gamma_f) \sin \alpha\}^2]^{1/2}, \text{ and}$$

$\phi$  = the angle of repose of the riprap.

On the banks of straight reaches, such as the upstream slopes of embankments, the angle,  $\lambda_1$ , approaches zero, and the relationship for the stability coefficient becomes  $K_1 = K_2^{1/2}$ . This equation and the equation for the bank of a bend require iterative solutions for  $\eta$ . Appendix C contains a useful computational procedure for solutions of  $\eta$ .

On the bed of a straight reach, the stability coefficient may be obtained from

$$\eta = \frac{1.146(\gamma_s - \gamma_f) \tan \phi}{V_b^2 (1 + 0.85 \tan \phi)}.$$

For designs which require the estimation of stable rock sizes from given flow velocities, Figure 8 may be used for an initial estimate of the riprap  $d_m$ , and Figure 9 for an estimate of the angle of repose of the riprap. The value estimated from Figure 8 is maintained throughout the design, and its stability is checked in Figure 7 at the completion of the design. If the value from Figure 8 proves to be unstable, then changes in  $d_m$  and a repetition of the design are needed until stability is indicated.

### Lift Forces

The above procedure for stability analysis considers only the resistance to the drag and slope forces exerted on the particles. Vertical lift forces due to pressure differences exerted on the surface of a particle must also be considered.

A lift force coefficient, similar to the drag force stability coefficient, is plotted in Figure 10 along with the Reynold's number. For this case, the flow Reynold's number is used, where

$$R = V_b D / \nu ,$$

where the terms are defined as

$V_b$  = bottom velocity (fps), or 0.8 times the mean velocity,

$\nu$  = kinematic viscosity (ft<sup>2</sup>/sec) of the fluid,

and

$D$  = depth of flow (ft).

The lift force coefficient, with  $d_m$  substituted for  $d_{50}$ , is defined by Bhowmik as

$$\frac{1}{\psi} = \frac{V_b^2}{(S_s - 1) g d_{50}} \left( \frac{\rho_f}{\rho_s} \right) \left( \frac{d_{85}}{d_m} \right)^3 ,$$

where  $S_s$  is the specific gravity of the riprap, and  $d_{85}$  is defined as the sieve size for which 85 percent (by weight) of the riprap is smaller.

A value of  $d_m$  which is stable from drag forces according to Figure 7 will not necessarily be stable from lift forces. If the  $d_{85}$  size of the proposed riprap is too large, turbulent eddies are created which may lift the smaller  $d_m$  stones from the surface. The lift force

factor for the riprap must fall in the stable region of Figure 10 for any design.

In order to utilize Figure 10, the  $d_{85}$  size of the riprap must be estimated. Figure 11 presents Bhowmik's estimate for the bed material  $d_{85}$  size. A value chosen from this figure should insure that large-scale eddies produced by the larger  $d_{85}$  rocks do not lift the smaller  $d_m$  stones. For design, the shear stress for Figure 11 should be computed as  $1.5 \gamma DS$  to account for turbulent fluctuations from the average shear stress.

For banks, the shear stress varies with the depth, but may be related to the bed shear stress by

$$\left(\frac{\tau_s}{\tau_o}\right)^2 + \frac{\tau_s}{\tau_o} \frac{(1 + 0.85 \tan \phi)}{(1 - 0.72 \tan^2 \phi)} (1.7 \cos \alpha \tan \phi) = K_4 ,$$

where  $\tau_s$  is the bank shear stress,  $\tau_o$  is the bed shear stress,  $\phi$  is the angle of repose of the bank riprap, and

$$K_4 = \frac{(1 + 0.85 \tan \phi)^2 (\cos^2 \alpha \tan^2 \phi - \sin^2 \alpha)}{\tan^2 \phi (1 - 0.72 \tan^2 \phi)} .$$

Solution of this equation for  $\tau_s$ , and an increase of the value to  $1.5 \tau_s$ , provides a design ordinate for Figure 11 when considering riprap lift-stability on banks.

Another estimate for the  $d_{85}$  size may be obtained by first combining Bhowmik's (8) relationship between stable riprap sizes and Manning's roughness factor,  $37.6n = d_m^{0.178}$ , with Lane's (42) relationship between the  $d_{75}$  size and Manning's factor,  $39n = d_{75}^{1/6}$ . Eliminating  $n$  from the two equations results in  $d_{75} = 1.265 d_m^{1.07}$ , which may be solved for  $d_{75}$ . An estimate of  $d_{85}$  may be obtained from

a straight-line extrapolation on a standard sieve analysis curve, using  $d_m$  as a value for  $d_{50}$  on the curve.

After obtaining values of  $d_m$  and  $d_{85}$  which satisfy the stability requirements of Figures 7 and 10, similar parameters from available riprap are computed and compared. The required value of  $d_m$  is intended as a minimum value, meaning that the available riprap must have a value of  $d_m$  greater than or equal to the required value of  $d_m$ , regardless of the  $d_{50}$  size or any other size. Also, the  $d_{85}$  size computed by the design is intended as a maximum  $d_{85}$  size, and the available riprap need only have a  $d_{85}$  size equal to or less than the required value. The straight-line interpolation in the last paragraph substitutes the  $d_m$  value as a  $d_{50}$  value only to determine an estimate for the  $d_{85}$  size. Once an acceptable  $d_{85}$  size is determined, the remaining gradation curve may lie anywhere, as long as the whole curve produces the required value for  $d_m$ , and passes through the required  $d_{85}$  point or some smaller  $d_{85}$  point. This flexibility in the design of riprap should be borne in mind, especially in the design example of Chapter V. Figures 39 and 40 are intended only as methods of determining a maximum acceptable  $d_{85}$  size and are not presented as final gradation curves. The final curves may lie anywhere as long as the  $d_{85}$  sizes and  $d_m$  sizes are maintained as maximum and minimum values, respectively.

#### Wave Forces

Wind-generated waves can contribute to particle instability on the upstream and downstream sides of an embankment. For the upstream side, wave action and flowing water can contribute individually or collectively to the instability of riprap particles.

The downstream slopes of embankments are not subjected to flowing water, and riprap sizes predicted for wind or turbulence-generated waves are suggested for this region.

Hudson (30) presents an equation for the stone size resistant to wave forces as

$$W_s = \frac{\gamma_s H^3}{3.2 (S_s - 1)^3 \cot \alpha},$$

where  $\gamma_s$ ,  $S_s$ , and  $\alpha$  have been defined, and

$W_s$  = weight of stone required for wave stability (lb), and

$H$  = significant wave height (ft).

Hudson does not specify which stone size is to have the weight,  $W_s$ , and the  $d_m$  size is used in this report. The factor 3.2 is an empirical value obtained from quarry stone.

The significant wave height in shallow water for fetch widths approximately equal to fetch lengths is obtained (23) from

$$\frac{gH}{V_w^2} = 3.23 \times 10^{-3} (g F / V_w^2)^{0.435},$$

in which

$V_w$  = wind velocity (fps), and

$F$  = fetch length (ft), or length of the river subjected to wind.

The fetch widths are usually different from the fetch lengths for rivers, and an effective fetch length,  $F_e$ , is suggested (66) as

$$F_e = 1.17 F^{1/3} W_F^{2/3},$$

where  $W_F$  is the fetch width in feet.

When wave motion and flowing water occur simultaneously, the waves induce an additional bottom velocity given (9) by

$$V_{wm} = \frac{\pi H}{T} \frac{1}{\sinh \frac{2\pi D}{L_w}},$$

where

$T$  = wave period (sec),

$L_w$  = wave length (ft), and

$D$  = depth of flow (ft).

When considering stability for these conditions, the velocity vector  $\bar{V}_{wm}$  must be added to the flow velocity vector to obtain the resultant velocity.

#### Freeboard

Embankments that may be overtopped during floods act as broad-crested weirs and require spillway designs on their downstream sides. Due to the high-velocity supercritical flow directly down the slope, very large riprap sizes would be required for this region, and other protection forms should be considered (60).

The usual alternative to flow over the embankments is a provision for sufficient embankment height to prevent overflow. Backwater and possible wave heights should be added to normal stage when determining minimum embankment heights. Wave height considerations may not be necessary in semi-arid regions where flood hydrographs having high peaks and short bases are common. When waves are anticipated, the suggested freeboard above normal stage may be found from

$$F_b = h_1^* + H + h_s,$$

where  $H$  and  $h_1^*$  have been defined, and  $h_s$  is a safety height dependent on the judgment and experience of the design engineer.

### Scour at Abutments

Whenever scour of the bed material is anticipated at the abutment toe, protection of the toe must be carried below the expected scour depth to prevent undermining of the abutment. Three types of scour (69) are possible at bridge crossings, and are additive if all three occur at the same time. Local scour is defined as the scour near a pier or abutment due to the physical presence of the structure in the flow. Bridge piers and approach embankments reduce the net flow area and increase the flow velocity, causing contraction scour of the entire bed in the vicinity of the crossing. Natural scour, or degradation of the entire river channel, may also be occurring, and the measured bed elevation used for design purposes is not dependable. Natural scour is difficult to predict and is omitted in the design procedures. Whenever natural scour data is available at a proposed site, its effect should be included in protection designs.

For vertical wall or wing-wall abutments, protection may be provided by founding the wall below the expected scour depth or by using vertical sheet piles driven at the toe. Spill-through abutments may also be protected by sheet piles, or by creating a horizontal or sloping apron of riprap protection around the toe. The apron must either prevent scour at the abutment, or be placed so that the apron will fall into the scour hole as it develops. If the stream bed is not rigid, riprap protection may be buried along the abutment slope to a depth beneath the scour level, especially at the upstream corner where maximum bed material scour is expected (53, 54).

The flow at abutments may be either clear or sediment-laden, and different scour analyses are required for each case. Clear-water scour occurs at relief bridges or at abutments which are set back from the low-flow channel banks (Figure 3e). For the setback case, the low-velocity flood plain flow carries little sediment, and clear water scour occurs.

Laursen (45) proposes Figures 12 and 13 for the relationship among clear-water contraction scour at piers and abutments, critical tractive shear stress, and the geometry of the contraction.

The values in the figures are defined as

$d_{se}$  = equilibrium scour depth (ft), measured below mean bed elevation,

$h_1$  = flow depth in the main channel upstream of the pier or contraction (ft), including backwater,

$L_e$  = length of the approach embankment (ft),

$\tau'_o$  = shear stress attributed to the grain roughness in the constriction (psf),

$\tau_c$  = critical tractive shear stress for incipient motion of the bed material at the contraction (psf),

$d_{se}/r$  = scour in a long contraction, and

$r$  = a coefficient relating the scour in a long contraction to the scour,  $d_{se}$ , in a shorter contraction, where the scour in the long contraction is  $d_{se}/r$ .

Figure 13 also contains Laursen's curve for sediment-laden flow at the abutments. This curve may be used for sediment-laden flow whenever the bed between the abutments is unprotected, and when the sediment transported as bed load is the same size as the bed material. For



riprap-protected beds, the flow is always considered clear because of the large difference between the riprap and bed-load sizes.

The values from Figure 13 are based on the assumption that the scour holes from abutment to abutment, or from pier to abutment, do not overlap. Laursen states that a clear opening between the abutments greater than  $5.5 d_{se}$  should insure non-overlapping scour holes. No analyses presently exist for overlapping scour holes when piers are present, or when opposite abutments are close to each other.

Laursen's estimates for values of  $\tau_o'$  and  $\tau_c$  in Figure 13 are

$$\tau_o' = \frac{V_1^2 D_s^{1/3}}{30 h_1^{1/3}} \quad (\text{psf}) ,$$

and

$$\tau_c = 4D_s \quad (\text{psf})$$

where

$D_s$  = the bed mean particle diameter in the constriction (ft), and

$V_1$  = velocity of flow in the uncontracted reach upstream of the abutment (fps).

The equation for  $\tau_o'$  arises from the Manning and Strickler equations, and the equation for  $\tau_c$  agrees with White's (80) and Shield's critical shear for silica sands and turbulent flow.

Figure 13 is derived from model data only, and predicts unusually large scour depths for prototype structures, especially for clear water scour conditions. Caution and judgment are advised in applying the results of Figure 13 to these cases. The curves should be considered as a guide until future measurements at prototype crossings are available for modifications of the method.

### Scour at Piers

Shen (69) proposes the following analyses for local scour at piers, based on the cases of clear-water scour and scour with continuous sediment motion.

For clear water scour, Shen proposes the equation

$$d_{se} = 0.00073 \bar{R}^{0.619} \quad (\text{ft}) ,$$

where

$\bar{R}$  = pier Reynolds number defined as

$$\bar{R} = \frac{2aV_{\infty}}{\nu} ,$$

where

$a$  = half width of the pier, or radius of the pier (ft),

$V_{\infty}$  = the average upstream, undisturbed flow velocity (fps), and

$\nu$  = the kinematic viscosity of the fluid ( $\text{ft}^2/\text{sec}$ ).

This equation was derived from laboratory and field data collected in several investigations (69).

For the case of sediment-laden flow, deposition causes the scour depth to fluctuate about a mean value. Defining  $d_{se}^*$  as the maximum equilibrium scour depth measured from mean bed elevation, Shen recommends either

$$d_{se}^* = 1.4b_p ,$$

or

$$d_{se}^* = 1.42 K_b p^{0.75} ,$$

in which

$b_p$  = width of pier projected on a plane normal to the undisturbed flow (ft), and

$K$  = a coefficient of pier shape, recommended as 1.0 for cylindrical piers and 1.4 for rectangular piers.

The first equation for  $d_{se}^*$  is more conservative, and the second agrees better with the available data.

Whenever dunes are expected to pass through the scour hole, Shen suggests that half the expected dune height be added to  $d_{se}^*$  for estimations of scour depths. Dune heights, however, are usually small compared to scour depths, and may usually be neglected unless data are available for the design site.

When piers or pier bents are not aligned with the flow, Laursen and Toch (51) predict a larger scour depth than for piers aligned with the flow. Figure 15 provides a correction coefficient,  $K_{\alpha 1}$ , to be multiplied by the equilibrium scour depth for piers aligned with the flow.

#### Lateral Extent of Scour

Estimates of the lateral extent of possible scour at abutments and piers are required for the design of widths of horizontal aprons or riprap mats around the structures. Laursen (47) suggests a width of  $2.75 d_{se}$  for abutments and piers. This value is measured horizontally from the face or toe of the pier or abutment, and is recommended as a minimum value.

Field (23) participated in the research and recommends the use of Figure 14, obtained from this research, for determining the lateral extent of scour at abutments. The distance,  $z$ , along either face of the abutment defines the conical scour hole boundary, and  $d_{se}$  is the

equilibrium scour depth obtained from Figure 13. Note that the value of  $z$  along the upstream face for an angle,  $\theta$ , of 90 degrees and an angle of repose of  $21^{\circ} 31'$  becomes identical to Laursen's value of  $z = 2.75 d_{se}$ . The principal advantage of Field's figure is its estimate of lateral extent for skewed abutments.

## Chapter III

## PROPOSED DESIGN PROCEDURES

This chapter presents a step-by-step outline of design principles based on the derivations in Chapter II and from this research and the design recommendations summarized from the literature. Laboratory verification of the procedures are presented in Chapter IV, and an example of the design of protection for a prototype bridge is presented in Chapter V.

The presented design steps use the backwater and scour predicted from the literature. The results of this research included in the steps are the derivation of the vena contracta design velocity, the velocities along the upstream slopes of the approach embankments, the amount of riprap wrap-around for spill-through abutments, the terminal points for riprap placement on the side slopes of approach embankments, the length along the side slopes requiring buried toe protection, and the riprap sizing and gradation designs computed from the design bed velocities.

Stablization techniques are presented for bridge crossings assuming that the following quantities are given:

- (1) the desired crossing with design discharge,  $Q$ ;
- (2) normal flow stage for the design discharge;
- (3) the distribution of the design discharge across the unconfined channel;
- (4) the abutment type (Figure 2);
- (5) the geometric properties (Figure 3); and
- (6) the availability of riprap for protection.

The result of applying the design technique is the required riprap size and gradation. If only one size and gradation is available, the crossing

variables must be modified until the computed and actual riprap parameters match.

#### 1. Computed Parameters

Several values will be needed in the design, and they should be computed before proceeding.

a)  $A_{n2}$  - This is the flow area in the contraction beneath the unstricted flood stage, and it may be planimetered from a cross-section of the bridge site, or it may be computed as the area of an equivalent trapezoid (Figure 2c) for spill-through abutments, or as an equivalent rectangle for vertical wall or wing-wall abutments. For skewed crossings, the area is computed as the area projected on a plane normal to the flow direction. For designs allowing scour, the expected scour area is included in  $A_{n2}$  and is checked in steps 5a through 5c. Steps 1 through 5c are repeated for scoured designs until estimated and computed values of scour agree.

b)  $\bar{h}_{n2}$  - This is the average depth in the constriction measured below the unstricted flood stage (Figure 2c).

c)  $Q_b$  - For wing-wall or vertical wall abutments,  $Q_b$  is the unstricted flow confined to the opening width,  $b$ , shown in Figure 2d. For spill-through abutments, the value of  $B = A_{n2}/\bar{h}_{n2}$  is used in determining  $Q_b$ . For skewed crossings,  $Q_b$  is determined from the average width of the opening projected on a normal to the flow direction (Figure 3h).

d)  $M$  - Compute the bridge opening ratio,  $M$ , as  $Q_b/Q$ , or as  $K_b/K$  if the conveyances of the sections for the unstricted flow are known.

e)  $A_n = A_{n1} = A_{n4}$  - All of these are the cross-sectional flow area in the unstricted channel flowing at the design discharge, and they may be planimeted from a survey of the channel cross-section.

f)  $V_n = V_{n1} = V_{n4}$  - All are the average velocity in the unstricted channel flowing at design discharge. The equation is

$$V_n = Q/A_n .$$

g)  $V_{n2}$  - This is the average velocity in the constriction, or

$$V_{n2} = Q/A_{n2} .$$

h)  $h_{2c}$  - This is the average critical depth in the constriction for the design discharge. For an equivalent rectangle

$$h_{2c} = \left( \frac{Q^2}{g b_r} \right)^{1/3} ,$$

where  $b_r$  is the width of the rectangle. For an equivalent triangle

$$h_{2c} = \left( \frac{2Q^2}{gm^2} \right)^{1/5} ,$$

where  $m$  is the triangle side-slope rise for a unit run. For an equivalent trapezoid

$$h_{2c} = \left[ \frac{Q^2}{g} \frac{\left( \frac{b_r}{h_{2c}} + 2m \right)}{\left( \frac{b_r}{h_{2c}} + m \right)^3} \right]^{1/5} ,$$

where  $b_r$  is the base width of the trapezoid. This last equation requires a trial and error solution, and a trial value of  $b_r/h_{2c} = 2$  usually produces convergence after a few iterations. Each iteration

is made by replacing  $h_{2c}$  in the right side of the equation with the value computed from the last iteration.

i)  $V_{2c}$  - This is the critical velocity in the constriction for design discharge, computed from

$$V_{2c} = Q/A_{2c} ,$$

where  $A_{2c}$  is the equivalent rectangular, triangular, or trapezoidal flow area below  $h_{2c}$ . Combinations of equivalent shapes may be treated by solving the equation  $Q^2 B = g A_c^3$ , where  $A_c$  is the flow area for critical conditions.

j)  $h_{1c} = h_{4c} = h_{nc}$  - All of these are the critical depth in the unstricted channel flowing at design discharge. The equations in step 2h may be used if equivalent channel shapes exist.

k)  $\alpha_{1n}$  = This is the unstricted velocity correction coefficient at the section of maximum backwater. If the discharge and average velocity in each of  $p$  subsections (flood plains and low flow channel) are known, then

$$\alpha_{1n} = \frac{\sum_{i=1}^p Q_i V_i^2}{Q V_{n1}^2} .$$

## 2. Backwater

a) Method - Select a suitable method for determining the backwater that will be produced by the crossing. Reference 14 is recommended for this step, and has been summarized in Appendix B.

b)  $h_1^*$  and  $\Delta h$  - Compute the backwater,  $h_1^*$ , and the total drop through the abutments,  $\Delta h$ , by the chosen method. The determination of



backwater should assume a non-scoured condition in the gap unless it is known that the flood gradually rises to its peak with sufficient time for gradual scour, or if the bed material in the gap is to be removed during construction. The flow classification in accordance with Figure 1 may be determined, after finding  $\Delta h$ , by computing

$h_3 = h_n + h_1^* - \Delta h + S_o L_{1-3}$ , where  $L_{1-3}$  is obtained from Figure B.13 in Appendix B.

c) Waves - If wind waves are anticipated during the design flood, estimate the wind velocity,  $V_w$ , fetch length and width,  $F$  and  $W_F$ , and compute the significant wave height from

$$H = \frac{V_w^2}{g} 3.23 \times 10^{-3} (g F_e / V_w^2)^{0.435},$$

where

$$F_e = 1.17 F^{1/3} W_F^{2/3}.$$

d) Freeboard - Verify that the proposed embankment height equals or exceeds the sum of normal stage at design discharge, backwater,  $h_1^*$ , and wave height,  $H$ . Allow a safety factor between 1 and 3 feet as desired. The Wyoming Highway Commission (82) suggests a height of protection extending three feet above the maximum backwater for spill-through abutments.

### 3. Design Velocity

a)  $\alpha_1$  - Compute or estimate a value of the velocity head correction coefficient at the point of maximum backwater. The value obtained for unconfined flow at design discharge (step 1k) may be used as an estimate. For flow in wide channels the coefficient is close

to unity. For the overbank case, the velocity variation significantly increases the coefficient.

If the distribution of flow between the flood plains and the low-flow channel can be determined, an estimate of  $\alpha_1$  may be obtained from

$$\alpha_1 = \frac{\sum_{i=1}^p Q_i V_i^2}{Q V_1^2} ,$$

where  $Q_i$  and  $V_i$  are the discharge and velocity in each subsection, and

$$V_1 = Q/A_1 ,$$

where  $A_1$  is defined as the area, including backwater, at the upstream section of maximum backwater.

c)  $V_d$  - Compute the design velocity

$$V_d = \sqrt{\alpha_1 V_1^2 + 2 g \Delta h} .$$

This value should be multiplied by a value of 1.2 to allow for turbulent fluctuations of the velocity and to provide a design bed velocity, or

$$(V_b)_{\text{design}} = 1.5(0.8 V_d) = 1.2 V_d .$$

#### 4. Toe Protection

a) Shear Ratio - If the abutments are constructed on a rigid bed, proceed to step 4h. For alluvial beds, the toe of the abutment will require protection from undermining, and the design velocity for the non-scour case should be used if the flood rapidly rises to its peak. For designs allowing scour of the bed material, the scour is first

estimated prior to step 1. The backwater and upstream depth (including backwater) are then computed for the scoured opening from steps 1a through 2b. Steps 4b, 4c, and Figure 14 provide computed values for the depth and extent of the scour caused by the flow. This procedure would need to be repeated until the estimated scour and computed scour had the same value at the beginning and end of the trial. A similar process would be required for scour at piers, utilizing steps 1 through 3a, 9a, and 9c.

Regardless of the form chosen for protection (riprap, sheet piles, etc.) an estimate of the equilibrium depth of scour is required. Using the bed material mean particle diameter,  $D_s$ , and the velocity,  $V_1$ , from step 3a provide values for the solution of

$$\frac{\tau_o'}{\tau_c} = \frac{V_1^2}{120 D_s^{2/3} h_1^{2/3}},$$

where  $h_1$  is the flow depth including backwater directly upstream of the abutment.

b) Effective Length of Approach Embankment - The effective length,  $L_e$ , of the approach embankment is the roadway approach length for vertical wall or wing-wall abutments. For spill-through abutments,

$$L_e = L + \frac{b' - b}{2}$$

where  $L$  is the roadway approach length,  $b'$  is the top-width between the abutments, and the value of  $b$  was found in step 1e.

c) Scour Depth - Compute the ratio,  $L_e/h_1$ , and obtain a value of  $d_{se}$  from Figure 13. This depth may be increased by half the

expected dune height for sediment transporting flow, or by a factor of safety for clear water scour. In either case, a minimum total of five feet is suggested (68).

d) Sheet Piles - If sheet piles are used to protect the abutment toe, they must be driven at least to the depth determined in step 4c, and must act as retaining walls after scour has removed the bed material. Additional driving depth may be needed to provide this support.

e) Riprap Depth - If riprap is to be buried along a slope for toe protection, it must extend at least to the depth determined in step 4c, and should be placed on a slope less than the submerged angle of repose of the riprap. Wyoming practice employs a depth to competent rock or three feet below the expected scour depth, whichever occurs first (82). Wire-enclosed riprap may be placed at any angle less than the angle of repose of the baskets. This angle can be approximated by the angle for riprap having the same size as the baskets.

f) Alluvial Bed Riprap - Horizontal aprons dumped at bed level are not recommended in cases where scour may occur, unless the whole bed between the abutments is to be protected.

If bed-level aprons are used, sufficient material should be dumped to allow the apron to fall into the scour hole as it develops. The length of protection extending from the toe should equal or exceed  $d_{se}/\sin\phi$ , where  $\phi$  is the submerged angle of repose of the riprap.

g) Riprap Thickness - Various investigators suggest values for the thickness of riprap protection that are equal to the maximum stone size (68), 1.5 to 2.0 times the maximum diameter (15), or 3.0 times the maximum diameter (30). If the gradation of the riprap can be maintained during placement, thicknesses from 1.5 to 2.0 times the maximum

diameter are recommended. Values between 2.0 and 3.0 are suggested when dumping or mishandling produces possible segregation of the particles. For horizontal aprons which are dumped at bed level and are expected to slough into the scour hole as it develops, the thickness determined above should be increased by a factor of 1.5.

h) Rigid-Bed Riprap - If the abutments are constructed on a rigid bed, or if the bed material cannot be excavated, the toe should be protected with a horizontal apron of riprap extending a minimum distance of 6 feet (68) from the abutment toe. The thickness of the layer may be determined as 1.5 times the value obtained from step 4g, with a minimum of 3 feet.

i) Riprap  $d_m$  - If riprap is to be used for toe protection, the  $d_m$  and  $d_{85}$  sizes can be determined from steps 5b through 5h. Any riprap having these two values should be stable from lift and drag forces as discussed in Chapter II. The design bed velocity,  $V_b$ , for the toe protection was determined in step 3b, and the value of  $D$  for step 5e may be taken as  $\bar{h}_{n2}$  for subcritical flow in the constriction, or  $h_{2c}$  (step 1h) for critical flow.

## 5. Riprap Sizing

a) General - This step is used to compute the  $d_m$  and  $d_{85}$  sizes mentioned in step 4i. The procedures in this section are also recalled in later steps to find  $d_m$  and  $d_{85}$  sizes for other zones requiring protection.

The following steps are based on the assumption that riprap is to be used for protection. If wire-enclosed riprap is to be used, the size and gradation computed in these steps will not be required. The requirements for wire-enclosed riprap are that the baskets are thick

enough and contain riprap particles of sufficient size to prevent pumping of the embankment material through the riprap voids. These considerations are only mentioned herein, and other reports (15, 77) are suggested for more thorough discussions.

Wire-enclosed rock protection is not recommended in designs where corrosion from alkali or abrasion from coarse-gravel bed loads may occur. Costs of hand placing the baskets should also be considered when end-dumping of riprap may prove more economical, especially for submerged zones requiring protection. A combination of dumped riprap at low points of abutments and smaller, wire-enclosed riprap at higher points may prove to be economical for these troublesome areas.

b) Trial  $d_m$  - Having selected a design bed velocity,  $V_b$ , and after applying the appropriate factor of safety, choose a trial value of  $d_m$  from available riprap or from the design curve in Figure 8, and select an angle of repose from Figure 9.

c) Stability Coefficient - Compute the value of the particle stability coefficient,  $\eta$ , from one of the following equations:

Beds:

$$\eta = \frac{1.146(\gamma_s - \gamma_f) \tan \phi}{V_b^2 (1 + 0.85 \tan \phi)}$$

Banks of straight reaches:

$$K_1 = K_2^{1/2}$$

Banks of spill-through abutments in the constriction:

$$K_1 = [K_2 + 1.74 V_b^2 \eta (\gamma_s - \gamma_f) \sin \alpha \sin \lambda_1]^{1/2},$$

where  $\tan \lambda_1 = 2h_A/W \sin \alpha$ , and  $h_A = h_n$ . Appendix C presents computational aids for solutions of  $\eta$ .

d) Particle Reynolds Number - Compute the riprap particle Reynolds number from the relationship

$$R_p = V_b d_m / \nu ,$$

and determine if the chosen riprap falls in the stable region of Figure 7. If instability is indicated, select a larger value for  $d_m$ , and repeat steps 5c and 5d. If the riprap falls well within the stable region of Figure 7, a smaller value for  $d_m$  may be selected, providing that the lift forces in the following steps are not too great.

e) Flow Reynolds Number - Compute the flow Reynolds number from

$$R = V_b D / \nu ,$$

where  $D$  is the predicted depth of flow at the bed of the zone being protected.

f)  $d_{85}$  Size - Compute the  $d_{75}$  size (in.) of the riprap from the relationship

$$d_{75}^{1/6} = 1.04 d_m^{0.178} ,$$

and plot the  $d_m$  and  $d_{75}$  sizes on semi-log paper which has riprap size as the logarithmic ordinate, and values from zero to one hundred on the rectangular abscissa. The  $d_{85}$  size may be estimated from a straight-line extrapolation of a line connecting the two plotted points, where the  $d_{50}$  size is approximated by the value of  $d_m$ .

g) Lift Force Factor  $1/\psi$  - Compute the lift force factor,  $1/\psi$ , from

$$\frac{1}{\psi} = \frac{v_b^2}{(S_s - 1) g d_{50}} \left( \frac{\rho_f}{\rho_s} \right) \left( \frac{d_{85}}{d_m} \right)^3 .$$

h) Lift Stability - Using the flow Reynolds number from step 5e and the lift force factor from step 5g, determine if the riprap is stable from lift forces from Figure 10. If instability is indicated, repeat steps 5c through 5h with a larger value of  $d_m$ . If extreme stability is indicated, the  $d_{85}$  size may be increased to provide a better riprap gradation.

#### 6. Abutment Spill-Slope Protection

a) Riprap  $d_m$  - The spill-slopes of spill-through abutments can be protected with riprap by using the design bed velocity from step 3b and the relationships for slopes of spill-through abutments in steps 5b through 5h. The value for  $D$  in step 5e should be the same as computed in step 4i, and the side slope angle,  $\alpha$ , should be less than the angle of repose of the riprap.

b) Riprap Thickness - The thickness of the nose protection on spill-through abutments is determined from step 4g. If desired, the thickness can be increased at the points of greatest scour potential.

c) Riprap Extent - The riprap size obtained in step 6a can be placed on all the slopes of the spill-through abutment or limited to the nose if a sufficient quantity of the riprap is not available for the sides. Steps 7 and 8 provide values for the smaller riprap sizes required on the side slopes.

Turbulent eddies from the wake of separation require placement of the large riprap around the downstream shoulder at least to the tangent with the embankment side slope (point G in Figure 5). Extreme



velocities and plunging flow produce the same requirement for the upstream shoulder (Point E in Figure 5).

One estimate of the distance requiring protection along the upstream side slope of spill-through embankments is obtained (82) from the rational equation

$$L = [1 - (V_n/V_2)] L^* ,$$

where

$L$  = the length (ft) requiring the protection, measured from the beginning of curvature on the upstream side slope of the spill-through abutment,

$V_n$  = the average flood velocity (fps) in the unconstricted channel (step 1f),

$V_2$  = the constricted flood velocity (fps), and

$L^*$  = the distance to the point of maximum backwater (ft) obtained in step 2b.

Another estimate for  $L$ , obtained from the research, is presented in step 8.

d) Filter Layer - Filter layers may not be required when the riprap is well-graded with a minimum size equal to the size of the embankment material, or when the riprap is dumped, causing the smaller material to settle against the slope. When filters are required, filter cloth, graded gravel, or some other suitable material may be used. The recommended Terzaghi-Vicksburg (T-V) specifications (60) for graded-gravel riprap are

$$\frac{d_{15}(\text{Filter})}{d_{85}(\text{Base})} < 5 ,$$

and

$$4 < \frac{d_{15}(\text{Filter})}{d_{15}(\text{Base})} < 20 ,$$

and

$$\frac{d_{50}(\text{Filter})}{d_{50}(\text{Base})} < 25 .$$

The thickness of the filter layer may be determined from step 4g.

#### 7. Downstream Side Slope Protection

a)  $d_m$  - If the riprap size determined in step 6a is not plentiful, a smaller size may be used on the side slopes of the embankments. The riprap must be of sufficient size to withstand expected wave forces, and the weight of the  $d_m$  size is estimated from

$$W_s = \frac{\gamma_s H^3}{3.2(S_s - 1)^3 \cot \alpha} ,$$

where

$W_s$  = weight of stone (lb) required for stability,

$H$  = wave height (ft) from step 2c,

$S_s$  = specific gravity of the riprap, and

$\alpha$  = side slope angle with the horizontal.

b) Turbulent Waves - If wind-generated waves are not anticipated, the waves from the turbulent mixing downstream of the crossing will determine the required size of riprap if an estimate of the wave height is available.

c) Extent - The riprap on the downstream slope should be placed to a height equal to the anticipated downstream depth plus the wave height. Downstream depths are generally less than normal stage, and the use of  $h_n$  would provide a conservative estimate. Figure 14, and the value of  $d_{se}$  from step 4e, will produce an estimate of the length along the abutment toe requiring buried protection.

d) Filter Layer - The filter layer for the downstream embankment slope may be determined from step 6d.

## 8. Upstream Side Slope Protection

a) General - Upstream side slopes of embankments may be protected with riprap designed for wave and drag forces. The size computed in step 7a should be considered a minimum size, and the stability from drag and lift forces may be checked as follows:

b) Velocities - For skewed crossings, expected velocities are obtained from Figure 4 and should be increased by 50 to 100 percent for design. For normal crossings, the experimental curves of Figure 35 are suggested for values of  $x/L$  greater than the value at the intersection of the experimental and theoretical curves. The experimental curves indicate that the parameter  $VM'/V_n$  becomes zero at a value of  $x/L$  close to 0.3. Stagnation (defined by  $V = 0.0$ ) did occur at this point for the model embankments, but other investigators (10, 36) report that stagnation in prototype crossings occurs at a value of  $x = 0.0$ . For this reason, the theoretical values should be used for values of  $x/L$  less than the intersection value. These curves produce stagnation at a value of  $x/L = 0.0$ .

c) Riprap  $d_m$  - After obtaining design velocities along the upstream slope, the required riprap size and gradation at any point are

found from steps 5b through 5h. The riprap size determined for waves in step 7a must be used if the size required for drag stability is smaller.

A riprap size that is stable at any point along the upstream slope could be placed along the slope to the point where  $x = 0$ . One required size may be determined at a single point (e.g.,  $x/L = 0.8$ ), and this size may be placed from that point to the point defined by  $x = 0.0$ . If desired, a third riprap size could be placed from some other point (e.g.,  $x/L = 0.4$ ) to the point defined by  $x = 0.0$ . This procedure would result in a small riprap size from  $x = 0.0$  to  $x/L = 0.4$ , a larger size from  $x/L = 0.4$  to  $x/L = 0.8$ , and the largest size (step 6a) from  $x/L = 0.8$  around to the downstream slope of the embankment.

If different sizes of riprap are to be used along the upstream slope, each must be larger than the size required for anticipated wave action, and the large riprap from step 6a should always extend at least to the beginning of curvature (point E in Figure 5), or to the distance  $L$  from step 6c.

If wave action is not anticipated on the upstream embankment side slope, the riprap placement can be terminated at a point where the actual velocity equals the critical erosive velocity for the embankment core material. This point is defined by the distance,  $x$ , from Figure 35 at which the velocity,  $V$ , is equal to the velocity which causes movement of the embankment material. To obtain this value of  $x$ , the critical design velocity for movement of the embankment core material is found and substituted for  $V$  in Figure 35. The critical velocity can be found by selecting a trial value for  $V_b$  and by using the known  $d_m$  size and angle of repose of the embankment core material

to obtain values of the stability coefficient,  $\eta$ , and the particle Reynolds number,  $R_p$ . If these parameters plot as a point in the stable region of Figure 7, then the critical bed velocity,  $V_b$ , is accepted or can be increased to shift the point closer to the design curve. If instability is indicated, the trial velocity is too large and must be decreased. An initial trial velocity can be obtained from the design curve of Figure 8.

After obtaining a bed velocity with values of  $\eta$  and  $R_p$  which plot near the design curve in Figure 7, the bed velocity should be increased to a depth-averaged velocity by dividing by 0.8. Turbulent fluctuations and safety require a reduction of the design velocity obtained by dividing by 1.5. This process results in the maximum safe velocity,  $V$ , for use in Figure 35. Riprap placement can be terminated at the resulting value of  $x$  because the embankment core material will safely withstand the smaller velocities between this point and the point at which  $x = 0.0$ .

This result of the research indicates a considerable saving in the initial cost of protection for a structure which would previously be protected to a value of  $L$  (step 6c) greater than determined by this new method.

d) Toe Protection - The toe along the upstream slopes of embankments is vulnerable to scour, especially in cases of embankments which are skewed downstream (Figure 14).

During the construction of an embankment, the flood plain along the upstream slope is sometimes cleared to facilitate equipment. This practice leaves a low-resistance channel along the embankment toe, creating greater scour hazards from increased velocities. If this

condition cannot be avoided, the toe of the embankment should be protected with buried riprap.

e) Riprap Size and Extent - The riprap size determined in step 8c should be placed to the height determined in step 2d. Buried riprap is to begin at a point determined from Figure 14, using the value of  $d_{se}$  determined in step 5c. The depth of buried riprap should vary from the bed level at this point to the depth,  $d_{se}$ , at the point of maximum scour.

f) Filter Layer - The particle size and thickness of the filter layer for the upstream slopes are determined from step 6d.

g) Spur Dikes - If spur dikes are used to reduce scour at the abutment, the dikes should be protected as if they were abutments. References 14, 27, and 37 present discussions of the need for spur dikes and the optimum size and shape required. Reference 2 provides an estimate of the anticipated scour at spur dikes, and the extent of riprap protection is discussed in reference 38.

## 9. Pier Protection

a) Scour Depth - For piers at relief bridges or on the flood plains, compute the clear-water scour depth from the relationship

$$d_{se} = 0.00073 \bar{R}^{0.619},$$

where

$$\bar{R} = \frac{2aV_1}{v}.$$

The mean velocity of the undisturbed flow,  $V_1$ , was found in step 3a, and the radius or half-width of the pier is known from structural requirements.

For piers at locations which are exposed to sediment transporting flow, compute the scour depth from the equation

$$d_{se}^* = 1.42 K b_p^{0.75} .$$

Values of 1.0 for cylindrical piers and 1.4 for rectangular piers may be substituted for  $K$ . Half the expected dune height should be added to  $d_{se}^*$  for design.

b) Pier Alignment - Minimum scour occurs for piers which are aligned with the flow direction. Cylindrical piers eliminate alignment problems, but structural requirements frequently call for "Hammer Head" piers or pier bents composed of multiple columns or piles. If the piers are not aligned with the flow direction, the depth of scour obtained in step 9a should be multiplied by the value of  $K_{\alpha 1}$  obtained from Figure 15.

c) Extent of Protection - If piers are not founded on competent rock or below the possible scour depth, the footings may be lost during a flood. Footings or piles which are designed from soil strength and structural considerations should be placed at or below the expected scour depth. Buried riprap protection could be placed around the piers, and an estimate of the extent of the riprap may be obtained from step 4f.

#### 10. Protection of Special Cases

a) Flood Plains - If the flood plains between the abutments at a setback crossing (Figure 3e) are to be maintained for livestock passage beneath the superstructure, protection may be placed at bed level on the flood plains and on the low-flow channel side slopes. Livestock are reluctant to cross loose riprap, and a soil cover or concrete or

grouted riprap path may be required. It may be more economical to bury the horizontal layer of riprap beneath a foot or more of earth, and replace the soil cover after each flood. The size of the riprap is determined from step 4i for flood plains and from steps 5b through 5h for the low-flow channel sides. The thickness of the riprap layer is determined from step 4g.

The horizontal extent of flood plain protection will be determined by the degree of setback and other factors. Figure B.13 in Appendix B could be used as an estimate of the upstream distance requiring protection. The dashed line encloses the region of flow acceleration, and velocities are small at other upstream points.

Downstream protection is difficult to evaluate. If the protection is placed for a short distance downstream and then terminated, the extreme roughness difference between the protected zone and the unprotected zone may produce vertical scour at the terminus of the protection. Undermining could eventually cause the loss of the livestock plains. Smooth transitions between the riprap and the flood plain material, or buried riprap or sheet piles might be used to alleviate this problem.

b) Eccentric Crossings - Backwater and protection for eccentric bridge crossings (Figure 3d) may be determined by treating each abutment as half of an equivalent non-eccentric crossing. The equivalent crossing would consist of each abutment and its mirror image reflected from the center of the flow distribution.

An estimate of the backwater for eccentric crossings may also be obtained by applying an empirically determined correction coefficient to the backwater for non-eccentric crossings. This procedure is presented in Appendix B.



## Chapter IV

## LABORATORY VERIFICATION OF DESIGN PROCEDURE

Laboratory investigations of the validity of the design procedures developed in Chapter II and presented in Chapter III were conducted in the engineering research facility at Colorado State University. The research included studies of spill-through bridge abutments protected with riprapped spill-slopes and side-slopes. The design of the riprap was tested for all the model abutments, and velocity and depth data were collected for several of the abutments.

The facilities, test program, data reduction, data analysis and the verification of design are presented in this chapter.

Facilities

Two laboratory flumes were used for the tests of spill-through abutment models with riprap-protected slopes. Smaller models were tested in the 6-foot wide by 64-foot long horizontal recirculating flume, and larger models were constructed in the 20-foot wide by 180-foot long outdoor flume. The flumes were capable of discharges of 10 and 100 cfs, respectively, and the outdoor flume was equipped with a 30-foot long recessed section which was filled with 5 feet of river sand having a medium fall diameter of 0.47 mm. Models constructed on the sand bed in the outdoor flume were used to investigate the bed scour characteristics and abutment riprap stability of bridge crossings constructed on alluvial beds. Most of the models were constructed on rigid beds because of the assumption that flood waves rapidly rise to a crest with little or no time for bed scour.

### Models

Table 1, with reference to Figure 16, describes the models tested in the two flumes. The models were constructed with a core of river sand protected by rock riprap having a thickness,  $t$ , equal to twice the maximum stone size. The first three models were constructed on a sand bed, and all the rest were built on plywood or broken-concrete beds.

Wide channel (W.C.) models were constructed in both rectangular flumes, with skewed and normal spill-through abutments constructed on sand and plywood beds.

By assuming that the flow through a normal bridge crossing is symmetrical about the flow centerline, only half the channel and one abutment would need to be studied. This assumption is not valid for skewed or eccentric crossings which are not symmetrical with respect to the flow centerline. Symmetry was assumed for all the tests in the 6-foot wide flume, and the model abutments were constructed from one flume wall only. This assumption places the flow centerline along one wall and produces an effective width of 12 feet for the 6-foot wide flume. Three of the tests in the outdoor flume assumed flow symmetry, and the other four tests employed abutments from both walls of the flume, reducing the widths in Table 1 to 20 feet.

All the overbank (O.B.) models were constructed perpendicular to the flow direction. The small values of width-to-depth ratios that would be produced by two abutments prevented the construction of skewed abutment models from both walls of the 6-foot wide flume.

The low-flow channel and flood plain shown in Figure 16b were constructed of plywood, and the flood plain was raised 0.25 feet above

Table 1. Summary of Model Geometry Values for  
Spill-through Abutments (see Figure 16)





































Model No.	Channel Type	B (ft)	h (ft)	W (ft)	L (ft)	r (ft)	$\alpha$	$\theta$ deg	$d_m$ (in)	$d_{50}$ (in)	t (in)		
1	W.C.	20	1.5	1.0	4.25	3.0	2:1	90	2.50	-	2.50		
2		20	1.5	1.0	4.25	3.0		90	1.25	1.20	3.00		
3		40 <sup>a</sup>	3.2	2.0	8.68	6.4		90	1.25	1.20	3.00		
4		40 <sup>a</sup>	3.2	2.0	8.68	6.4		90	1.25	1.20	3.00		
5		40 <sup>a</sup>	3.0	2.0	10.1	6.0		120	1.25	1.20	3.00		
6		20	2.0	1.0	6.40	4.0		60	.405	.311	2.00		
6A	W.C.	20	2.0	1.0	6.40	4.0	2:1	120	.405	.311	2.00		
1 <sup>b</sup>	O.B.	12 <sup>a</sup>	1.0	1.0	1.50	2.0	2:1	90	.238	.230	1.00		
2 <sup>b</sup>					1.50								
3 <sup>b</sup>					2.25								
4 <sup>b</sup>													
5 <sup>d</sup>													
6												1.0	1.0
7			0.5	0.5	3.25	1.0		0.75					
7A						1							
8													
9						0.5						0.5	3.25
10			1.0	1.5	2.50	2.0		.519	.517	1.25			
11						2.50							
12						2.50							
13						2.75							
14												.519	.517
15												.238	.230
16	.238	.230											
17	3.00	.519				.517							
18		.519				.517							
19		.553 <sup>r</sup>				.548							
19A		.553 <sup>r</sup>				.548							
20		.553 <sup>r</sup>	.548	1.25									
21									.705	.698	2.00		

Table 1. Summary of Model Geometry Values for Spill-through Abutments (see Figure 16) (Continued)

Model No.	Channel Type	B (ft)	h (ft)	W (ft)	L (ft)	r (ft)	$\alpha$	$\theta$ deg	$d_m$ (in)	$d_{50}$ (in)	t (in)
22					3.00				.705	.698	2.00
23					2.00				.519	.517	1.25
24											
24A											
25					2.00				.519	.517	1.25
26					0.00				.238	.230	0.75
26A											
27											
28											
29 <sup>d</sup>	O.B.	12 <sup>a</sup>	1.0	1.5	0.00	2.0	2:1	90	.238	.230	0.75
1	W.C.	12 <sup>a</sup>	1.0	1.0	1.5	2.0	2:1	90	2.50	-	c
2									0.75	.705	c
3									0.19	.180	c
3A											c
4 <sup>b</sup>											0.75
4A <sup>b</sup>											
4B <sup>b</sup>											
4C <sup>b</sup>									0.19	.180	0.75
5 <sup>b</sup>	W.C.	12 <sup>a</sup>	1.0	1.0	1.5	2.0	2:1	90	0.75	.705	2.00

<sup>a</sup>These models were constructed from one wall only, doubling the effective flume width by assuming symmetry.

<sup>b</sup>These models were constructed with a roughened plate beneath the models.

<sup>c</sup>The riprap extended to the flume floor with no sand core.

<sup>d</sup>The flood plain and low flow channel sides for models 5 through 29 were coated with the  $d_{50} = 0.230$  inch riprap.

<sup>r</sup>The riprap was extremely rounded.

the bed of the low-flow channel. The assumed symmetry of flow produces a low-flow channel 2.0 feet wide from bank to bank.

Side slopes in the low-flow channel and on the abutments were 2H:1V, producing an angle,  $\alpha$ , of  $26^{\circ} 34'$ .

Lengths of the overbank models were varied to investigate the effects of setback shown in Figure 3e. The case in Figure 3f was produced in Models 17 through 22.

Widths of embankments in the direction of flow were also varied to investigate the effect of this variable on the flow field and stability of the embankment material.

Mean riprap sizes for the model spill-through abutments ranged from 0.19 to 2.50 inches in diameter. Sieve analyses of samples of each class were taken to obtain the  $d_m$  values.

#### Testing Procedure

In order to evaluate the validity of the design procedures in Chapter III, all the model embankments in Table 1 were tested to failure.

Incremental increases in the discharge were applied until the beginning of visual losses of embankment material. After determining if the losses were continuous or intermittent, the discharge was again increased by small increments until continual failure of the embankment material occurred.

Testing to failure was accomplished in the outdoor flume with repeated increases of the discharge. The upstream water surface and velocity distribution were smoothed with a series of floating baffles and hardware-cloth screens, and the discharge was measured with a rectangular 24 by 36 inch orifice in the supply line. The orifice was calibrated in January, 1969.

Testing to failure in the 6-foot wide flume was accomplished with control of the depth downstream of the model. The discharge was increased to a point close to failure conditions, and the tailwater was adjusted to a pre-determined value by the addition or release of water in the recirculating flume. This process allowed measurements of velocity and depth data for different values of tailwater with all other variables being held constant. Additional increments of discharge were then applied until failure occurred. The depths upstream and downstream of the model were recorded for each increment of discharge, providing a record of the depth field during failure conditions. An 11 by 14 inch orifice in the supply line for this flume was used for discharge measurements. The orifice was calibrated in May, 1969.

Depths in the 6-foot wide flume for the overbank tests were controlled in order to approximate prototype design floods with a return period between 50 and 100 years. Flood plain depths of flow equal to approximately twice the depth above the low-flow channel bed were observed from available prototype crossings, and this ratio was applied in the tests.

#### Velocity Data

In order to describe and evaluate the flow properties in the vicinity of spill-through bridge abutments, velocity and depth data were taken at constant discharge for several of the models listed in Table 1. The discharge used for data collection was slightly less than the failure discharge for each model.

Vertical distributions of velocity were recorded at various points in the flow field with a Prandtl pitot tube. The pressure differences from the static and stagnation holes in the pitot tube were converted to velocity values using a pitot calibration obtained earlier in the

investigation. A differential pressure transducer and strip-chart recorder provided time-averaged values of the velocity at each depth of the vertical profile. Depth-integrated averages at each vertical provided a mean velocity through the depth.

Average velocities through the depth were obtained for points upstream and downstream of the constrictions, and for points directly in the flow area between the abutments. Figures 17 and 18 are typical drawings of the velocity measurements taken, and similar data plots for the other models are available on request.

#### Depth Data

Depth data were taken in both flumes at various points of a square grid superimposed on the flow field. For the outdoor flume, a two by two foot grid was used with smaller subdivisions in the region of rapidly changing depth. A one by one foot grid was used for the 6-foot wide flume with the overbank models.

Traversing point gauges with a measuring accuracy of 0.001 ft were referenced to the mean flume bed at each point in the grid and were used for flow depth and bed scour measurements.

Water surface contour maps were drawn from the depth measurements to provide a visual interpretation of the flow. Figures 19 and 20 are typical drawings of the patterns noted.

Characteristics common to all the model embankments included the steep water surface gradients at the nose, the standing surface waves in the contraction, the flow separation at the abutment, and contracting jet downstream, and the turbulent wake and stagnation zones bordering the expanding jet.

### Photographic Data

To provide a visual record of the model abutment failures, still photographs of the flow and scoured abutments were taken at different discharge values during the failure of each abutment. These photographs were later used for qualitative interpretation of critical scour zones and extent of scour at various discharge values.

Figures 21 through 28 depict a typical sequence of photographs taken during the failure of one of the wide-channel models listed in Table 1. The first photograph is a view looking downstream in the 20-foot wide flume showing the headbox, instrument carriage, and the series of floating baffles. Figures 22 and 23 illustrate the water surface characteristics at a discharge of 11.1 cfs. Some scour and deposition of the left abutment material due to the discharge of 11.1 cfs can be seen in Figure 24. Figure 25 reveals the failed form after passing a discharge of 12.7 cfs. The scoured material was for the most part deposited on the abutment slope in the separation wake.

Scour on the right abutment in Figure 24 was minor at the discharge of 12.7 cfs. In order to facilitate failure of this abutment, the downstream abutment was protected with a larger riprap size. Figures 26 through 28 reveal the scour stages for the upstream abutment after the downstream abutment had been armored.

Figures 29 through 34 illustrate a typical series of photographs taken during the testing of an overbank model. In this case the abutment was set back from the bank of the low-flow channel shown on the right in Figure 30. Scour of the riprap material was occurring when both Figures 31 and 32 were taken.



### Data Analysis

The objective of the experimental program was the verification of the proposed design procedures for model embankments. Due to the limited number of tests for which velocity and depth data were collected, experimental relationships among the many possible variables could not be derived. Future research and additional analyses of the data from this research are necessary to provide these relationships.

Sufficient velocity and depth data at discharges less than the failure discharge were collected for comparison with the theoretical design velocity,  $V_d$ , given in the last chapter, and with the theoretical backwater,  $h_1^*$ , and water surface drop,  $\Delta h$ , computed from reference 14. Verification of the riprap design was based on the assumption that the theoretical design velocities and backwater were correct at failure conditions.

### Backwater and Design Velocities

The backwater,  $h_1^*$ , and the total water surface drop,  $\Delta h$ , through the constriction were computed using the methods in Chapter III for each of the models for which velocity and depth data were taken. Comparisons of measured values with theoretical values are shown in Table 2. Verification of the methods in reference 14 are presented therein, and Table 2 is intended only as a comparison of measured and theoretical values. Verification of the stable design of riprap is presented in the next section.

The velocity,  $V_d$ , listed in Table 2 was computed from the theoretical value of  $\Delta h$  and the equation

$$V_d = \sqrt{2g\Delta h + \alpha_1 V_1^2} \quad .$$

Table 2. Comparison of Measured and Theoretical Velocities and Backwater for Spill-through Abutments

Model No.	Chnl Type	Maximum <sup>a</sup> Recorded Velocity (fps)	Theory V <sub>d</sub> (fps)	Max h <sub>1</sub> minus Min h <sub>3</sub> (ft) <sup>3</sup>	Theory Δh (ft)	$\frac{\Delta h_m - \Delta h_t}{\Delta h_m}$ (%)	$\frac{V_{Toe}^d}{V_d} = \frac{Q_b^M}{Q}$ (%)	
1	W.C.	2.05 <sup>b</sup>	3.01	.128	.133	-3.9	65.7	.359
2	↓	2.57 <sup>b</sup>	3.10	.145	.141	2.8	82.9	.361
3		3.80 <sup>b</sup>	4.75	.228	.335	-46.9	80.0	.339
4		4.73 <sup>b</sup>	6.57	.430	.656	-52.6	69.7	.331
5		5.08	4.98	.468	.366	21.8	60.8	.396
6		W.C.	3.44 <sup>b</sup>	4.20	.201	.271	-34.8	81.9
1	O.B.	2.44	2.74	.099	.102	-3.0	89.0	.559
2	↓	2.80 <sup>b</sup>	3.42	.143	.167	-16.8	79.5	.574
3		2.51 <sup>b</sup>	3.14	.120	.146	-21.7	74.5	.455
4		3.11	3.74	.188	.209	-11.2	71.9	.480
5		2.45 <sup>b</sup>	3.47	.131	.176	-34.4	65.7	.525
6		3.13	3.80	.207	.212	-2.4	65.8	.547
7		2.53 <sup>b</sup>	3.18	.129	.146	-13.2	79.6	.574
11		4.06	4.16	.296	.258	12.8	62.2	.475
14		4.58	4.41	.347	.293	15.6	69.8	.427
19		4.04	4.50	.303	.308	-1.7	72.2	.406
24		4.37	4.34	.317	.274	14.6	72.1	.537
29	O.B.	3.50	3.73	.192	.138	28.1	86.9	.813

<sup>a</sup>Averaged through the depth.

<sup>b</sup>These velocities are the values at the model centerline or in the expanding jet -- vena contracta velocities were not recorded.

<sup>c</sup>The maximum depth excludes the stagnation depth.

<sup>d</sup>The average velocity through the depth at the toe along the abutment centerline.

Most of the velocity data were taken in the vicinity of the embankment side slopes and abutment nose near the riprap surfaces. As a result, the maximum velocities in the vena contracta were not recorded for all the models. However, the agreement between the measured and theoretical design velocities for the cases where vena contracta velocities were measured suggests that the theoretical values of  $V_d$  closely approximate the maximum values in the flow field.

Ratios of the toe velocity at the abutment centerline to the design velocity are tabulated in Table 2, indicating that values approximating the maximum velocity may occur within the constriction. The suggested use of  $V_d$  for design of the toe and abutment protection was based on this laboratory observation.

Values of velocity greater than the values at the centerline toe were recorded upstream of the model centerline at the point of maximum curvature of the toe. Studies by other investigators (53, 54) revealed the greatest scour at this point in the flow, and these observations indicate that the greatest amount of toe protection is required for this region.

Computed and measured values of  $\Delta h$  deviate significantly for some of the models listed in Table 2. Depth measurements for the wide channel flow models 3, 4, and 6 were not taken far enough upstream to include the point of maximum backwater. The water surface contours for these models indicated an increasing water surface elevation at the farthest upstream point for which data were taken. The measured values of  $\Delta h$  for the models are therefore less than the actual drop.

Model 5 was skewed from one wall of the flume only, thereby violating the assumption of symmetry for one-sided models. The

theoretical water surface drop was derived using the assumption of symmetry, and this may account for the difference indicated in Table 2.

Maximum backwater was measured for the overbank flow cases listed in Table 2, and comparisons with theoretical values of  $\Delta h$  are tabulated. Deviations greater than 20 percent were found for three of the models, and the discrepancies may be attributed to the use in horizontal flumes of theoretical values derived from sloping flumes and river channels. Normal stage does not exist in horizontal flumes, and recommendations found in the literature suggest that the average depth in the upstream portion of the constriction may be used for  $h_n$  in backwater computations. The average depth above the low-flow channel across the channel from point A in Figure 5 was substituted for  $h_n$  in computing the theoretical backwater and water surface drop for the models listed in Table 2.

#### Upstream Velocities

Values of depth-averaged velocities were recorded at several points along the upstream slopes of the embankments for all the models listed in Table 2. Figure 35 illustrates a comparison of the measured and theoretical upstream velocities. The solid lines are based on data from the models listed in Table 2, and the dashed lines are reproductions of Fields' curves from Figure 4. Insufficient data were taken for the skewed models, and the curves in Figure 35 apply only to normal crossings. Eccentric crossings (Figure 3d) may be treated as two non-eccentric abutments by assuming symmetry for each side with respect to the flow centerline.

For values of  $M$  greater than 0.20, the solid experimental curves in Figure 35 predict larger values of upstream velocities than do the

theoretical curves. Stagnation, or zero velocity, occurred for all the model embankments at a value of  $x/L$  approximately equal to 0.5. Stagnation for prototype crossings does not occur, and the solid curves are not extended to the abscissa for this reason. Any design based on Figure 35 should utilize the empirical curve for large values of  $x/L$  and the theoretical curve for smaller values.

#### Riprap Stability

Stability of riprap on the spill-slopes of spill-through abutments was investigated for both overbank and wide channel flow conditions. Stability in other regions of the flow was not investigated due to the occurrence of greatest instability on sloping surfaces. Riprap that is stable on sloping surfaces should also be stable on channel beds in the vicinity of the slopes.

Table 3 lists the measured failure discharge and computed parameters for all the model abutments that were tested to failure. The listed failure discharges represent the values at which riprap particles were being lifted from the slope and washed downstream. These values all fell between the points of initial loose-gravel movement and continual losses.

Abutment riprap for models 1, 2, and 3 in the 20-foot outdoor flume (Table 1), and for model 1 in the 6-foot wide flume with wide channel flow could not be failed due to oversized riprap or from riprap sloughing into the scour hole downstream of the models. Abutment spill-slope riprap failure from drag and lift forces occurred for all the models listed in Table 3.

Initial riprap losses for the model abutments usually occurred on the upstream abutment shoulder whenever the flow depth was great enough

Table 3. Computed Values at Failure Conditions for  
Model Spill-through Abutment Riprap.

Model No.	Chnl Type	Failure $Q_f$	Stab Coef $\eta$	Lift Force $1/\psi$	$\Delta h$ @ $Q_f$	$V_d$ @ $Q_f$	$R_{PV} (10^4)$ $\frac{V_d^3}{v} =$	$R (10^5)$ $\frac{V_d^3 h_A}{v} =$	M $\frac{Q_b}{Q}$
4	W.C.	85.6	0.82	5.68	.618	6.39	5.33	8.38	.341
5	↓	96.8	1.26	3.70	.392	5.17	4.30	7.31	.408
6		15.2	1.08	20.00	.407	5.14	1.11	4.61	.221
6A	W.C.	10.3	1.62	13.33	.271	4.20	.91	3.35	.207
1	O.B.	7.40	3.04	6.37	.128	3.06	.49	1.23	.561
2	↓	4.30	3.03	7.09	.147	3.23	.52	.71	.564
3		3.50	2.57	8.33	.182	3.50	.56	.79	.453
4		2.64	2.66	9.09	.199	3.65	.58	.54	.500
5		3.14	2.50	8.62	.184	3.55	.57	.79	.526
6		3.32	1.77	12.66	.274	4.29	.69	.83	.542
7		1.88	2.89	7.09	.151	3.23	.52	.44	.593
7A		2.20	2.64	7.58	.162	3.33	.53	.53	.568
8		2.08	1.92	10.87	.236	3.99	.64	.51	.607
9		2.64	3.17	6.06	.128	2.98	.48	.67	.526
10		4.50	1.99	4.31	.263	4.20	1.51	1.28	.467
11		5.06	1.52	5.68	.351	4.83	1.73	1.44	.468
12		4.90	1.50	5.81	.358	4.88	1.75	1.39	.471
13		4.60	1.77	4.72	.292	4.40	1.58	1.48	.423
14		4.66	1.44	5.99	.372	4.95	1.78	1.50	.429
15		2.66	2.06	12.35	.273	4.25	.68	.82	.478
16		2.82	1.75	14.71	.326	4.64	.74	.87	.483
17		3.60	1.52	5.81	.364	4.89	1.75	1.33	.397
18		3.42	1.50	6.02	.378	4.97	1.79	1.25	.405
19		3.40	1.45	5.13	.350	4.79	1.82	1.25	.401
19A		3.54	1.46	5.02	.343	4.74	1.80	1.30	.396
20		3.72	1.26	5.85	.400	5.11	1.95	1.37	.398
21		4.48	1.57	3.56	.336	4.70	2.28	1.66	.377
22		6.16	1.11	4.90	.464	5.52	2.67	2.26	.371
23		5.88	1.68	5.16	.309	4.59	1.65	1.35	.539
24		6.42	1.79	4.67	.279	4.38	1.57	1.47	.534

Table 3. Computed Values at Failure Conditions for Model  
Spill-through Abutment Riprap (Continued)

Model No.	Chnl Type	Failure $Q_f$	Stab Coef $\eta$	Lift Force $1/\psi$	$\Delta h$ @ $Q_f$	$V_d$ @ $Q_f =$	$R_p (10^4)$ $\frac{V_d V_{d,m}}{v} =$	$R (10^5)$ $\frac{V_d^h A}{v} =$	M $\frac{Q_b}{Q}$
24A	↓	5.80	1.75	4.95	.297	4.51	1.62	1.33	.539
25		5.80	1.67	5.21	.312	4.62	1.66	1.34	.540
26		5.52	2.76	9.01	.147	3.63	.58	.74	.805
26A		6.54	2.62	9.01	.144	3.65	.58	.86	.804
27		7.44	2.53	9.09	.141	3.64	.58	.97	.804
28		7.78	3.03	7.30	.106	3.27	.52	.98	.805
29		O.B.	2.11	4.00	.174	4.05	1.46	1.32	.808
2		W.C.	3.36	2.36	.124	3.06	1.50	1.98	.587
3		6.80	3.55	7.25	.104	2.74	.34	1.25	.535
3A		5.00	5.89	4.39	.062	2.14	.27	.93	.531
4	↓	5.80	4.56	5.65	.081	2.43	.30	1.07	.533
4A		6.20	4.10	6.29	.090	2.56	.32	1.14	.534
4B		6.00	4.31	5.99	.085	2.49	.31	1.11	.533
4C		6.20	4.10	6.29	.090	2.56	.32	1.14	.534
5		W.C.	3.55	2.23	.115	2.98	1.46	2.08	.601

to approach the roadway elevation and produce a small radius of curvature of the flow around the shoulder. However, when the radius became larger due to shallow upstream and downstream depths relative to the embankment height, initial riprap losses occurred slightly downstream of the embankment centerline near the toe of the spill-slope. Insufficient data were obtained to accurately define the parameters that determine which mode of failure will occur. The radius of curvature, the water surface drop through the abutments, the length of the embankment in the flow direction, and other variables require further research to accurately define this phenomenon.

The total water surface drop,  $\Delta h$ , through the constriction was computed for each model in Table 3 using the methods presented in reference 14 and Appendix B. Normal depth,  $h_A$ , was defined as the average stage across the channel at point A in Figure 5, and the failure discharges in Table 3 were substituted for design discharges in the computations of  $\Delta h$  for each model.

Figure 36 is a reproduction of a portion of Figure 7, showing that instability was indicated for each of the tests at failure conditions. The particle Reynolds numbers were based on a value of  $V_d$  obtained from

$$V_d = \sqrt{2g\Delta h + \alpha_1 V_1^2} \quad ,$$

and the stability coefficient was computed from the relationship for stability on abutment spill-slopes. Values of angle of repose for the various sizes and shapes of riprap were obtained from Figure 9.

Two of the wide channel tests in the 6-foot wide flume produced parameters which plotted in the stable region of Figure 36. Only a few



riprap particles for both models had moved at the stated discharges, and failure conditions were probably not indicated by the discharges of 12 and 13 cfs, respectively, for models 2 and 5. The suggested design safety-factor produced by the use of  $1.5 V_d$  would shift both points into the unstable region, and a design would require a larger riprap size for the same flow conditions.

Figure 37 is a reproduction of Figure 10 revealing that the spill-slope riprap for the model abutments qualified as stable, relative to the lift turbulence generated by the  $d_{85}$  size. Stability in this figure does not imply stability in Figure 36, and a design riprap must have parameters which fall in the stable regions of both figures.

The small values of lift force factor in Figure 37 arise from the uniform size distribution of the model abutment riprap. The lift force factor  $1/\psi$  is proportional to the cube of the ratio  $d_{85}/d_m$ , and uniform gravels have small values for this ratio.

Uniform size distributions are not recommended in prototype designs. A design resulting in stable indications from Figure 7 and 10 will be adequate, but if the design point falls well below the curve in Figure 10, riprap uniformity is indicated, and the required  $d_{85}$  size should be increased to provide a more graded riprap. Increasing the  $d_{85}$  size to a point which falls in the unstable region of Figure 10 means that the  $d_m$  and smaller sizes are no longer safe from lift forces.

### Summary

Verification of the design of riprap for the sloping tips of spill-through abutments was accomplished by a "reverse" design consisting of measured failure conditions and theoretical indications of instability.

The validity of this method is based on the theoretical indication of instability when instability did in fact occur. Another way to verify the design method would be to compute theoretically stable riprap sizes for the given flow and geometric conditions. Tests could then be conducted to determine if the designed riprap was in fact stable at the design discharge.

As stated earlier, effects of each possible variable for bridge crossings were not evaluated. The design procedure includes most of the variables in some form, and the parameters which were varied in the experimental program appeared to incorporate satisfactorily into the design procedure. Various values of set back, riprap angularity, flow depth, channel type, riprap size, abutment width, skewness, and bed scour conditions all entered the computations for stability, resulting in the points plotted in Figure 36.

Prototype construction based on the design methods will provide the final verification of the theory presented herein. Data from prototype crossings enter in the computations of the water surface drop,  $\Delta h$ , through the constriction, but no data were available for prototype verification of the proposed riprap designs.

## Chapter V

## DESIGN EXAMPLE

An example of the design of stable riprap protection for a prototype bridge crossing is presented in this chapter. The example was obtained from reference 14, which included the backwater computations for the crossing. Stabilization techniques based on all the steps in Chapter III are presented and summarized in Figure 41 to illustrate the intended design procedures.

Design Example (Normal Crossing with Spill-through Abutments Set Back from the Low-Water Channel)

Given:

Design discharge = 19,500 cfs

$h_n = 28.0$  ft above datum

$S_o = 2.6$  ft/mi = 0.00049 ft/ft

Spill-through abutments with 2H:1V side slopes

Cross section and plan shown in Figure 38

Step 1. Computed Parameters

- a) By planimeter,  $A_{n2}$  is found to be 2,534 sq ft, assuming no time for scour to occur.
- b) From the equivalent trapezoid (Figure 38),  $\bar{h}_{n2}$  is 12.35 ft.
- c) For the spill-through abutment, the value of  $b$  is found from  $b = A_{n2}/\bar{h}_{n2} = 2,534/12.35 = 205$  ft, and  $Q_b$  is computed by Mannings' equation as 12,040 cfs. This is the unstricted design discharge flowing in the width,  $b$  (Figure 38).
- d) The opening ratio is found from  $M = Q_b/Q = 12,040/19,500 = 0.62$ .

e) The cross-sectional flow area,  $A_n$ , in the unconstricted channel is planimetered from Figure 38 and found to be 5,664 sq ft.

f) The average velocity in the unconstricted channel is

$$V_n = Q/A_n = 19,500/5,664 = 3.44 \text{ fps.}$$

g) The average velocity in the constriction is

$$V_{n2} = Q/A_{n2} = 19,500/2,534 = 7.70 \text{ fps.}$$

h) The critical depth in the constriction at design discharge for the equivalent trapezoid is  $h_{2c} = 6.76$  ft. This value required seven iterations of the method presented in Chapter III, using  $b_r = 190$  ft, and  $m = 2.0$ .

i) The critical average velocity in the constriction is

$$V_{2c} = Q/A_{2c} = 19,500/1,376 = 14.17 \text{ fps.}$$

j) The critical depth in the unconstricted channel flowing at design discharge is not required for this design because the flow is assumed subcritical. Critical depth for the whole channel would be less than critical depth for the constricted channel.

k) The velocity correction coefficient for the seven subsections in Figure 38 is

$$\alpha_{1n} = \frac{\sum_{i=1}^7 Q_i V_i^2}{Q V_n^2} = \frac{374,895}{19,500(3.44)^2} = 1.62$$

## Step 2. Backwater

a) The methods of reference 14 are selected for backwater computation (Appendix B).

b) Using the computed values from step 1 and assuming a non-scoured condition, the backwater,  $h_1^*$ , is found to be 1.13 ft, and the total

drop through the constriction,  $\Delta h$ , is 1.89 ft. Checking the flow classification, the minimum depth above datum is  $h_3 = h_n + h_1^* - \Delta h + S_o L_{1-3}$ . From Figure B.13, using  $\Delta h/\bar{h}_{n2} = 1.89/12.35 = 0.153$  produces a value of 0.78 for  $L^*/b$ , and  $L^* = 0.78 \times 205 = 160$  ft. The embankments are 70 ft wide, and the minimum depth is  $h_3 = 28.0 + 1.13 - 1.89 + 0.00049 \times (160 + 70)$  or 27.3 ft above datum. Critical depth in the constriction was found to be 6.76 ft (step 1h) so that critical depth is  $6.76 + 15.65$  (Figure 38), or 22.41 ft above datum (Figure 38). The flow classification is therefore subcritical.

c) Assume that waves are expected at the upstream and downstream embankments during the flood. Assume also that the river is straight for a distance of 1500 ft in each direction, and that channel bends occur at both extreme points. The fetch length,  $F$ , is therefore 1500 ft, and the fetch width may be taken as the river width, or 745 ft. This analysis assumes that a 40 mph, or 58.7 fps, wind will come from the upstream direction.

The effective fetch length is computed as  $F_e = 1.17 \times (1500)^{1/3} \times (745)^{2/3}$ , or 1096 ft, and the significant wave height is

$$H = \frac{(58.7)^2}{32.2} \times 3.23 \times 10^{-3} \left[ \frac{32.2(1096)}{58.7^2} \right]^{0.435},$$

or  $H = 0.95$  ft.

d) The minimum embankment height above datum is the sum  $h_n + h_1^* + H$ , or  $28.0 + 1.13 + 0.97$ , or 30.1 ft. The proposed roadway is at an elevation of 30.0 ft.

Step 3. Design Velocity

a) Using the value from step 1k of  $\alpha_{1n} = 1.62$ , and computing  $A_1$  as  $A_n + h_1^*B$ , or  $5,664 + 1.13 \times 745$ , or 6506 sq ft, then  $V_1 = Q/A_1 = 19,500/6506$ , or  $V_1 = 3.00$  fps.

b) The design velocity is

$$V_d = \sqrt{2(32.2)(1.89) + 1.62(3.00)^2} ,$$

or  $V_d = 11.68$  fps. Multiplying this by 1.5 produces a value of 17.52 fps for the depth-averaged design velocity, and multiplying again by 0.8 produces a design bed velocity of 14.02 fps for use in Figures 7 and 10.

Step 4. Toe Protection

a) Assuming that the bed material in the constriction has a mean diameter of 0.8 ft, and obtaining  $h_1 = 8.6$  ft by adding  $h_1^*$  (1.13 ft) to the depth below normal stage at the abutment (7.5 ft), then

$$\frac{\tau_o'}{\tau_c} = \frac{(3.00)^2}{120(0.8)^{2/3}(8.6)^{2/3}} ,$$

or

$$\frac{\tau_o'}{\tau_c} = 0.0212 .$$

b) The average roadway approach length is 265 ft, and the effective length is

$$L_e = 265 + \frac{229 - 205}{2} = 277 \text{ ft.}$$

An eccentric crossing would require a value of  $L_e$  for each approach.

c) The ratio,  $L_e/h_1$ , is  $277/8.6$ , or 32.2. From Figure 13, the ratio of  $d_{se}/h_1$  is 1.5. Solving for  $d_{se}$  produces a value of

1.5 x 8.6, or 12.9 ft. A value of 15 ft would include some allowance for safety.

d) Sheet piles are not used for this crossing.

e) Riprap toe protection for this example is to be placed (on a slope of 2H:1V) to a depth of 12.2 ft plus 3 ft for safety, or to a depth of 15.0 ft below the bed.

f) Horizontal riprap layers at the abutment toe are not recommended for this design.

g) A thickness equal to 2.0 times the maximum diameter of the required riprap is suggested.

h) The bed material should be excavated and the riprap placed and backfilled with the excavated material.

i) For this example, the protection for the abutment toe is to be the same size and placed on the same slope as the riprap for the spill-slope above the bed level. The size will be determined in step 5 for the spill-slope and should extend from the roadway at the abutment top because of the results of step 2. The riprap should also be placed to the scour depth determined in step 4e. If field evidence indicates that the low-flow channel is migrating, precautions must be taken to prevent the channel from migrating over against one of the abutments. If migration is possible, training works will be required to either prevent migration or allow for abutment protection after migration. If migration is allowed, steps 1 through 5 will need to be repeated using a cross-section which places the low-flow channel against one of the abutments. The end result will be greater expected scour depths at the abutment, and greater depths requiring protection. Economic considerations will

determine if training works upstream or additional riprap protection at the abutment is better.

#### Step 5. Riprap Sizing

a) The riprap  $d_m$  and  $d_{85}$  sizes are determined here for the spill-slope of the abutment, and any riprap with these parameters is to be placed both above and below the bed level on the spill-slope.

b) Assume that the riprap is to be quarried and the minimum stable size is desired. A trial value of 12 inches for  $d_m$  is selected. An angle of repose of 42 deg is obtained from Figure 9 for very angular rock.

c) The stability coefficient for the riprap on the nose of the spill-through abutment is 0.223. In computing this, values of  $h_A = 8.35$  ft at the abutment,  $h = 10$  ft at the abutment,  $\alpha = 26^\circ 34'$ ,  $\phi = 42^\circ 00'$ ,  $\gamma_s = 165$  lb/cu ft,  $\gamma_f = 62.4$  lb/cu ft, and  $V_b = 14.02$  fps were used.

d) By substituting  $1.2 \times 10^{-5}$  sq ft/sec for  $v$ , the particle Reynold's number is  $R_p = 14.02 \times 1.0 / 1.2 \times 10^{-5}$ , or  $1.17 \times 10^6$ . This value and the value of  $\eta$  obtained in step 5c plot is a point slightly in the unstable region of Figure 7. The riprap size must therefore be increased.

A second trial using  $d_m = 15$  inches and  $\phi = 43$  deg results in the values of  $R_p = 1.46 \times 10^6$  and  $\eta = 0.231$ . These values plot as a point very close to the design curve in Figure 7. The riprap size could either be increased or accepted.

e) The flow Reynolds number for the 15-inch riprap is  $R = 14.02 \times 8.35 / 1.2 \times 10^{-5} = 9.76 \times 10^6$ .



f) An estimate of the  $d_{75}$  size is obtained from  $d_{75}^{1/6} = 1.04 d_m^{0.178}$ , or  $d_{75} = 1.265 d_m^{1.07}$ , or  $d_{75} = 1.265 \times (15)^{1.07}$ , or 23 in. This value and the value of  $d_m$  are plotted in Figure 39, and the  $d_{85}$  size is estimated as 25 inches. This size must now be checked for stability in Figure 10.

g) The lift force factor is computed as

$$\frac{1}{\psi} = \frac{(14.02)^2}{(2.65 - 1)32.2(1.25)} \left(\frac{1}{2.65}\right) \left(\frac{1.915}{1.25}\right)^3 ,$$

or

$$1/\psi = 4.02 .$$

h) The parameters from steps 5e and 5f plot in the unstable region of Figure 10, indicating that the  $d_{85}$  size from step 5f is too large. Decreasing the  $d_{85}$  size by 20 percent produces an estimated of 20 inches for  $d_{85}$  and a new value of  $1/\psi = 2.65$ , which results in a stable indication from Figure 10. Any available riprap which has a minimum  $d_m$  size of 15 inches and a maximum  $d_{85}$  size of 20 inches will be stable according to Figures 7 and 10. Flexibility as discussed in Chapter II may be used in obtaining the gradation for the riprap. Figure 39 is intended only as an estimate for the  $d_{85}$  size.

#### Step 6. Abutment Spill-slope Protection

a) Riprap having the  $d_m$  and  $d_{85}$  sizes determined in step 5 is to be placed as toe protection and as spill-slope protection. The extent of wrap-around for this riprap is determined for the upstream and downstream sides in step 7 and 8.

b) The  $d_{100}$  size from Figure 39 is 22.5 inches and the thickness of the spill-slope protection is found from  $2d_{100}$ , or 45 in. (step 4g).

c) Due to the large size of the spill-slope riprap, it is desired to use a smaller size of riprap on the sides of the approach embankments. The large riprap should begin at point G in Figure 5 and should terminate somewhere between points E and H. Using the value from step 2b of 160 ft for  $L^*$ , and substituting the value of  $V_{n2}$  for  $V_2$  results in a length,  $L$ , of

$$L = [1 - \frac{3.44}{7.70}]160 ,$$

or  $L = 88.6$  ft. The 15-inch riprap is to extend from point G, around the abutment, to point E or point H in Figure 5. Point H is chosen for this example even though point E or some point between E and H could be chosen. Step 8c illustrates a better method for determining the distance  $L$  when wave forces are not anticipated. Steps 7 and 8 provide the required riprap size for the remaining unprotected side slopes.

d) Either gravel or filter-cloth filter layers could be used beneath the riprap layer depending on economic considerations. Assume, for illustrative purposes, that a gravel layer is desired and that the embankments are constructed from a material having values of 0.2, 1.0, and 4.0 inches for the  $d_{15}$ ,  $d_{50}$ , and  $d_{85}$  sizes. The riprap filter layer determined from the T-V specifications would require values of

$$d_{15} \text{ (Filter)} < 20 \text{ in} ,$$

$$0.8 \text{ in} < d_{15} \text{ (Filter)} < 4 \text{ in, and}$$

$$d_{50} \text{ (Filter)} < 25 \text{ in} .$$

Any filter satisfying the three inequalities should prevent losses of the embankment material.

The thickness of the gravel filter layer should be computed as 2.0 or 2.5 times the maximum filter stone diameter.

#### Step 7. Downstream Side Slope Protection

a) The riprap size required for the downstream embankment side slopes is obtained from

$$W_s = \frac{165(0.95)^3}{3.2(2.65 - 1)^3(2)},$$

or  $W_s = 4.92$  lb per stone. The equivalent spherical diameter for a 4.92-lb stone is

$$d_m = \left[ \frac{8}{4\pi/3} \left( \frac{4.92}{165} \right) \right]^{1/3},$$

or 0.385 ft (4.62 in.). The downstream protection should be a well-graded riprap with  $d_m = 4.6$  in.

b) Wind-generated waves produced the required riprap size for the downstream slopes in the last step.

c) The 4.6-inch riprap for the downstream slopes should extend to the top of the embankment (elev. 30.0) because the sum of wave height and normal stage is found to be 29.0 ft.

Figure 14 produces a value of  $z \tan \phi / d_{se} = 0.69$  for the downstream face. Using the values of  $\phi = 38$  deg for the bed material and  $d_{se} = 12.2$  ft (step 5c) results in a value of  $z = 10.8$  ft for the length requiring buried toe protection on the downstream side. The depth of buried riprap is to vary linearly from bed level at a value of  $z = 11$  ft to a depth of 15 ft at a value of  $z = 0.0$  (Point G in Figure 5).

d) The same filter material determined from step 6d should be placed beneath the 6.5-inch riprap.

#### Step 8. Upstream Side Slope Protection

a) The 15-inch riprap is to extend to point H (step 6c) in Figure 5, and the size required at point H by the velocities of Figure 35 will be placed along the remaining upstream slope to a point where the velocities are smaller than the critical velocity for movement of the embankment material. A minimum value of 4.6 in. was determined from the wave analysis in step 7a.

b) For the normal crossing, point H in Figure 35 occurs at a value of  $x = 270 - 89 = 181$  ft (steps 4b and 6c). From Figure 35 and steps 1a and 1b,  $M' = 2,534 / (745 \times 12.35) = 0.275$ , and  $L = 270$  ft. The value of  $x/L$  is 0.67, and  $VM'/V_n = 0.325$  is found from the solid lines in Figure 35. Solving for  $V$ , and multiplying by 1.2 to include turbulence and bed corrections, produces a design value of  $V_b = 4.86$  fps at point H.

c) Repeating steps 5b through 5d with new values of  $d_m = 4.6$  in.,  $V_b = 4.86$  fps,  $\phi = 41^\circ$ ,  $\alpha = 26^\circ 34'$ ,  $\gamma_s = 165$  lb/cu ft, and  $\gamma_f = 62.4$  lb/cu ft, produces values of  $\eta = 4.58$ , and  $R_p = 1.55 \times 10^5$ . These values, when plotted in Figure 7, indicate stability. A smaller value of  $d_m$  would satisfy the stability requirements for  $V_b$ , but the wave analysis of step 7a produced a minimum size of 4.6 in.

For illustrative purposes, assume that wind waves are not expected, and it is desired to determine the point along the upstream slope of the approach embankment at which the velocity reduces to the critical value for movement of the embankment material. This point coincides with the

point of all riprap termination because the embankment material is no longer subjected to erosive velocities at this point. The method outlined in step 8c of Chapter III would proceed as follows:

Using the embankment core material  $d_m$  size of 1.04 inch (step 6d), and assuming an angle of repose of 40 deg (Figure 9), a trial value of  $V_b$  of 4.0 fps is obtained from Figure 8. For these values, the stability coefficient is computed as 6.72 and the particle Reynolds number is  $2.78 \times 10^4$ . These values plot as a point well within the stable region of Figure 7, and  $V_b$  must be increased to shift the point closer to the design curve. After several trials, a value of 9.0 fps for  $V_b$  produces values of 1.33 for the stability coefficient and  $6.25 \times 10^4$  for the particle Reynolds number. These parameters plot as a point slightly on the stable side of the design curve. For repeated trials of  $V_b$  equal to 4, 5, 6, 7, 8, and 9 fps, it was noted that the parameters plotted as a straight line in Figure 7 for fixed values of the angle of repose and  $d_m$  size of 1.04 in. This straight-line property could be used in future trials to expedite the solution for a value of  $V_b$  with parameters which plot as a point on the design curve in Figure 7.

Having the desired bed velocity of 9.0 fps, and dividing by 0.8 produces a value of 11.25 fps for the depth-averaged critical velocity. Dividing this value by 1.5 yields a design depth-averaged velocity,  $V$ , equal to 7.5 fps for use in Figure 35.

The final step for solution of  $x$  proceeds by computing the parameter  $VM'/V_n$ , or  $7.5(0.275)/3.44$ , or 0.6. From Figure 35, a value of  $x/L$  of 0.93 and a value of  $L$  equal to 270 ft produces a value of  $x$  equal to 251 ft. Point E in Figure 5 occurs at a value of  $x$  equal

to 270 ft, and the riprap for the case of no wind waves can be terminated at a point H where  $L$  is computed as  $270 - 251$ , or 19 ft. The embankment core material is theoretically stable on the remaining side slope of the approach embankment.

The flow depth upstream of the embankments is  $h_n + h_1^* = 8.4 + 1.13 = 9.53$  ft. Using this value for  $D$  produces a flow Reynolds number of  $4.86 \times 9.53 / 1.2 \times 10^{-5}$ , or  $3.86 \times 10^6$ . The  $d_{75}$  size is  $1.265(4.6)^{1.07}$ , or 6.48 in. (step 5f).

The  $d_m$  and  $d_{75}$  sizes are plotted in Figure 40, and the estimate for  $d_{85}$  is 7.4 in. Computing the lift force factor from

$$\frac{1}{\psi} = \frac{4.86^2}{(2.65 - 1)32.2(6.5)} \left(\frac{1}{2.65}\right) \left(\frac{7.4}{6.5}\right)^3,$$

or  $1/\psi = 0.083$ . This value, and the flow Reynolds number of  $3.86 \times 10^6$ , plot as a point well within the stable region of Figure 10. The resulting values of  $d_m = 4.6$  in. and  $d_{85} = 7.4$  in. are to be treated as minimum and maximum values as discussed in Chapter II for determining riprap size and gradation. Figure 40 is presented only as an estimate of the allowable  $d_{85}$  size.

d) If the flood plain along the upstream toe of the approach embankment is to be cleared during construction, the toe will require either buried riprap protection or some other desired form such as finger dikes or flow retards. Assume for this example that buried protection is to be used.

e) For the upstream face, Figure 14 produces a value of 1.0 for  $z \tan \phi / d_{se}$ . Using the values for  $\phi$  and  $d_{se}$  from step 7c produces a value of 15.6 ft for  $z$ . This value, rounded to 16 ft, is suggested as

an estimate for the length along the upstream face requiring buried riprap protection. The depth of buried riprap is to vary linearly from bed level at a value of  $z$  equal to 16 ft (Figure 41a) to a depth of 15 ft at a value of  $z = 0.0$  (Point E in Figure 5). The riprap should also extend to the top of the embankment (step 2d).

f) The filter layer determined in step 6d can also be used along the upstream embankment, because the same embankment material is being protected.

#### Step 9. Pier Protection

a) The piers for the crossing are shown in Figure 38. Three of the piers are placed on the flood plain, and the other two are founded in the low-flow channel.

For the flood-plain piers 1, 2, and 5, the clear water scour depth is

$$d_{se} = 0.00073 \left[ \frac{2(1.25)(3.00)}{1.2 \times 10^{-5}} \right]^{0.619},$$

or  $d_{se} = 2.81$  ft. For the other two piers, the scour is  $d_{se}^* = 1.42 (1.3)(3.0)^{0.75}$ , or  $d_{se}^* = 4.21$  ft.

b) Assume that piers 1 and 5 are positioned close enough to the abutments so that the issuing flow from the spill-slopes strikes the piers at an angle,  $\alpha$ , equal to 20 deg as shown in Figure 15. The ratio of  $l/a$  for the piers is  $22/1.25$ , or 17.6. From Figure 15, a value of 3.7 is obtained for  $K_{\alpha 1}$ , and the expected scour depth at these piers becomes  $3.7 \times 2.8 = 10.4$  ft. Better estimates of the angle of flow at these piers are hoped to be found from continued analytical and experimental work being conducted at CSU.

c) Due to the proximity of piers 1 and 5 with the abutment toes, the abutment protection and pier footings should be founded 15 feet below the bed (steps 5c and 9b). Pier 2 could be founded at any depth greater than 2.8 ft, although overlapping scour holes may cause greater depths than anticipated. Piers 3 and 4 should have footings located at depths greater than 4.2 ft below the low-flow channel bed. If the low-flow channel is allowed to migrate between the abutments (see step 5i) then the scour depths in steps 9a, b, and c, need to be re-computed using a cross-section which places the low-flow channel at all possible positions. As in step 4i, training works may be more economical than pier footings founded at greater depths.

Figure 41 summarizes all the recommended stabilization requirements for this example.

#### Step 10. Protection for Special Cases

a) For illustrative purposes, assume that the left flood plain between the abutment tip and the low-flow channel bank is to be maintained for livestock (Figure 38). Assume also that the riprap is to be placed as a horizontal apron and buried under 1 ft of soil as discussed in step 10a of Chapter III. The riprap size determined from step 4i may be used for the horizontal apron, even though a smaller size would be allowed. The size from step 4i was derived for a sloping apron, and steps 5b through 5h could be repeated using the relationships for horizontal aprons.

The side slope of the low-flow channel should also be protected to a depth of 15 ft below the channel bed (step 4c), preventing migration of the channel.



A value of  $L^*$  was obtained in step 2b, and the flood plain and channel wall could be protected for this distance upstream and possibly downstream of the crossing. This proposal entails a considerable amount of rock, and it may be more economical to allow the flood plains to scour instead. Occasional replacement of the flood plains could be accomplished during periods of low flow.

b) The bridge crossing shown in Figure 38 was treated as a non-eccentric crossing when the backwater and water surface drop were computed. The abutment lengths of 230 and 300 ft actually produces an eccentric crossing.

The first method of treating eccentric crossings (step 10b of Chapter III) would proceed by concealing half the crossing in Figure 38 and proceeding with steps 1 through 10 as if an identically symmetrical half were being concealed. This procedure would result in backwater values, design velocities, and riprap sizes for the unconcealed half. The process would be repeated for the opposite abutment, resulting in different backwater values, velocities, and riprap sizes. The basic assumption for validity of this procedure is that the flow conditions at the vertical "folding line" for each design are identical. A trial procedure would be required to locate the position of the folding line which provides the same backwater and velocity on each side of the line.

Reference 14 (Appendix B) provides a different method of computing backwater for eccentric crossings without using the trial folding technique. This backwater value can then be used with the folding line placed at the center of the flow distribution to design riprap protection for each side of the line. For this method, the eccentricity of a bridge crossing is defined as  $e = 1 - Q_c/Q_a$ , where  $Q_c < Q_a$  (the

values of  $Q_c$  and  $Q_a$  are defined in Figure 38). For this example,  $e = 1 - 1479/5980$ , or 0.753. Experimental results (14) indicate that backwater at an eccentric crossing is no different from backwater at a symmetrical crossing for values of  $e$  less than 0.8, and this explains the assumption of symmetry in the example.

Bridge crossings which are fully eccentric are defined as having a value of  $e$  equal to 1.0. This condition occurs at bends in natural channels or when a meandering low-flow channel migrates to one side of the flood plain. Under these conditions, only one approach embankment is used to constrict the flow. Reference 14 provides allowances for this possibility, and the backwater and other computed parameters can be used to design the protection for the single abutment in the same manner described for both abutments of symmetrical crossings. The channel wall and bridge footing across the channel from the single abutment can be protected as a channel side slope using Bhowmik's techniques for these reaches.

## BIBLIOGRAPHY

1. Ahmad, M., "Effect of scale distortion, size of model bed material, and time scale on geometrical similarity of localized scour," Proc. IAHR, The Hague, Netherlands, 1955.
2. Ahmad, M., "Experiments on design and behavior of spur dikes," 5th Congress, IAHR, Minneapolis, Minnesota, 1953, pp. 145-159.
3. Ahmad, M., "Spacing and projections of spurs for bank protection," Civil Engineering, London, March 1951.
4. Andre, P., "Study of scour at obstructions in non-cohesive bed," M.S. thesis, University of Alberta, Edmonton, Alberta, Canada, 1956.
5. Appel, D. W., "Flexible mats may reduce scour at piers of small bridges," Engineering News Record, May 25, 1950.
6. ASCE Subcommittee on Slope Protection of the Committee on Earth Dams of the Soil Mechanics and Foundations Division, "Review of slope protection methods," Proc. ASCE, Vol. 74:8, June 1948, p. 845.
7. ASCE Task Committee on Preparation of Sedimentation Manual, "Sediment transportation mechanics: Initiation of motion," Proc. ASCE, Vol. 92, HY2, 1966, pp. 291-314.
8. Bhowmik, N. G., "The mechanics of flow and stability of alluvial channels formed in coarse materials," Ph.D. dissertation, Colorado State University, Ft. Collins, Colorado, 1968.
9. Bhowmik, N. G. and D. B. Simons, "Stabilization of alluvial channels," preprint of paper presented at the Institute of River Mechanics, Colorado State University, Ft. Collins, Colorado, June 15-26, 1970, 28 pp.
10. Biery, P. F. and J. W. Delleur, "Hydraulics of single span arch bridge constrictions," Proc. ASCE, Journal of Hydraulics Division, HY2, Paper 3076, March 1962, pp. 75-108.
11. Bradley, J. N., "Hydraulics of bridge waterways," Bureau of Public Roads, U.S. Department of Commerce, Washington, D.C., August 1960.
12. Bradley, J. N., "Use of backwater in designing bridge waterways," Highway Research Board Bulletin 242, Washington, D.C., 1960, pp. 57-68.
13. Bureau of Public Roads, "Computation of backwater caused by bridges," preliminary draft by Division of Hydraulic Research, Washington, D.C., October 1958.

14. Bureau of Public Roads, "Hydraulics of bridge waterways," Hydraulics Branch, Bridge Division, Office of Engineering and Operations, reported by J. N. Bradley, consultant, 2nd edition, Hydraulic Design Series No. 1, U.S. Government Printing Office, Washington, D.C., 1970.
15. California Division of Highways, "Bank and shore protection in California highway practice," State of California, Department of Public Works, November 1960.
16. Campbell, F. B., "Hydraulic design of rock riprap," U.S. Army Engineer Waterways Experiment Station, Miscellaneous Paper No. 2-777, Vicksburg, Mississippi.
17. Carlson, E. J. and W. W. Sayre, "Canal bank erosion due to wind-generated water waves," U.S. Bureau of Reclamation, Progress Report 1, Hydraulic Laboratory, Report No. Hyd-465, 1961.
18. Carstens, M. R., "Similarity laws for localized scour," Proc. ASCE, Journal of Hydraulics Division, Vol. 92, HY3, Paper 4818, May 1966, pp. 13-36.
19. Davidian, J., P. H. Carrigan, Jr., and J. Shen, "Flow through openings in width constrictions," U.S. Geological Survey, Water Supply Paper 1369-D, U.S. Government Printing Office, Washington, D.C., 1962, 32 pp.
20. de Abreu-Lima, J. O. and W. B. Morgan, "Protection of earth embankments by riprap of uniform size," M.S. thesis, State University of Iowa City, Iowa, 1951.
21. de Souss, P. and L. Nelson, "Riprap protection against scour around bridge piers," M.S. thesis, State University of Iowa, Iowa City, Iowa, 1959.
22. Engels, H., "Experiments pertaining to the protection of bridge piers against undermining," ASME, Hydraulic Laboratory Practice, Chapter V, New York, 1929.
23. Field, W. G., "Flood protection at artificial river constrictions," Preprint 906, ASCE National Meeting on Transportation Engineering, Washington, D.C., July 21, 1969, 46 pp.
24. Gales, R., "Principles of river training for railway bridges and their application to the case of the Hardinge Bridge over the lower Ganges at Sara," Journal of the Institution of Civil Engineers, Paper No. 5167, December 1938.
25. Hallmark, D. E. and G. L. Smith, "Stability of channels by armor-plating," Proc. ASCE, Journal of Waterways and Harbors Division, Vol. 91, No. WW3, August 1965, pp. 117-135.

26. Hedman, E. R., "Effect of spur dikes on flow through contractions," ASCE, Journal of Hydraulics Division, Vol. 91, HY4, Paper 4412, July 1965, pp. 155-165.
27. Herbich, J. B., "Spur dikes prevent scour at bridge abutments," Lehigh University Institute of Research, Fritz Engineering Laboratory Report 280.20, Bethlehem, Pennsylvania, December 1966.
28. Herbich, J. B., R. J. Carle, and J. E. Kable, "The effects of spur dikes on flood flows through highway bridge constrictions," Lehigh University Institute of Research, Fritz Engineering Laboratory, Bethlehem, Pennsylvania, June 1959.
29. Herr, L. A., discussion of "Effect of spur dikes on flow through contractions," by E. R. Hedman, ASCE, Journal of Hydraulics Division, Vol. 92, HY2, March 1966, p. 430.
30. Hudson, R. Y., "Laboratory investigations of rubble mound breakwaters," Proc. ASCE, Journal of Waterways and Harbors Division, Paper 2171, September 1959.
31. Inglis, C. C. and D. V. Joglekar, "Investigations carried out by means of models at the Khodakwasla Hydrodynamics Research Station near Poona in connection with the protection of the Hardinge Bridge which spans the river Ganges near Paksey," East Bengal Railway, Public Works Department, Bombay, India, Technical Paper No. 55, 1936.
32. Isbash, S. V. and I. V. Lebedev, "Change of natural streams during construction of hydraulic structures," Proc. 9th Congress, IAHR, Dubrovnik, 1961, p. 1114.
33. Izzard, C. F., discussion of "Backwater effects of open-channel constrictions," by H. J. Tracy and R. W. Carter, Trans. ASCE, Vol. 120, 1955, pp. 1008-1013.
34. Izzard, C. F., discussion of "Tranquil flow through open-channel constrictions," by C. E. Kindsvater and R. W. Carter, Trans. ASCE, Vol. 120, 1955, pp. 985-989.
35. Izzard, C. F. and J. N. Bradley, discussion of "Flood erosion protection for highway fills," by C. J. Posey, Trans. ASCE, Vol. 122, 1957, p. 544.
36. Izzard, C. F. and J. N. Bradley, "Field verification of model tests of flow through highway bridges and culverts," Proc. 7th Hydraulics Conference, Studies in Engineering, Bulletin 39, State University of Iowa, Iowa City, Iowa, June 1958, p. 225.
37. Karaki, S. S., "Hydraulic model study of spur dikes for highway bridge openings," Colorado State University, Civil Engineering Section, Report CER59SSK36, Ft. Collins, Colorado, September 1959, 47 pp.

38. Karaki, S. S., "Laboratory study of spur dikes for highway bridge protection," Highway Research Board Bulletin 286, Washington, D. C., 1961, pp. 1-12.
39. Kindsvater, C. E., discussion of "Flood erosion protection for highway fills," by C. J. Posey, Trans. ASCE, Vol. 122, 1957, p. 548.
40. Kindsvater, C. E. and R. W. Carter, "Tranquil flow through open channel constrictions," Trans. ASCE, Vol. 120, 1955, pp. 955-980.
41. Kindsvater, C. E., R. W. Carter, and H. J. Tracy, "Computation of peak discharge at contractions," U.S. Geological Survey Circular 284, Washington, D.C., 1953, 35 pp.
42. Lane, E. W., "Design of stable channels," Trans. ASCE, Vol. 120, 1955, pp. 1234-1260.
43. Lane, E. W., "Experiments on the flow of water through contractions in an open channel," Trans. ASCE, Vol. 83, 1910-20, pp. 1149-1219.
44. Lane, E. W. and E. J. Carlson, "Some observations on the effects of particle shape on the movement of coarse sediments," Trans. AGU, Vol. 35, No. 3, 1954, pp. 453-462.
45. Laursen, E. M., "An analysis of relief bridge scour," Proc. ASCE, Journal of Hydraulics division, Vol. 89, No. HY3, Paper 3516, May 1963, pp. 93-118.
46. Laursen, E. M., "Progress report of model studies of scour around bridge piers and abutments," Highway Research Board, Research Report 13-B, 1951.
47. Laursen, E. M., "Scour at bridge crossings," Proc. ASCE, Journal of Hydraulics Division, No. 2369, February 1960.
48. Laursen, E. M., "Scour at bridge crossings," Trans. ASCE, Vol. 127, Part 1, 1962, pp. 166-179.
49. Laursen, E. M., "Scour at bridge crossings," Iowa Highway Research Board, Bulletin 8, August 1958, 53 pp.
50. Laursen, E. M. and A. Toch, "A generalized model study of scour around bridge piers and abutments," 5th Congress, IAHR, Minneapolis, Minnesota, 1953, pp. 123-131.
51. Laursen, E. M. and A. Toch, "Scour around bridge piers and abutments," Iowa Highway Research Board, Bulletin 4, May 1956, 60 pp.

52. Liu, H. K., J. N. Bradley, and E. J. Plate, "Backwater effects of piers and abutments," Colorado State University, Civil Engineering Section, Report CER57HKL10, Ft. Collins, Colorado, October 1957, 364 pp.
53. Liu, H. K., F. M. Chang, and M. M. Skinner, "Effect of bridge constriction on scour and backwater," Colorado State University, Civil Engineering Section, Report CER60HKL22, Ft. Collins, Colorado, 1961.
54. Liu, H. K. and M. M. Skinner, "Laboratory observations of scour at bridge abutments," National Research Council, Highway Research Board, Bulletin 242, January 1959, pp. 69-77.
55. Matthai, H. F., "Measurement of peak discharge at width constrictions by indirect methods," U.S. Geological Survey, Techniques of Water Resources Investigations, Book 3, Chapter A4, U.S. Government Printing Office, Washington, D.C., 1967, 44 pp.
56. Moore, W. L. and F. D. Masch, "The influence of secondary flows on local scour at obstructions in a channel," Proc. Federal Inter-agency Sedimentation Conference, Miscellaneous Publication No. 970, 1963.
57. Nagler, F. A., "Obstruction of bridge piers to the flow of water," Trans. ASCE, Vol. 82, 1918, p. 334.
58. Owen, H. J. and A. Sooky, discussion of "Hydraulics of single span arch bridge constrictions," by P. F. Biery and J. W. Delleur, Proc. ASCE, Vol. 88, HY5, Part 1, Paper 3076, September 1962, pp. 327-333.
59. Parkin, A. K., D. H. Trollope, and J. D. Lawson, "Rockfill structures subject to water flow," Proc. ASCE, Journal of Soil Mechanics and Foundations Division, Vol. 92, No. SM6, 1966, pp. 135-151.
60. Posey, C. J., "Flood erosion protection for highway fills," Trans. ASCE, Vol. 122, Paper 2871, 1957, pp. 531-542.
61. Posey, C. J., "Flood erosion protection for highway fills," Iowa Highway Research Board, Bulletin 13, December 1960, 27 pp.
62. Posey, C. J., "Rock 'sausages' provide economical protection against erosion," Engineering News Record, May 13, 1954, p. 45.
63. Posey, C. J., "Some basic requirements for protection against erosion," Proc. 5th Congress, IAHR, Minneapolis, Minnesota September 1-4, 1953, pp. 85-87.
64. Posey, C. J., "Why bridges fall in floods, model tests of erosion around bridge piers indicate depth of scour in erodible materials," Civil Engineering, February 1949, p. 42.



65. Sanden, E. J., "Scour at bridge piers and erosion of river banks," Department of Highways, Province of Alberta, Canada, October 3, 1960.
66. Saville, T., Jr., "The effect of fetch width on wave generation," Beach Erosion Board, Corps of Engineers, Tech. Memo No. 70, 9 pp.
67. Schneible, D. E., "Field observations on performance of spur dikes at bridges," paper presented at ASCE Transportation Engineering Conference, Philadelphia, Pennsylvania, October 17-21, 1966.
68. Searcy, J. K., "Use of riprap for bank protection," Bureau of Public Roads, Hydraulic Engineering Circular No. 11, U.S. Government Printing Office, Washington, D.C., June 1967, 43 pp.
69. Shen, H. W., "Scour near piers," preprint of paper presented at the Institute of River Mechanics, Colorado State University, Ft. Collins, Colorado, June 15-26, 1970, 23 pp.
70. Shen, H. W., V. R. Schneider, and S. Karaki, "Mechanics of local scour," Colorado State University, Civil Engineering Section, Report CER66HWS-VRS-SK-22, Ft. Collins, Colorado, 1966.
71. Shen, H. W., V. R. Schneider, and S. Karaki, "Mechanics of local scour and supplement methods of reducing scour," Colorado State University, Civil Engineering Section, Report CER66HWS-VRS-SK36, Ft. Collins, Colorado, 1966.
72. Simons, D. B., "Theory and design of stable channels in alluvial materials," Ph.D. dissertation, Colorado State University, Ft. Collins, Colorado, 1957, 394 pp.
73. Simons, D. B., G. L. Lewis, and W. G. Field, "Embankment protection at river constrictions," Proc. 11th Annual Bridge Engineering Conference, Colorado State University, Ft. Collins, Colorado, 1970, pp. 160-206.
74. Simons, D. B., M. A. Stevens, and F. J. Watts, "Flood protection at culvert outlets," Report prepared for Wyoming State Highway Department, Planning and Research Division, in cooperation with the U.S. Department of Transportation, Federal Highway Administration, Bureau of Public Roads, 1970
75. Tracy, H. J. and R. W. Carter, "Backwater effects of open-channel constrictions," Trans. ASCE, Vol. 120, 1955, pp. 993-1006.
76. U.S. Army Engineer Waterways Experiment Station, "Velocity forces on submerged rocks," Corps of Engineers, Waterways Experiment Station Miscellaneous Paper No. 2-265, Plate 1, Vicksburg, Mississippi, 1958.



77. U.S. Army Engineer Waterways Experiment Station, "Waterways Experiment Station hydraulic design criteria," Corps of Engineers, Vicksburg, Mississippi, 1960.
78. Vallentine, H. R., "Flow in rectangular channels with lateral constriction plates," *La Houille Blanche*, No. 1, January - February 1958, pp. 75-84.
79. Welty, K. H., M. L. Corry, and J. L. Morris, "Hydraulics of bridge waterways," Bureau of Public Roads, Electronic Computer Program HY-4-69, Washington, D.C., 1969.
80. Wend, J. H., "Stabilization of channels with gravel," M.S. thesis, Colorado State University, Ft. Collins, Colorado, 1967.
81. White, C. M., "The equilibrium of grains on the bed of a stream," *Proc. Royal Society of London, Series A*, Vol. 174, p. 331.
82. Wyoming Highway Department, Hydraulic Design Practice, Chapter 3, January 1966.
83. Yarnell, D. L., "Bridge piers as channel obstructions," U.S. Department of Agriculture, Technical Bulletin No. 442, U.S. Government Printing Office, Washington, D.C., November 1934, 52 pp.
84. Yarnell, D. L., "Pile trestles as channel obstructions," U.S. Department of Agriculture, Technical Bulletin No. 429, U.S. Government Printing Office, Washington, D.C., July 1934.
85. Yarnell, D. L. and F. A. Nagler, "Flow of flood waters over railroad and highway embankments," Public Roads, Vol. II, No. 2, April 1930.
86. Young, J. C., "Economics of self-protection of highways against flood damage," ASCE, *Journal of Highway Division*, HW3, Paper 1075, October 1956.

## APPENDIX A

## FIGURES

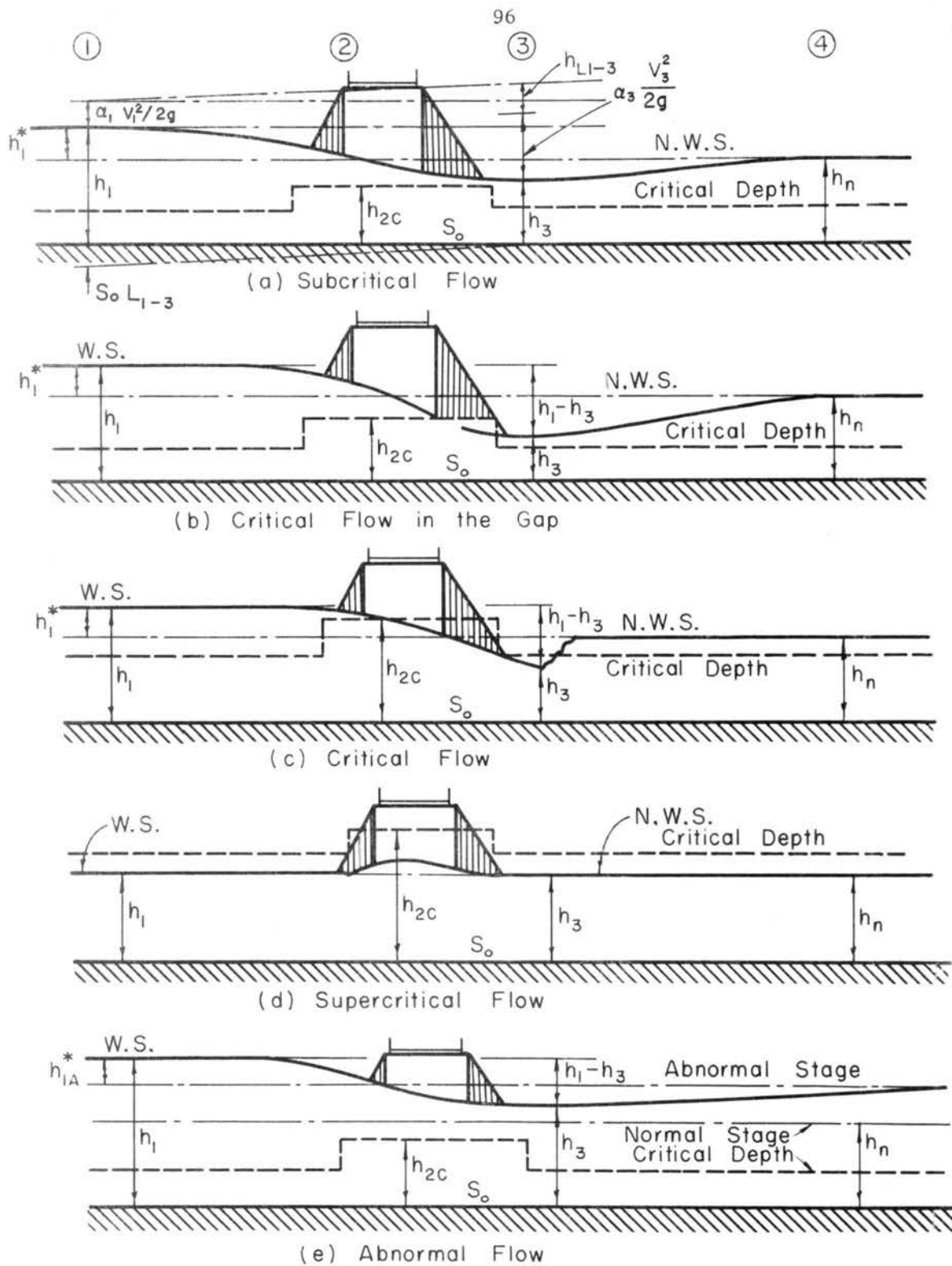


Fig. 1 Classification of Flow Conditions from Bradley (14)

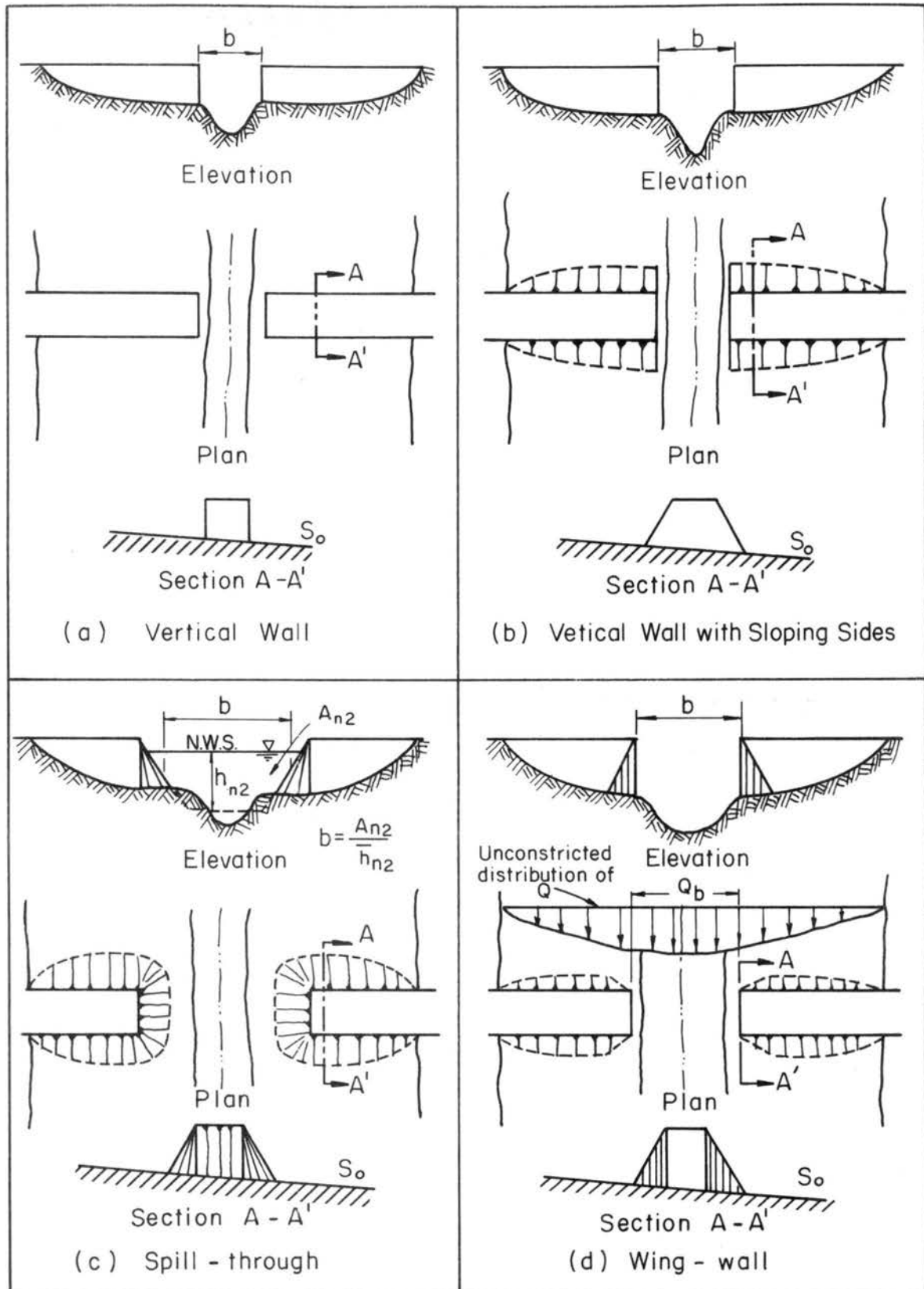


Fig. 2 Classification of Abutment Types

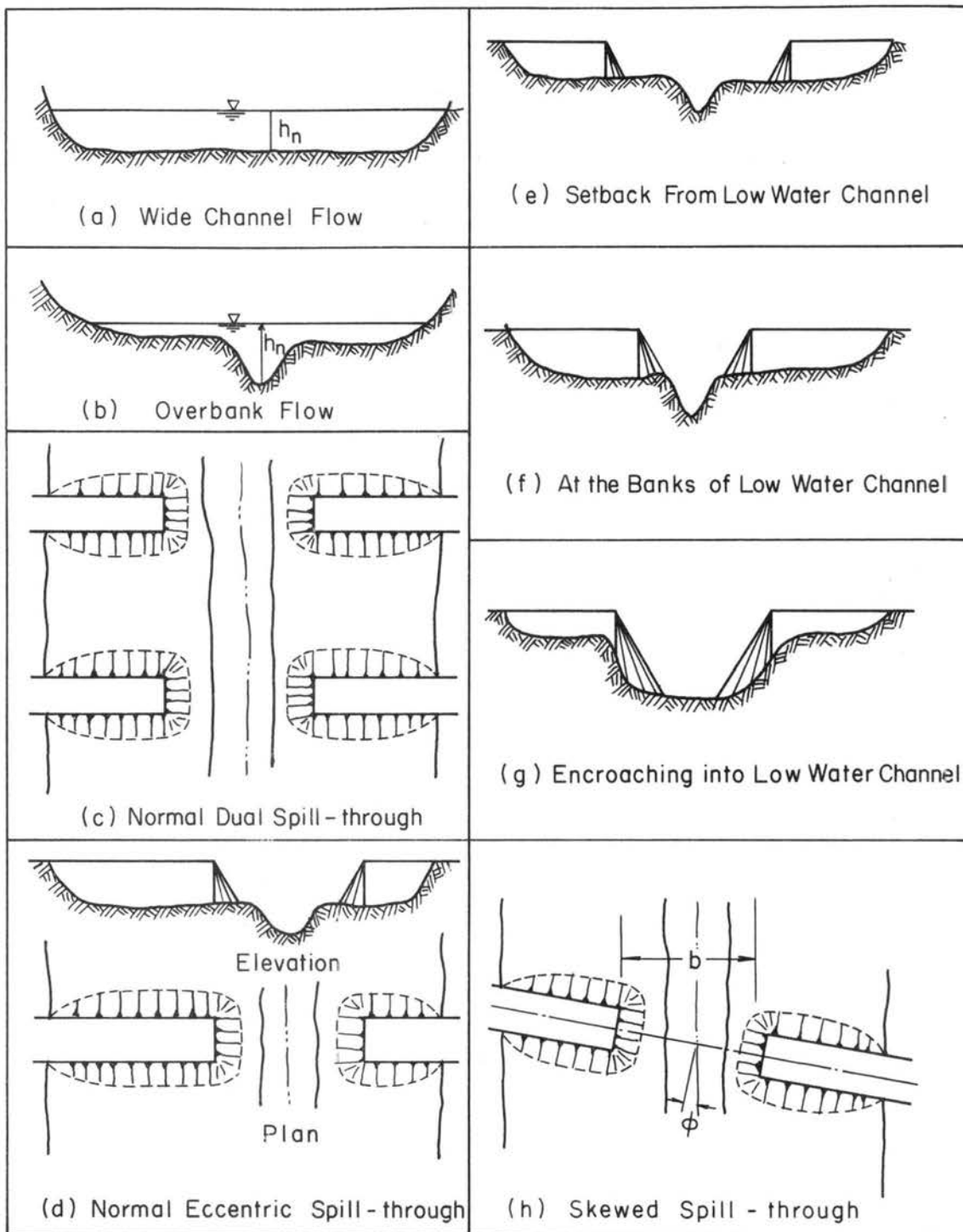


Fig. 3 Classification of Geometry

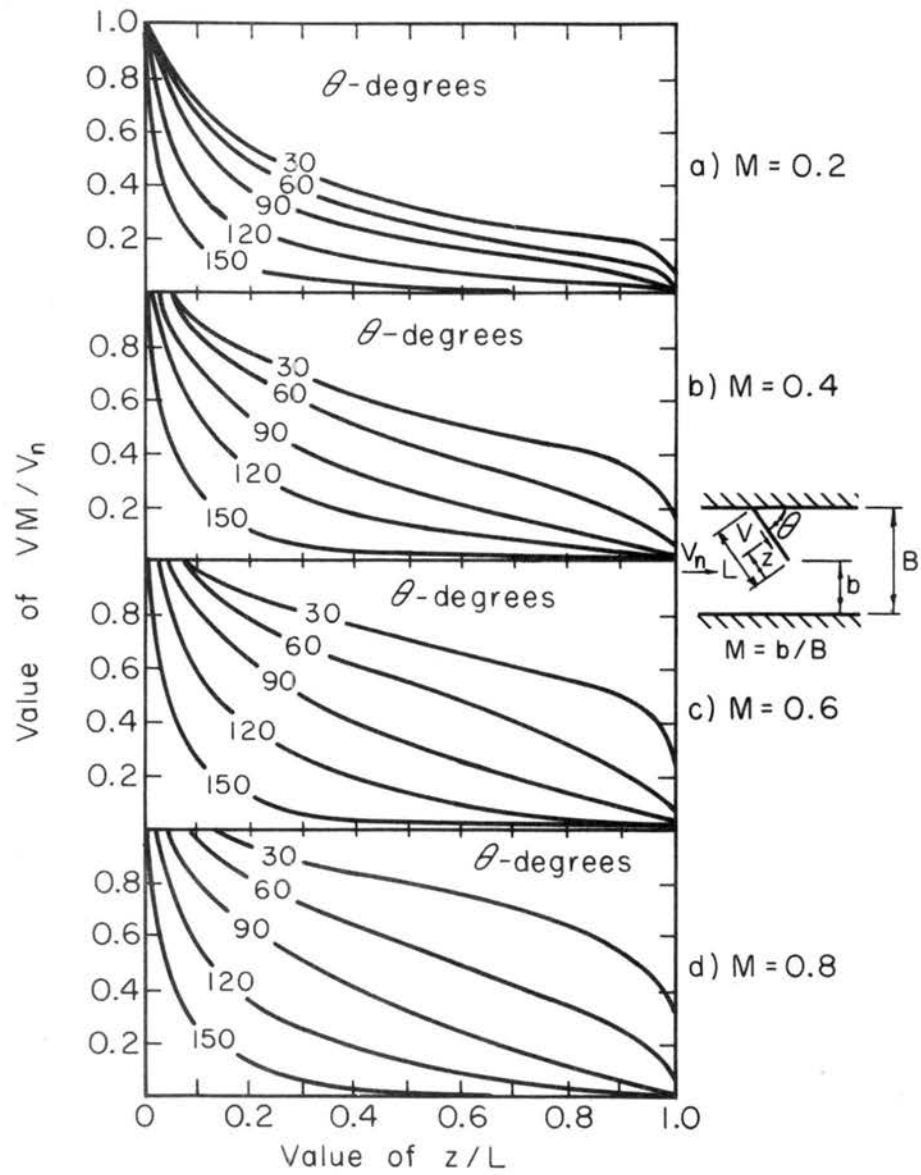


Fig. 4 Variation of Velocity along Embankment with Distance from Tip from Field (23)



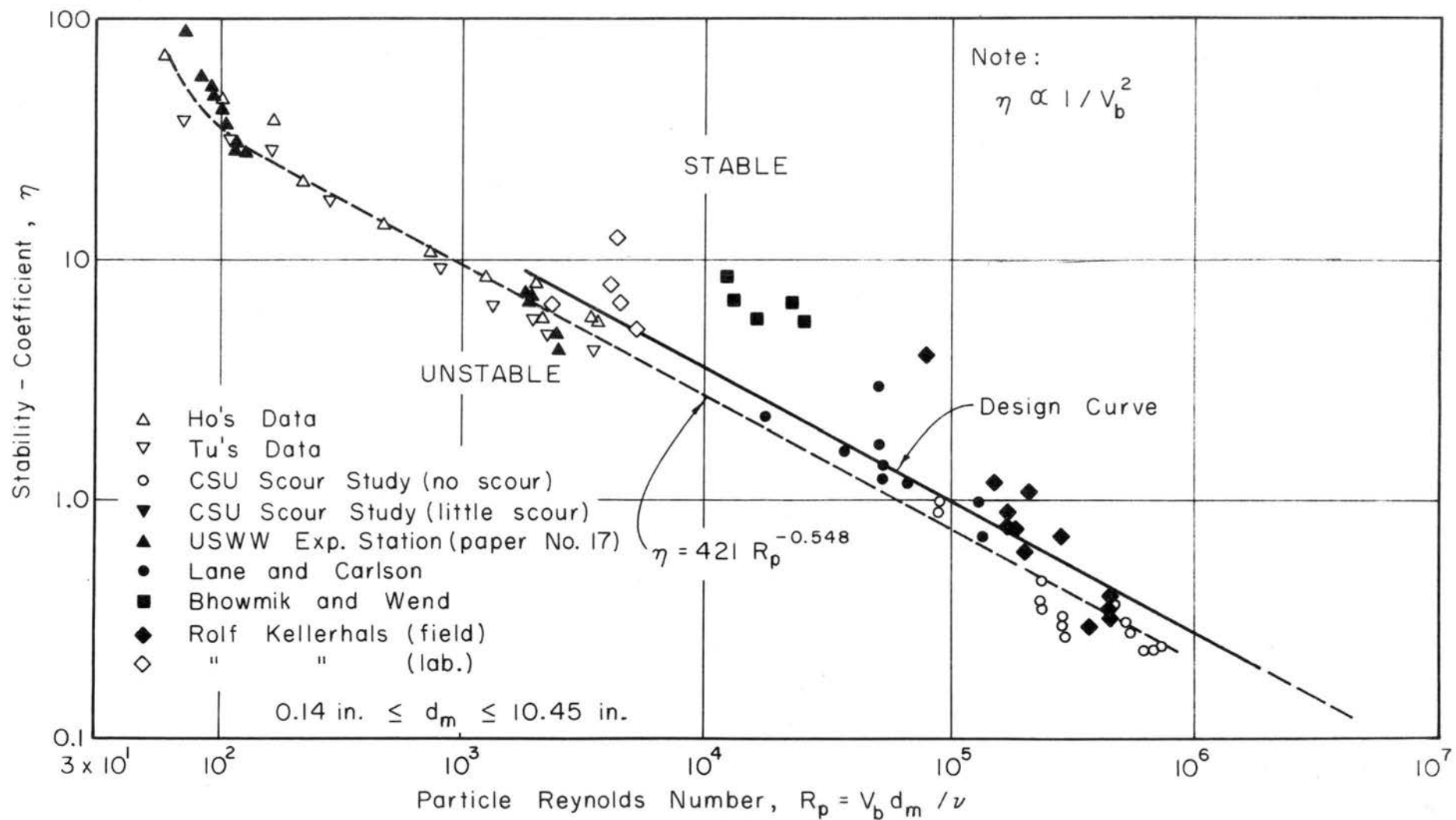


Fig. 7 Stability Coefficient,  $\eta$ , and Particle Reynolds Number from Bhowmik and Simons (9)



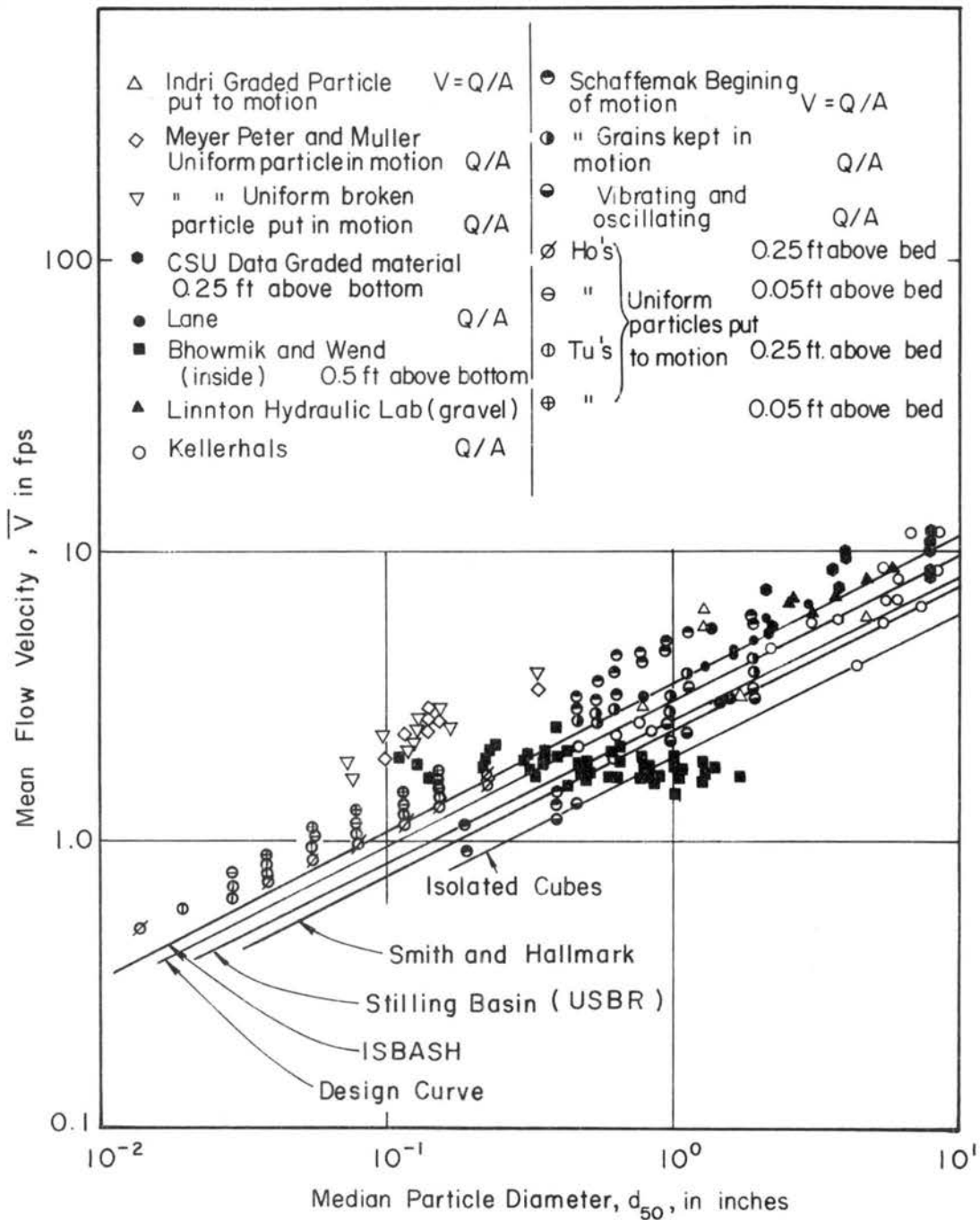


Fig. 8 Relation Between Mean Velocity and Stable Mean Particle Diameter from Bhowmik and Simons (9)

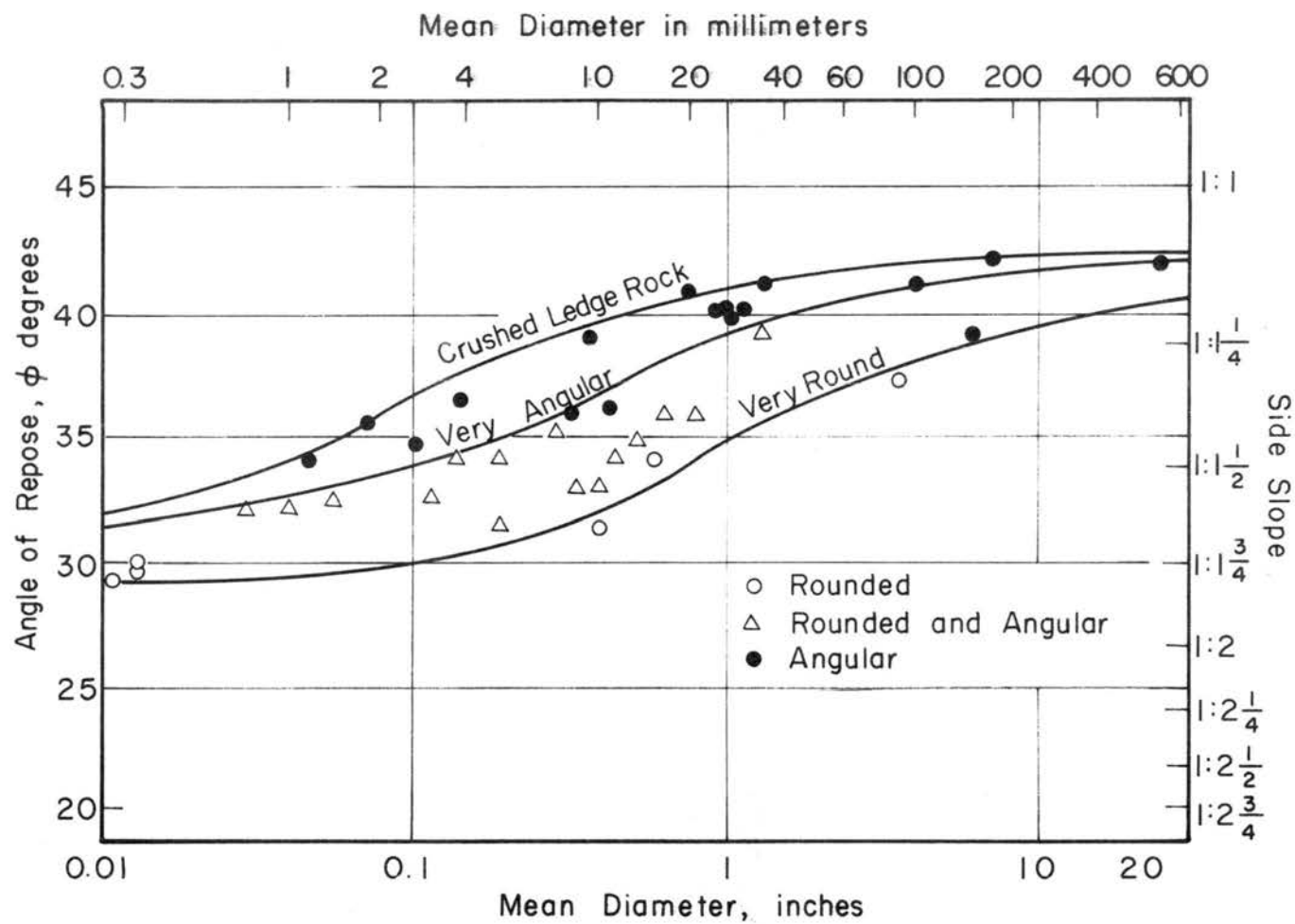


Fig. 9 Angle of Repose of Non-cohesive Material from Simons (72)

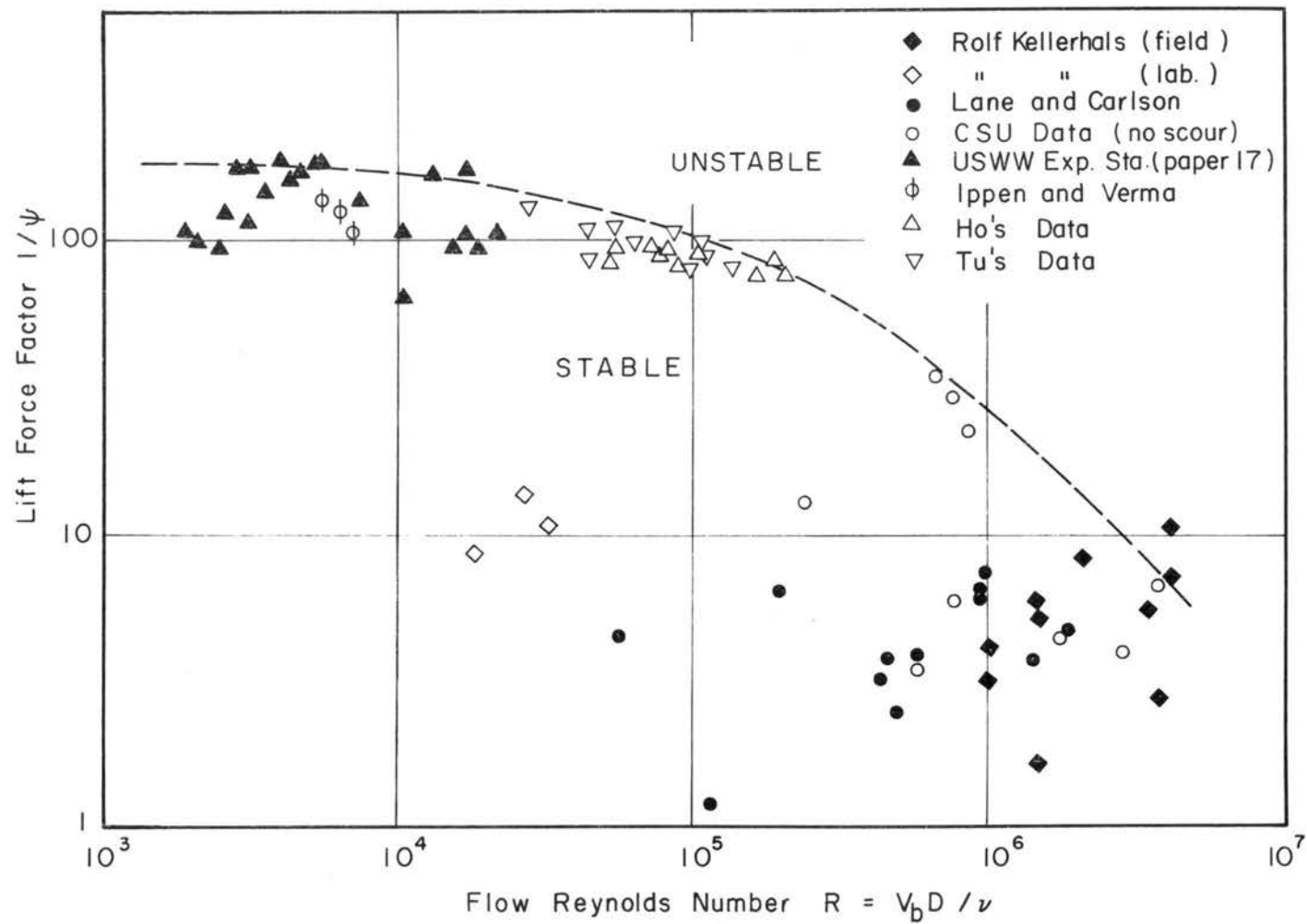


Fig. 10  $1/\psi$  Versus Flow Reynolds Number from Bhowmik and Simons (9)

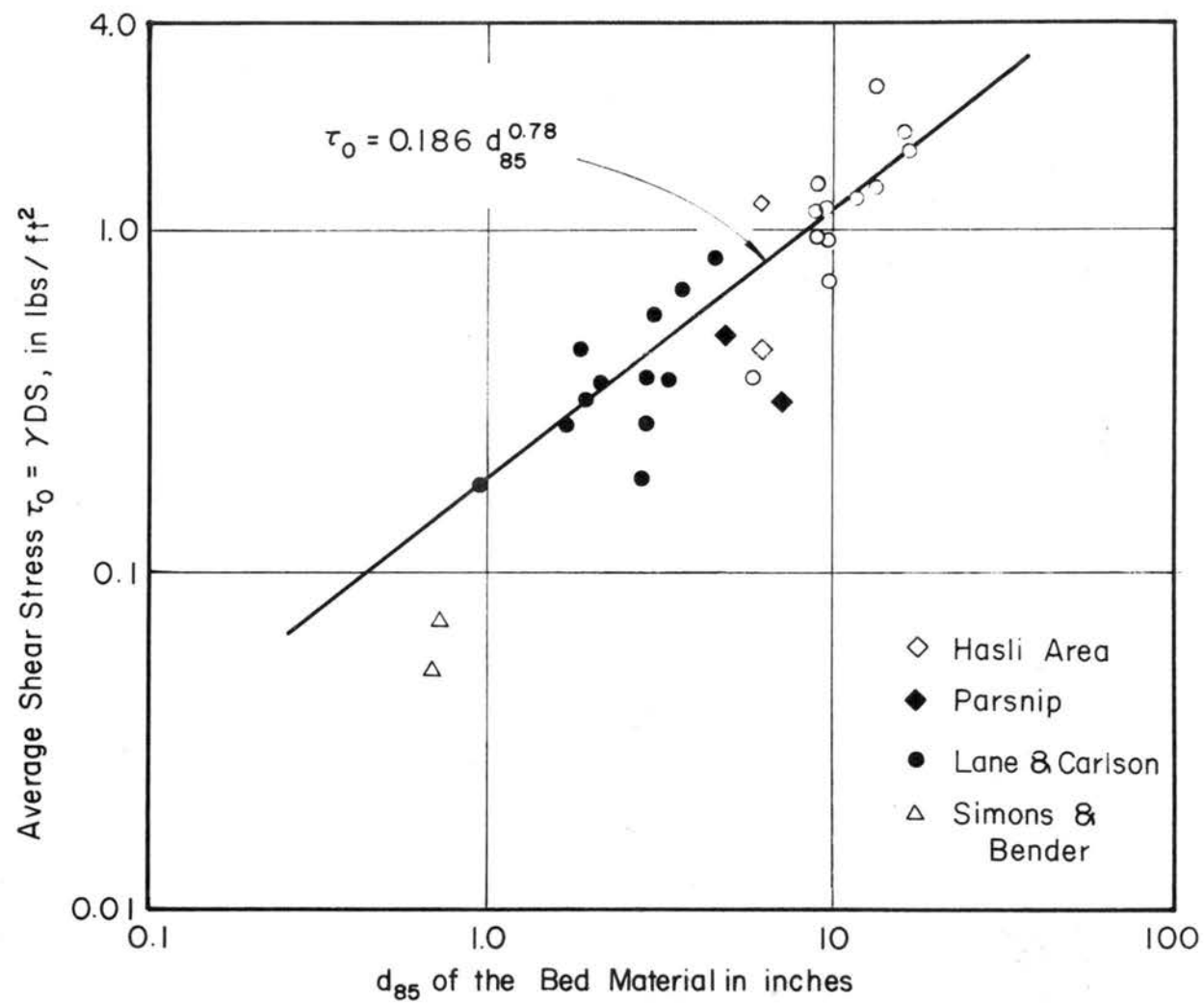


Fig. 11 Relation Between Average Shear Stress and  $d_{85}$  Size of the Bed Material from Bhowmik and Simons (9)

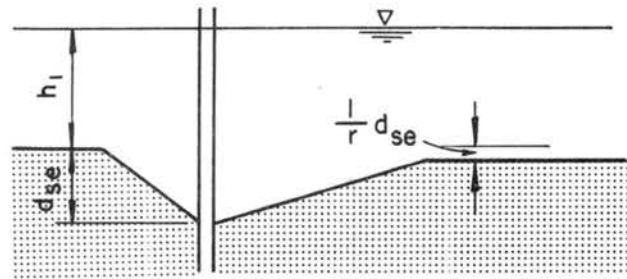


Fig. 12 Definition Sketch for Pier and Abutment from Laursen (45)

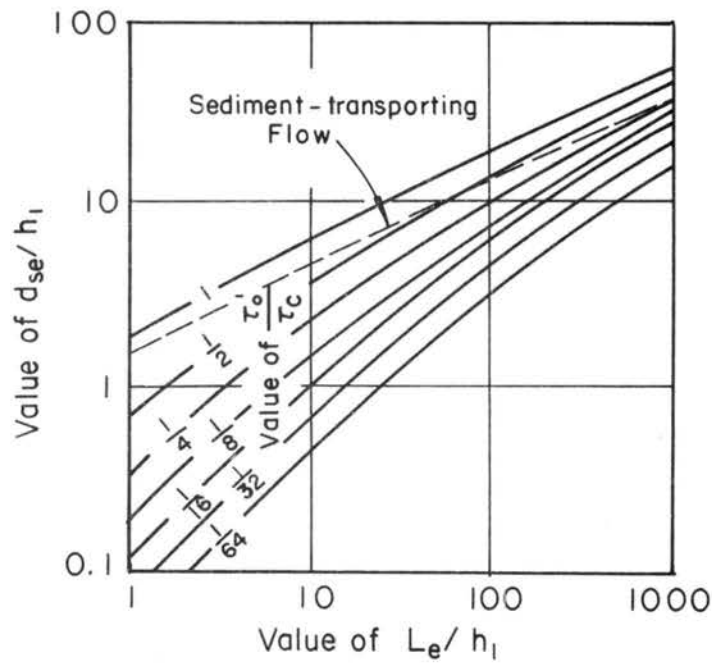


Fig. 13 Clear-water Scour at an Abutment from Laursen (45)

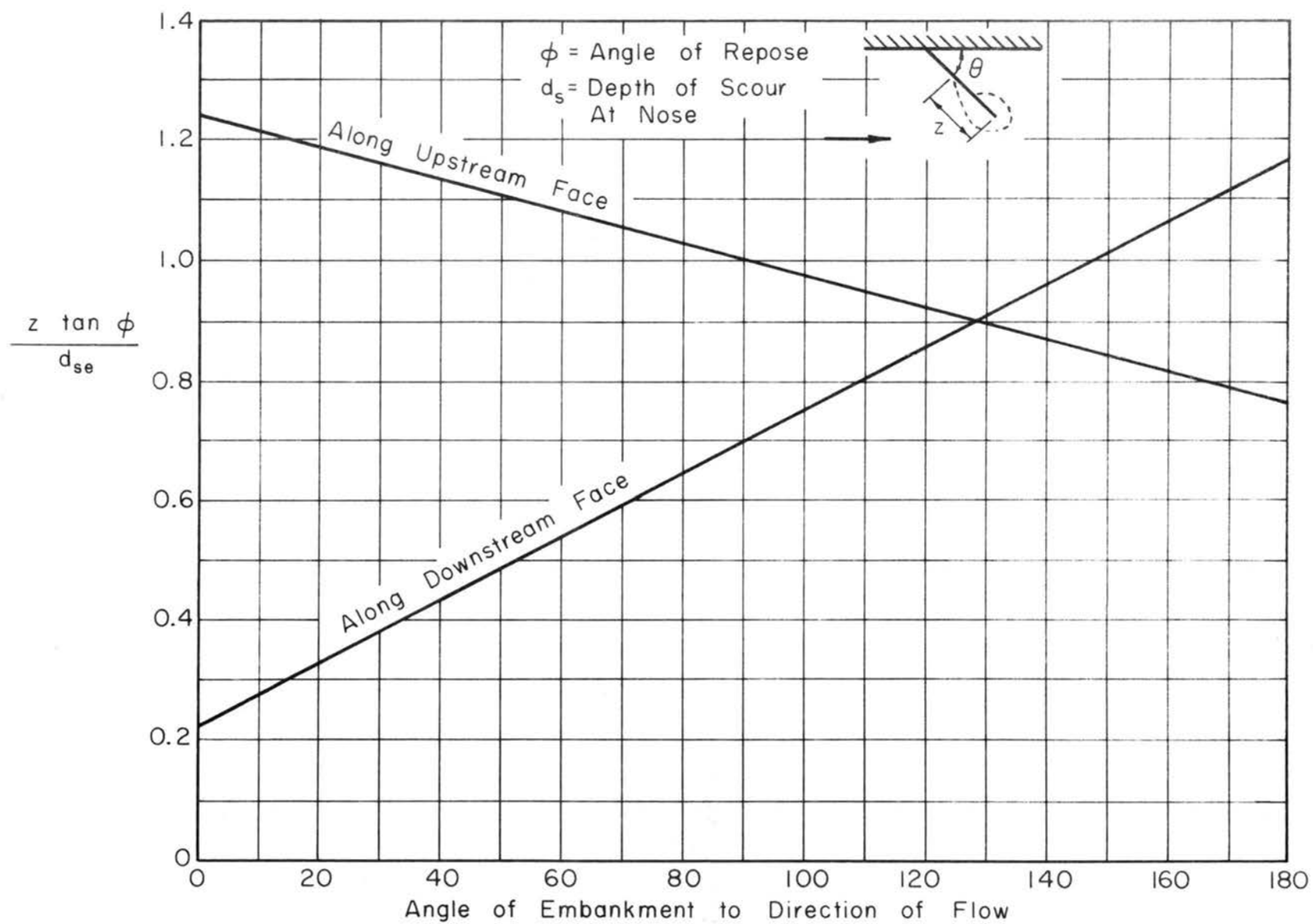


Fig. 14 Length Requiring Protection Against Scour as a Function of Embankment Skew from Field (23)

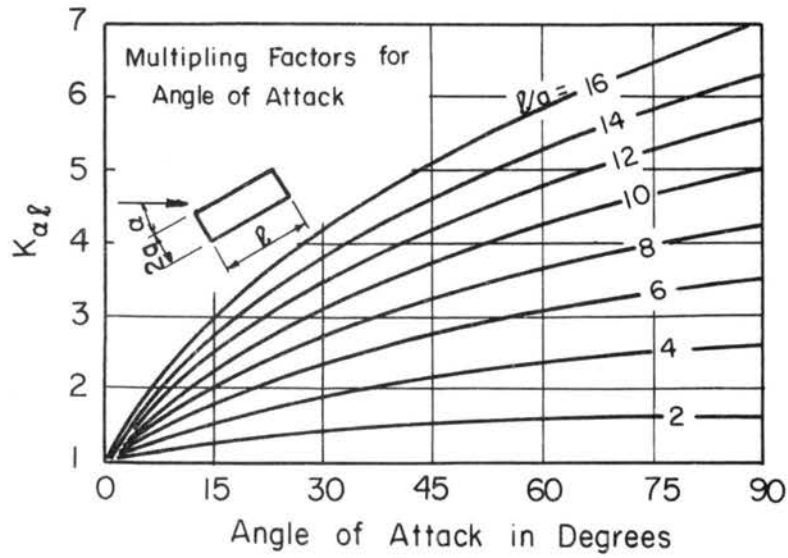


Fig. 15 Design Factors for Piers Not Aligned with Flow from Laursen and Toch (51)

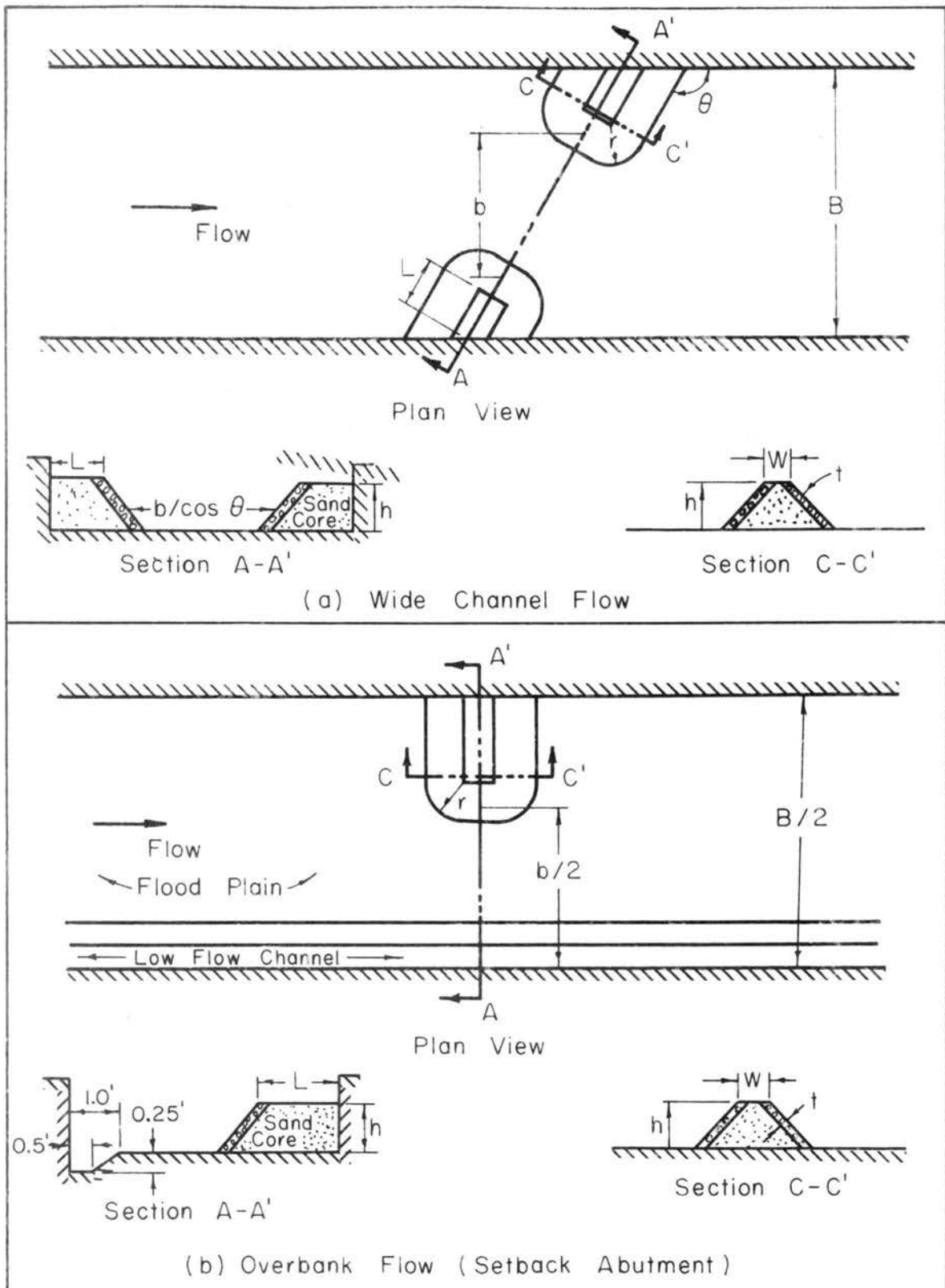


Fig. 16 Model Geometry Variables for the Spill-through Abutments in Table 1



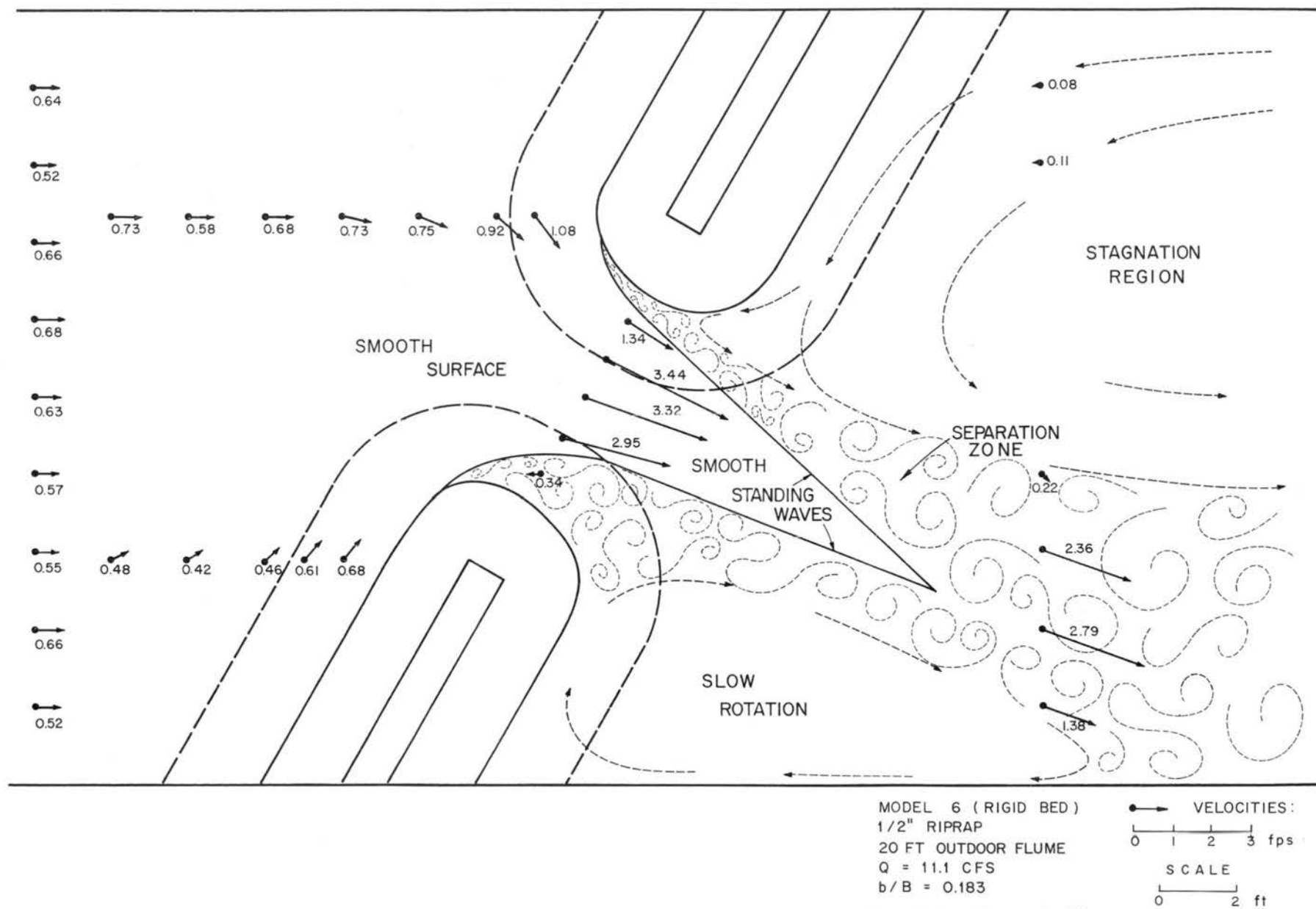
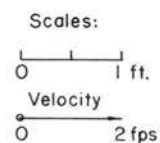
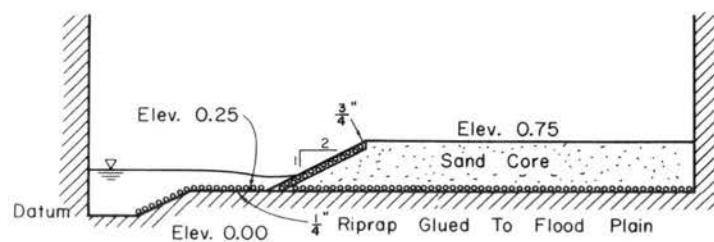
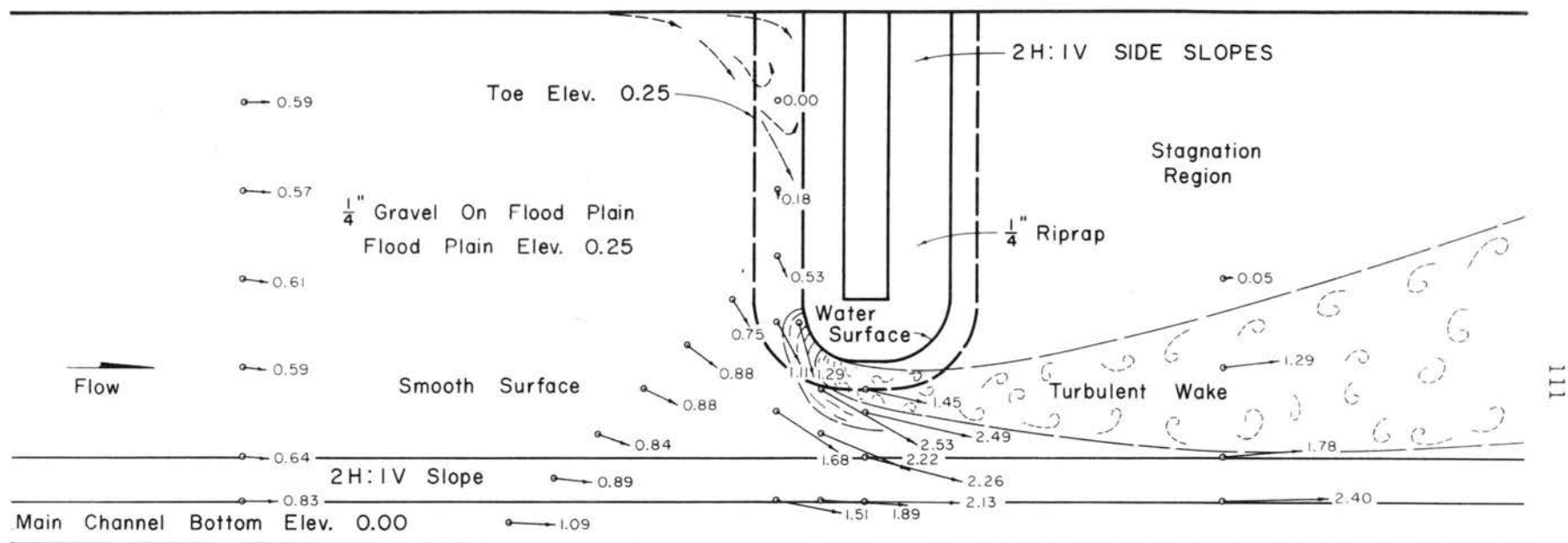
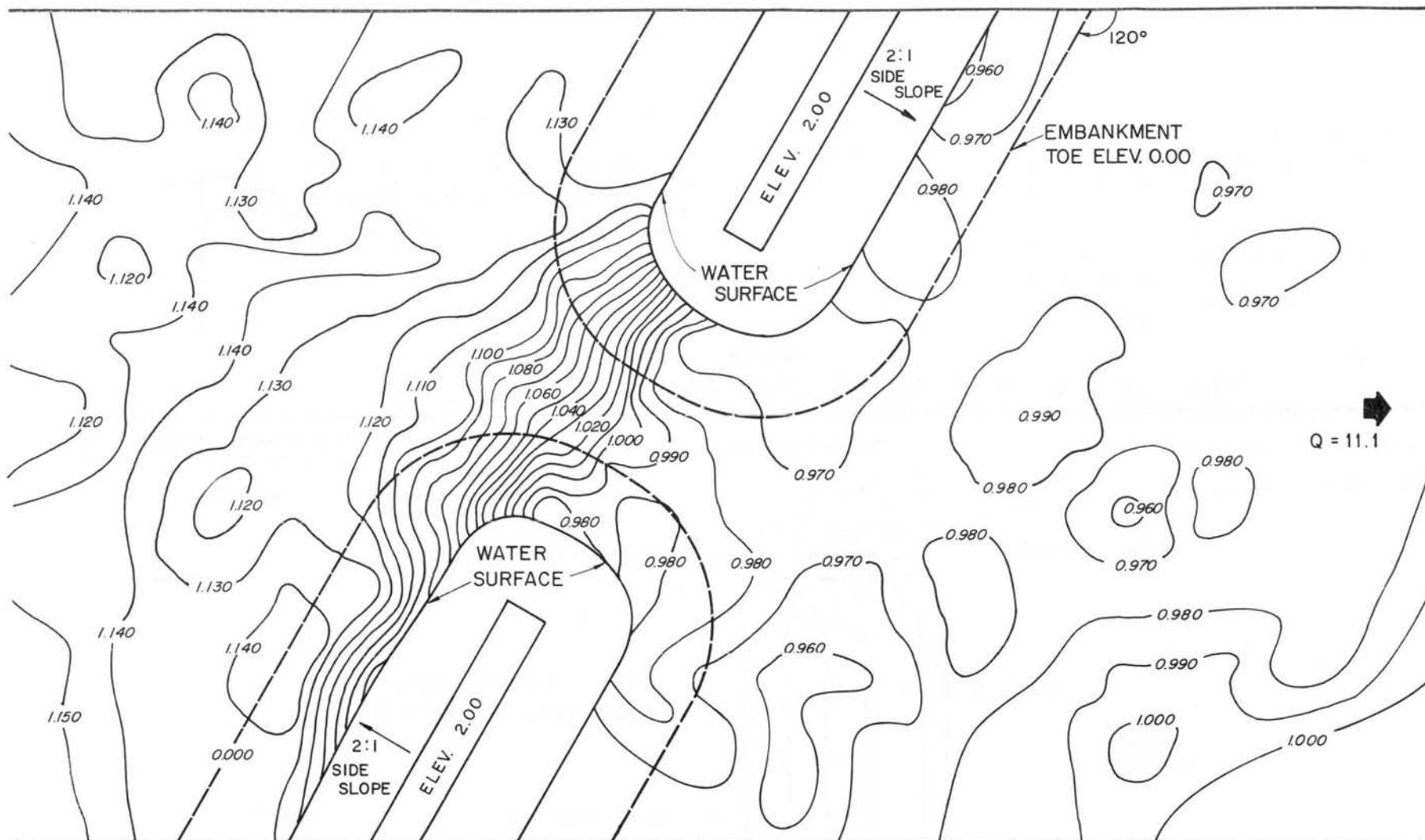


Fig. 17 Measured Velocities and Water Surface Patterns for Wide Channel Flow

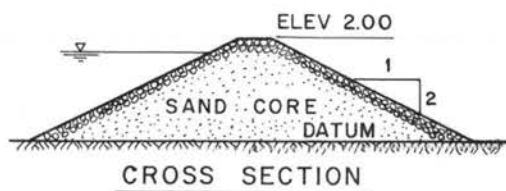


Overbank Flow  
 Model 7 Six-foot Wide Flume  
 Riprap  $d_{50} = 0.230$ " &  $d_m = 0.238$ "  
 $\frac{1}{4}$ " Riprap On Floodplain & Main Channel Wall  
 Plywood Main Channel Bottom  
 $Q = 1.02$  cfs  
 Flow Depth 16' Upstream Of  $\zeta = 0.529'$   
 Flow Depth 16' Downstream Of  $\zeta = 0.403'$   
 Velocities Are Averages Through The Depth  
 Velocity Directions From Dye Streaklines

Fig. 18 Measured Velocities and Water Surface Patterns for Overbank Flow



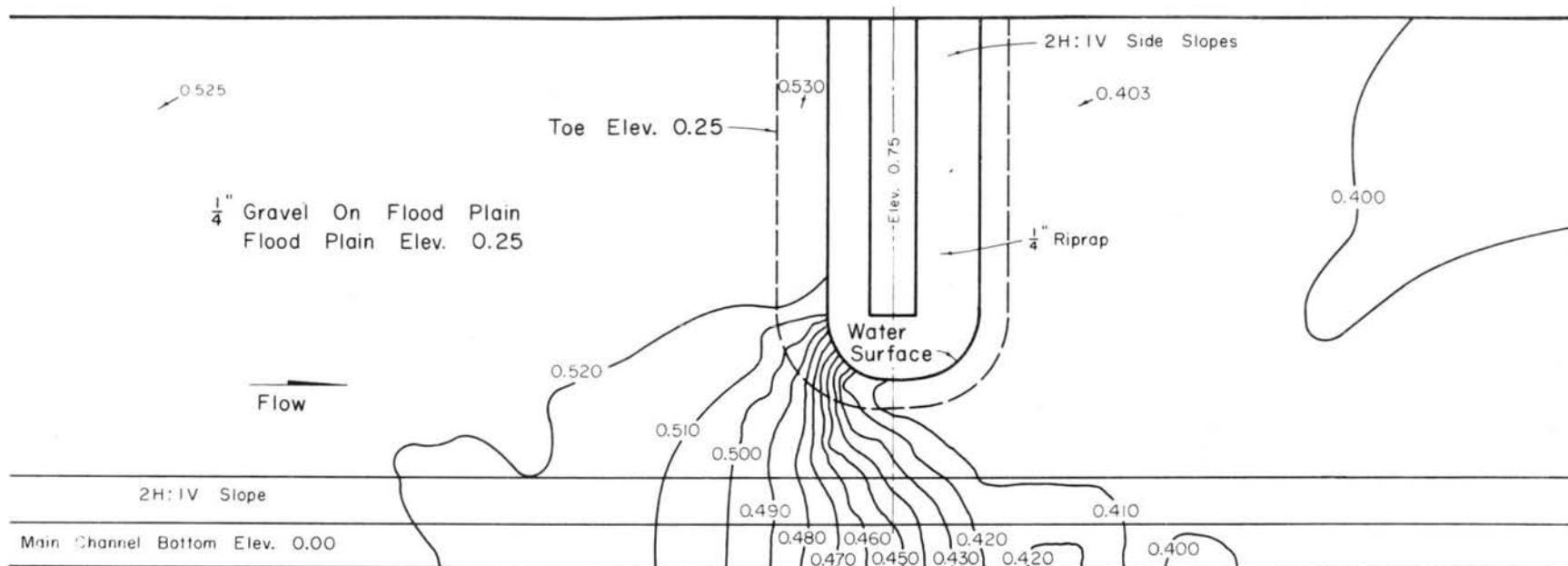
112



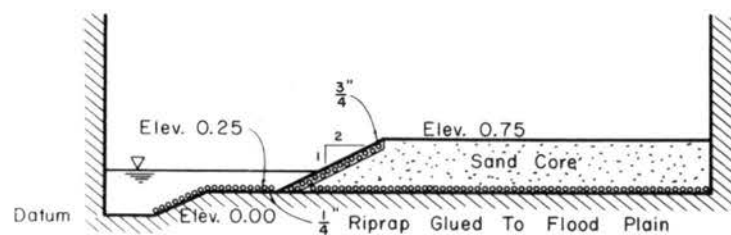
MODEL 6 (RIGID BED)  
1/2" RIPRAP  
20 FT OUTDOOR FLUME  
Q = 11.1 CFS  
b/B = 0.183

DATUM: FLUME BED  
SCALE  
0 2 ft  
INTERVAL = 0.010 FT  
FROM 2' x 2' GRID

Fig. 19 Water Surface Contours for Wide Channel Flow



### WATER SURFACE CONTOURS PLAN



### CENTERLINE CROSS SECTION

Scale  
0 1 ft.

Overbank Flow  
Model 7 Six-foot Wide Flume  
Riprap  $d_{50} = 0.230"$  &  $d_m = 0.238"$   
 $\frac{1}{4}$ " Riprap On Flood Plain & Main Channel Wall  
Plywood Main Channel Bottom  
 $Q = 1.02$  cfs  
Flow Depth 16' Upstream Of  $\zeta = 0.529'$   
Flow Depth 16' Downstream Of  $\zeta = 0.403'$   
Contour Interval = 0.010'  
Contours Drawn From 1' x 1' Grid

Fig. 20 Water Surface Contours for Overbank Flow

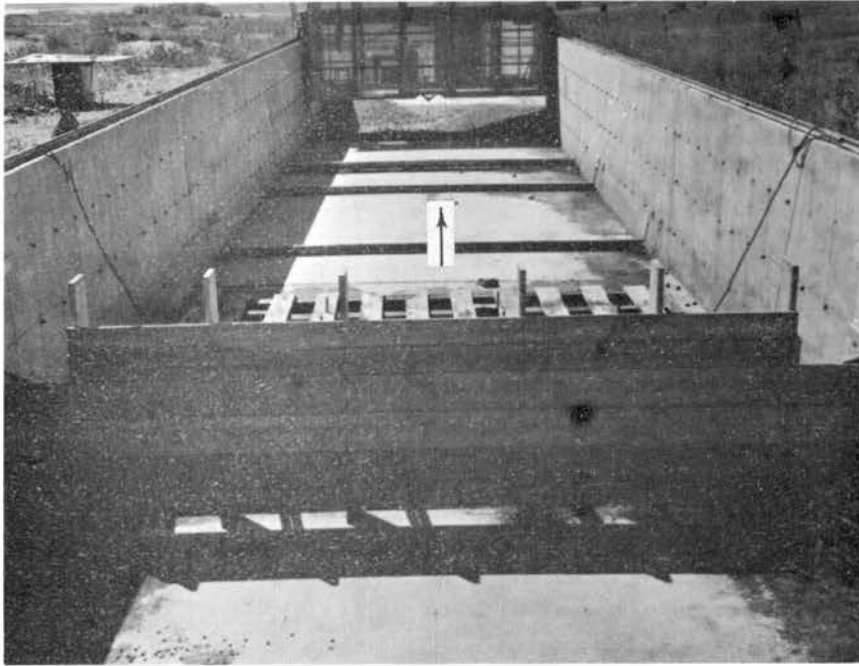


Fig. 21 - Photograph of the 20-foot wide flume showing the headbox, floating baffles, and rail-mounted instrument carriage



Fig. 22 - Photograph of the water surface characteristics for a skewed model at  $Q = 11.1$  cfs

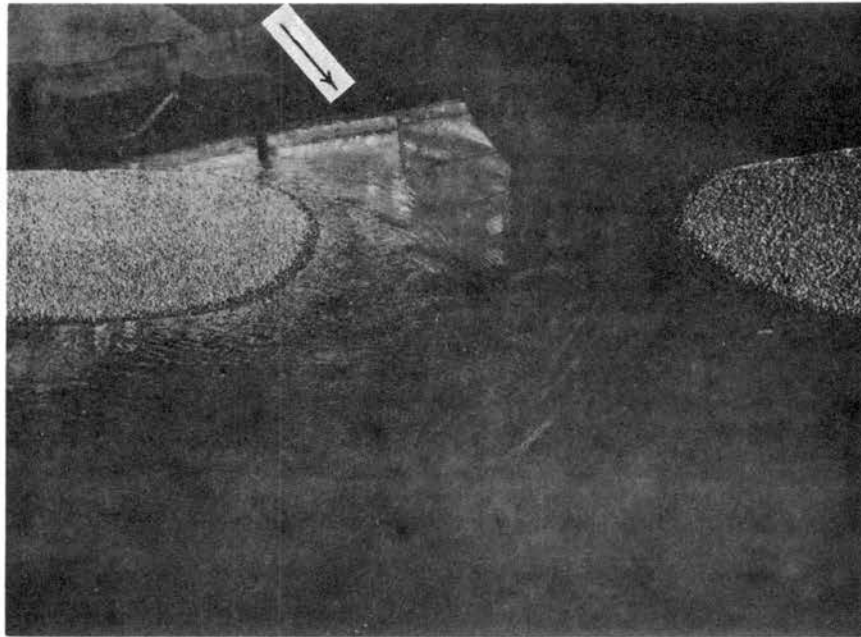


Fig. 23 - Photograph of the separation at the upstream embankment for the skewed model at  $Q = 11.1$  cfs

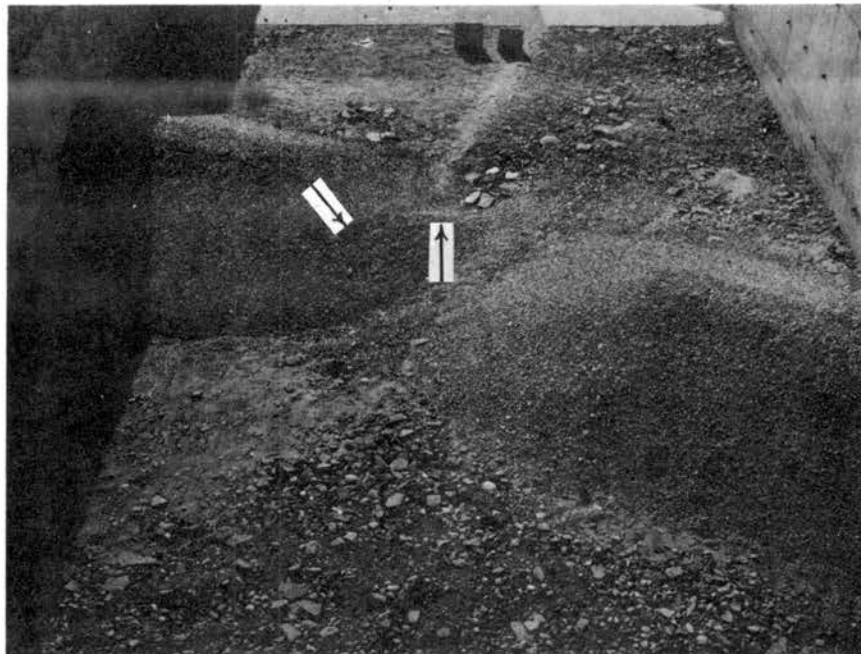


Fig. 24 - Photograph of the scour on the downstream abutment and the jet boundary for the skewed model at 11.1 cfs

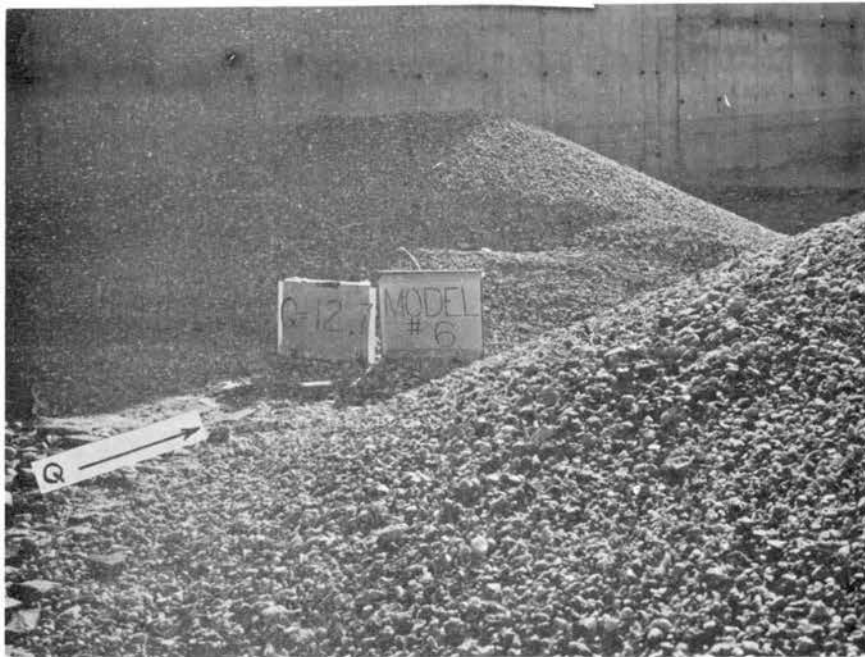


Fig. 25 - Photograph of the scour on the downstream abutment after increasing the discharge to 12.7 cfs



Fig. 26 - Photograph of the protected nose of the downstream embankment and the jet properties at  $Q = 13.9$  cfs



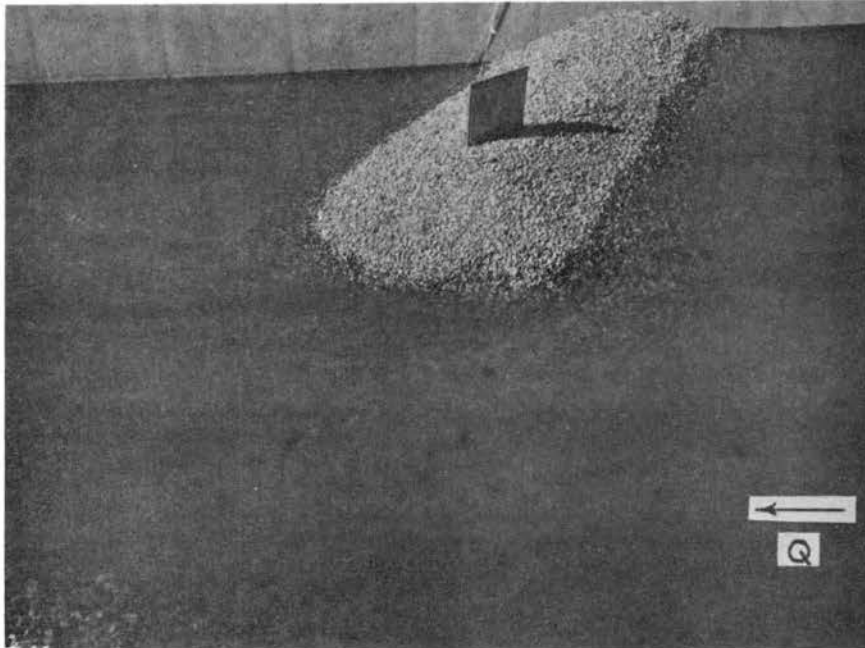


Fig. 27 - Photograph of the scour on the upstream abutment of Figure 26 for a discharge of 16.0 cfs

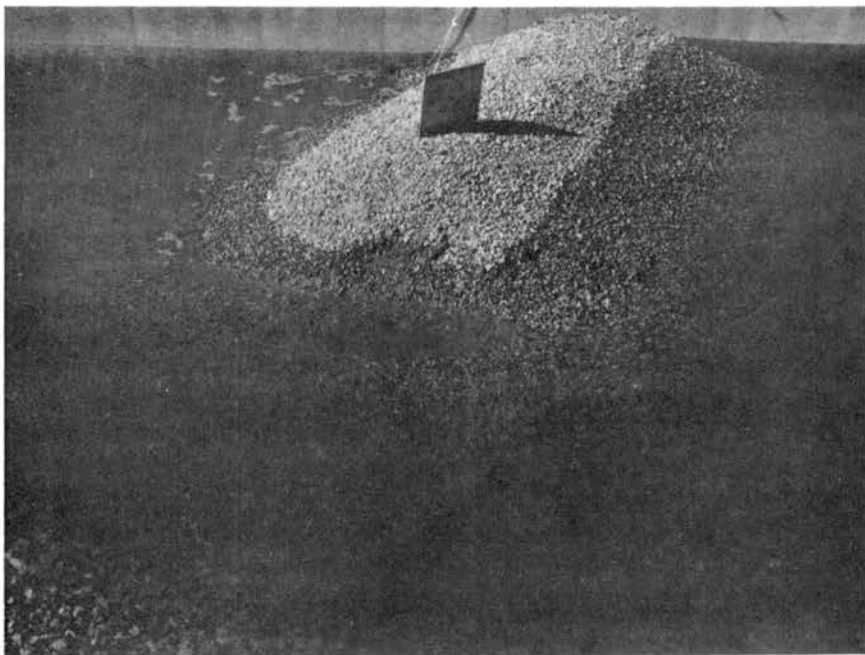


Fig. 28 - Photograph of the same abutment in still water after scour had reached the sand core



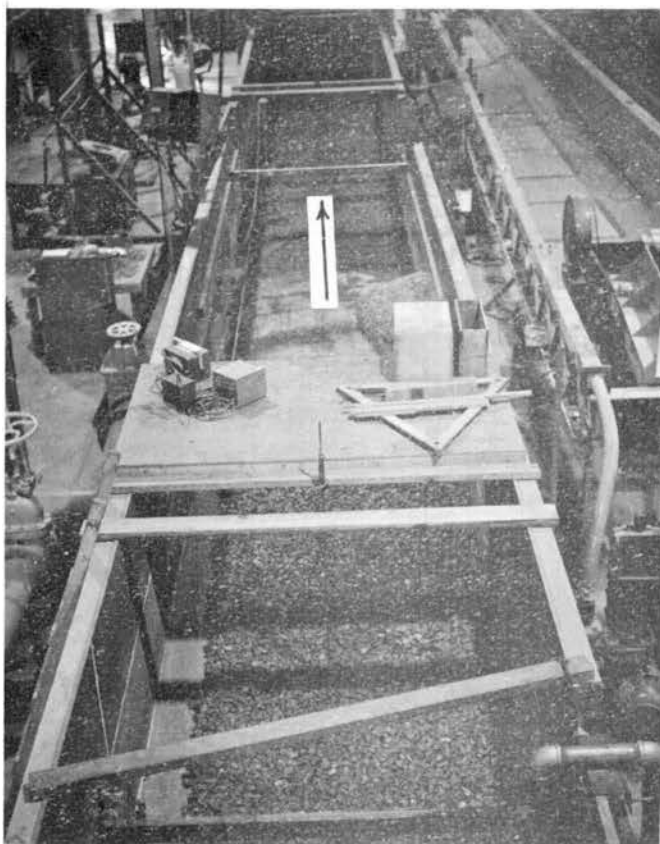


Fig. 29 - Photograph of the 6-foot wide flume showing the overbank-flow flood plain and the low-flow channel



Fig. 30 - Photograph of an overbank flow model which is set back from the low-flow channel

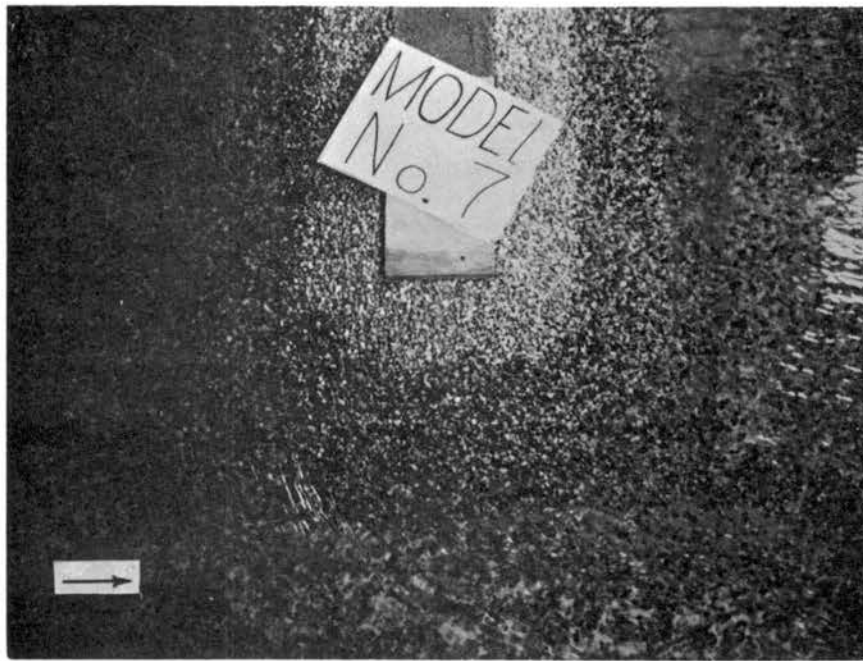


Fig. 31 - Photograph of the abutment for a discharge of 0.94 cfs showing the separation on the upstream (left) shoulder

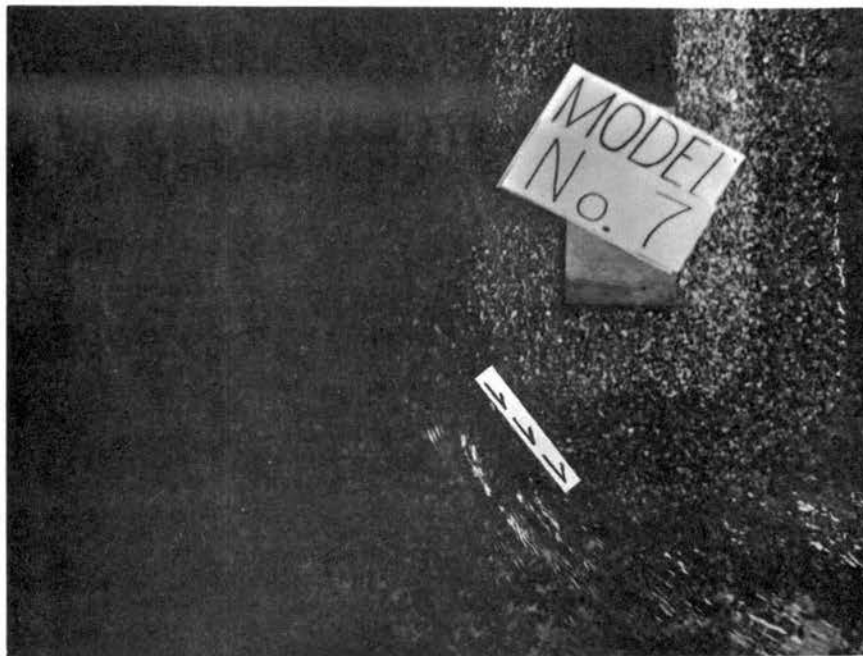


Fig. 32 - Photograph of the same abutment showing the scour at  $Q = 1.10$  cfs



Fig. 33 - Photograph of the abutment after draining the flume



Fig. 34 - Photograph looking downstream showing the scoured abutment and the deposition downstream

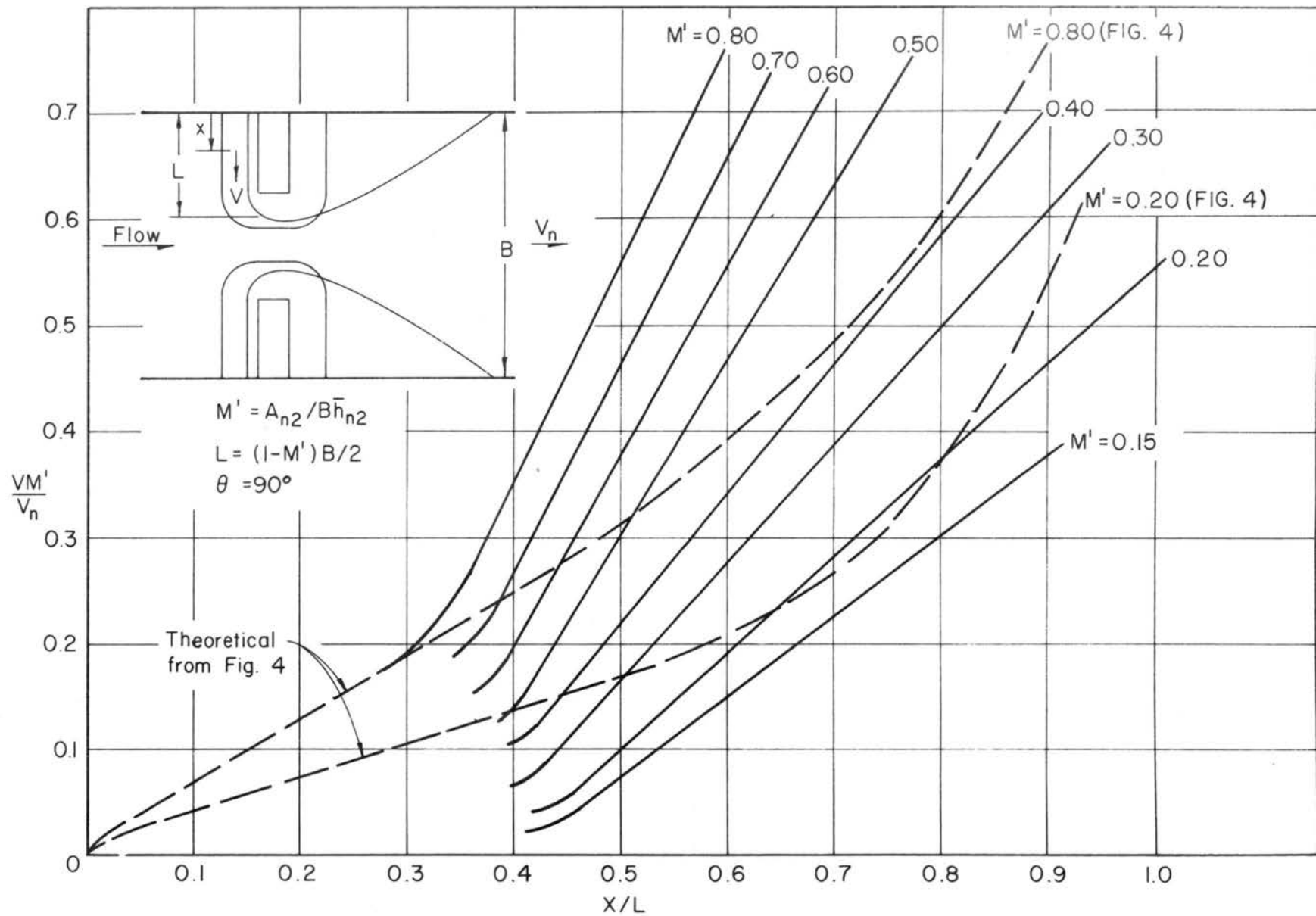


Fig. 35 Variation of Velocity on the Upstream Slopes of Approach Embankments

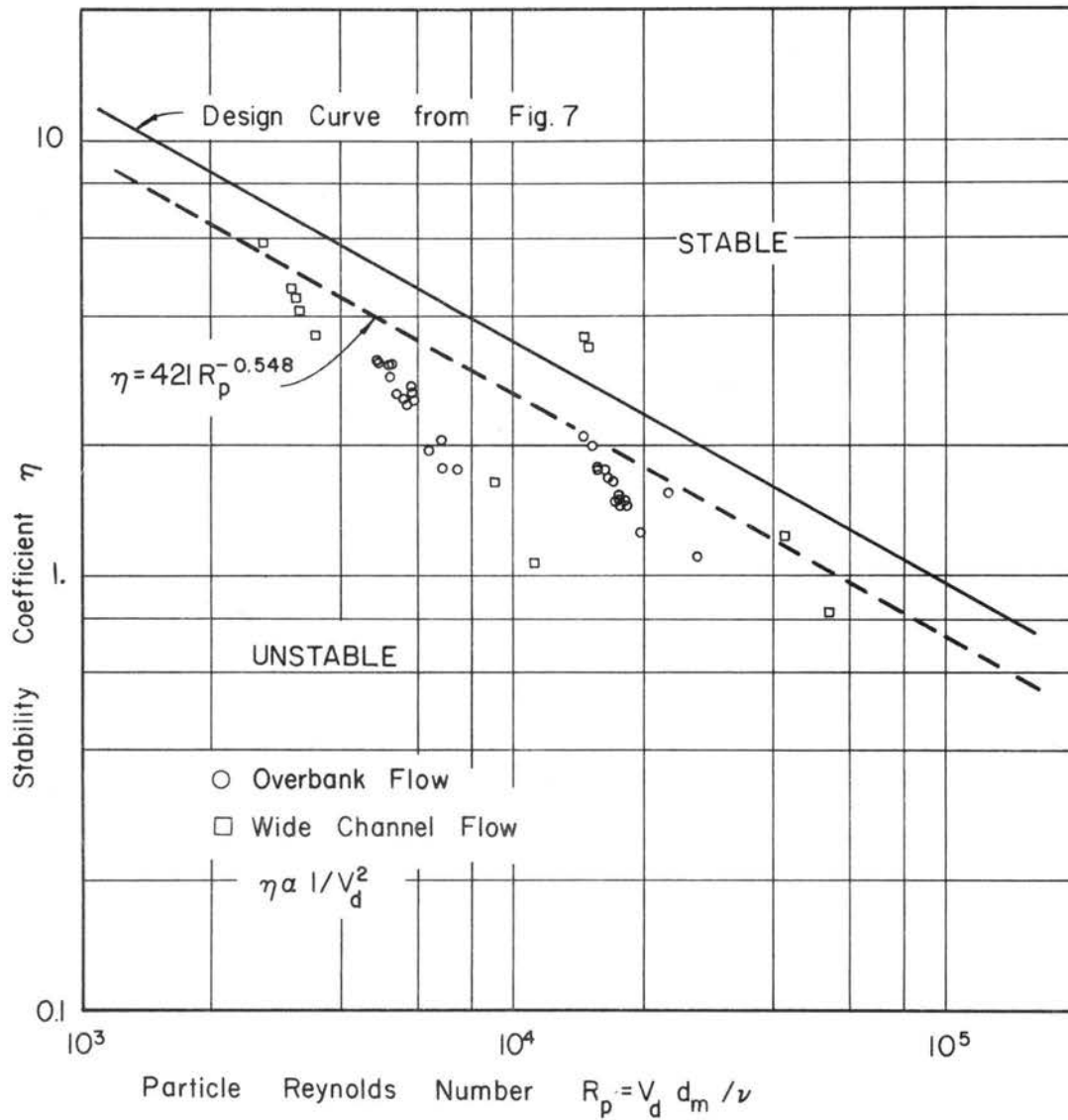


Fig. 36 Stability of Nose Riprap at Failure Conditions for Model Spill-through Abutments

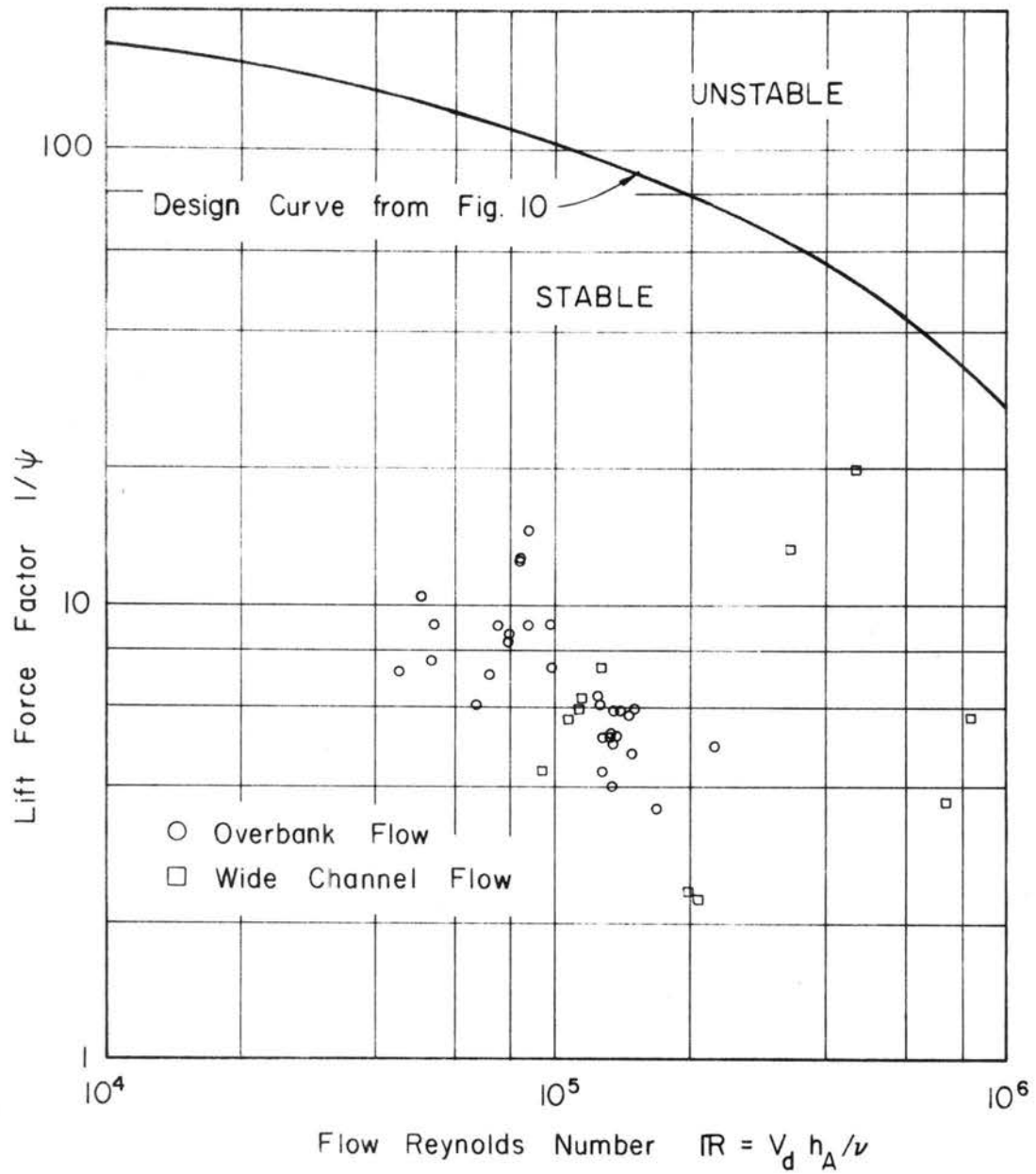


Fig. 37 Stability of the Nose Riprap  $d_m$  from Lift Forces Generated by the  $d_{85}$  Size for Model Spill-through Abutments

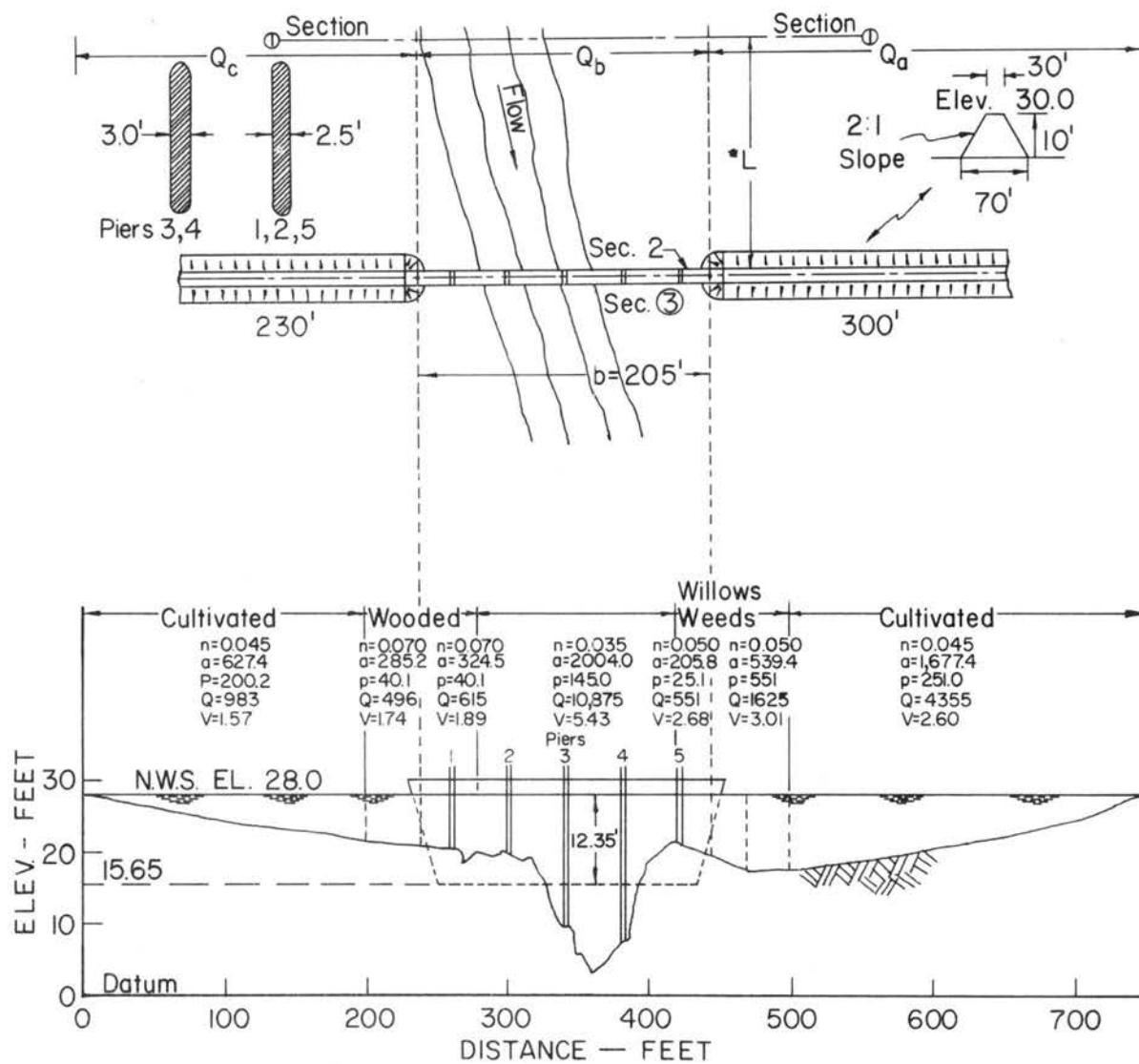


Fig. 38 Plan and Cross Section of Example Crossing from Bradley (14)

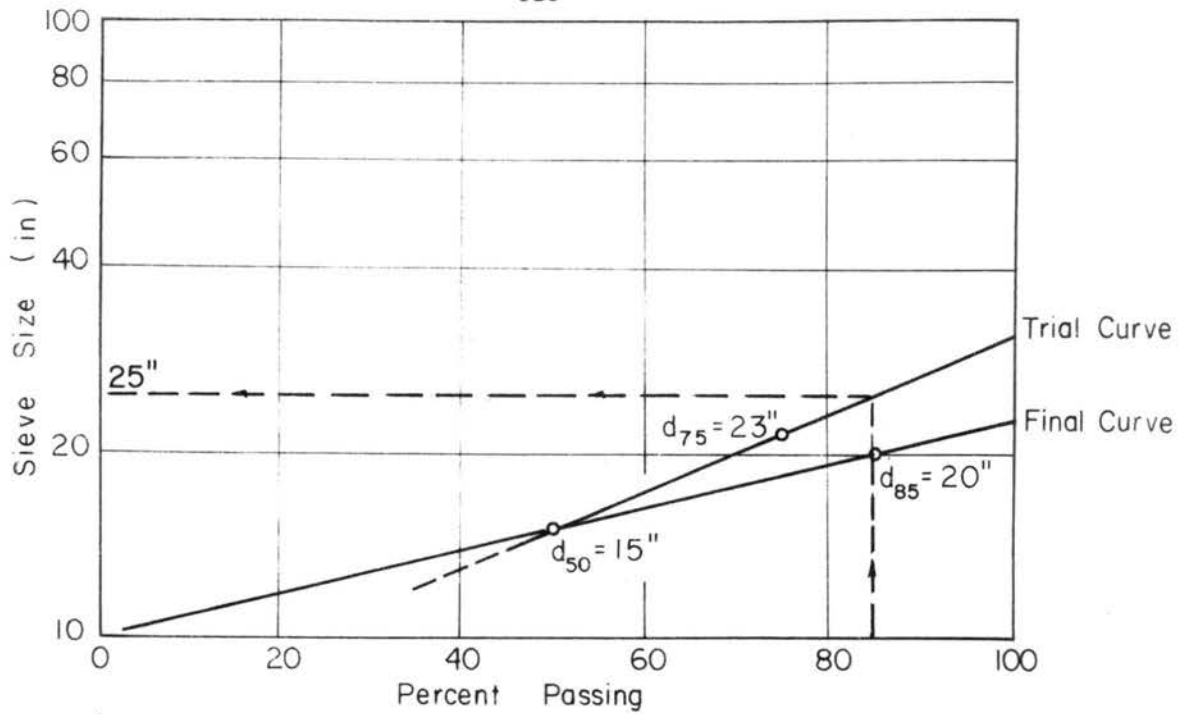


Fig. 39 Determination of  $d_{85}$  for Spill-slope Riprap in Example 1

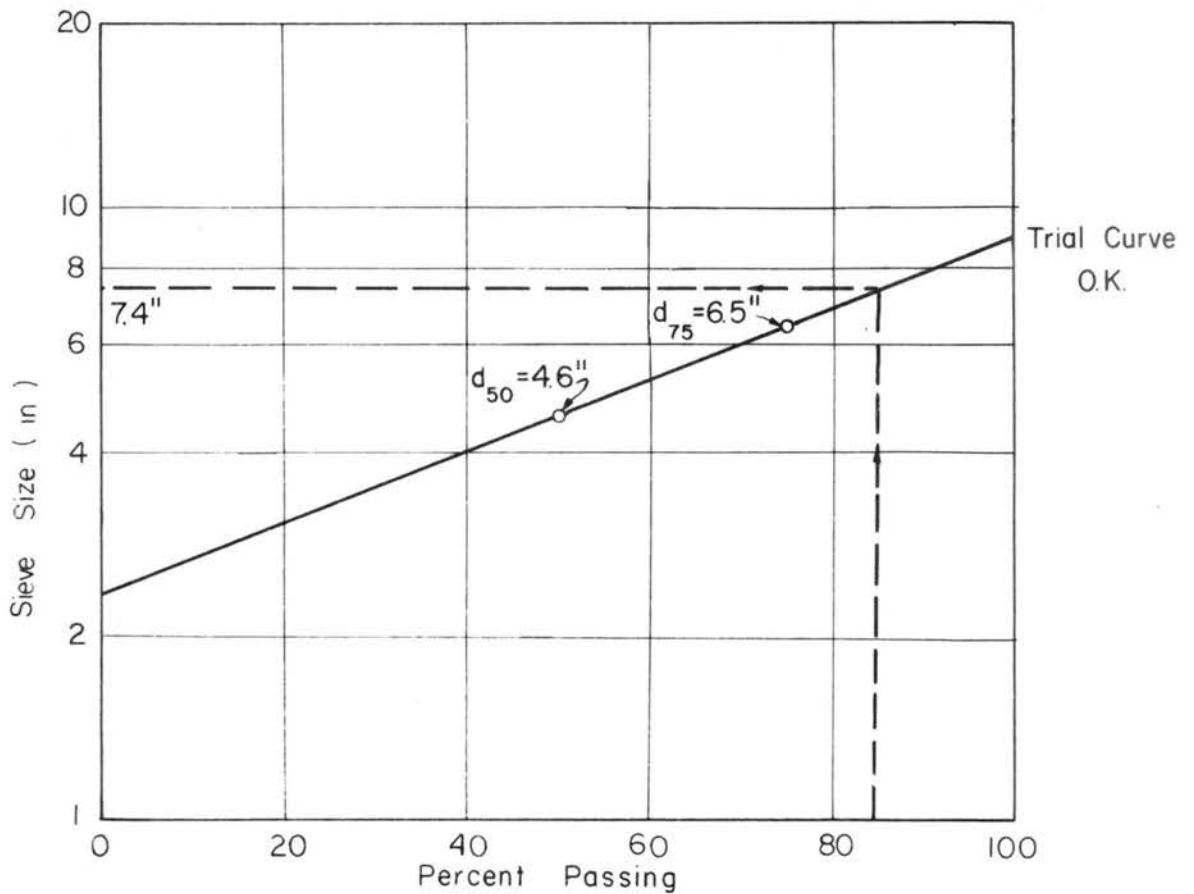
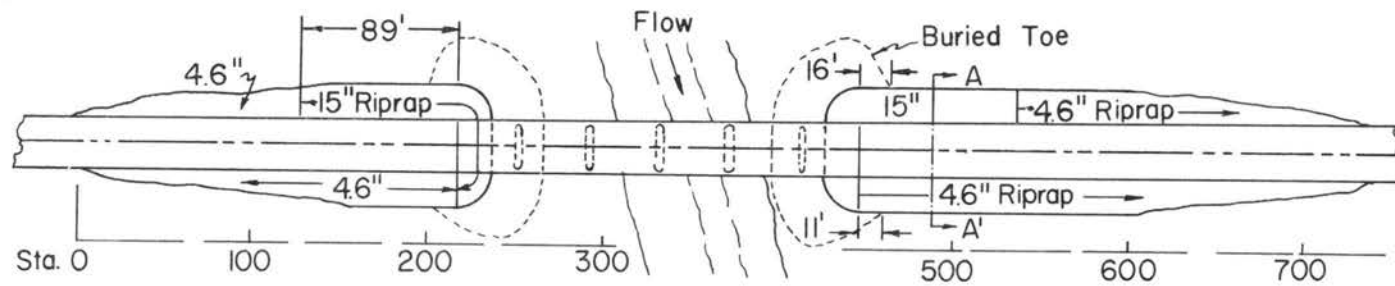
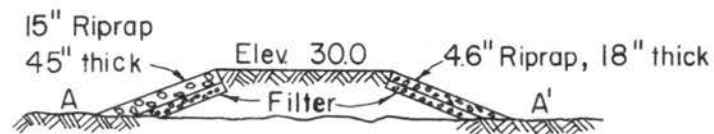


Fig. 40 Determination of  $d_{85}$  for Upstream Embankment Protection in Example 1

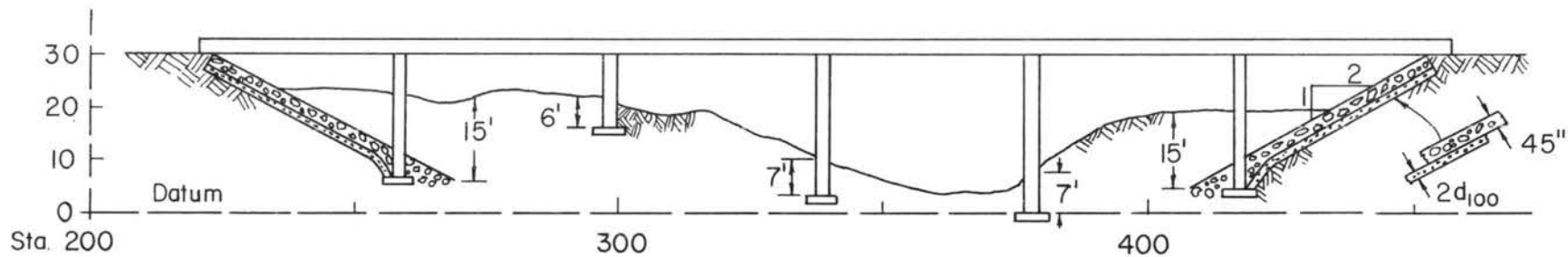




(a) Plan



(b) Section A-A'



(c) Elevation (Vertical Scale = Horizontal Scale)

Fig. 41 Summary of Design Requirements for Example

APPENDIX B  
BACKWATER AND TOTAL WATER SURFACE DROP  
THROUGH THE ABUTMENTS

# COMPUTATION OF BACKWATER AND TOTAL DROP THROUGH THE ABUTMENTS

Methods for computing the backwater and the total drop through the abutments are summarized here from "Hydraulics of Bridge Waterways" (14) for convenience in design. The methods are intended to be used for relatively straight reaches of streams having approximately uniform slope.

There are four types of flow which may be encountered in bridge waterway design. They are as follows:

Type I flow: Subcritical flow (Fig. 1a),

Type IIa flow: Critical flow in the gap (Fig. 1b),

Type IIb flow: Critical flow (Fig. 1c),

Type III flow: Supercritical flow (Fig. 1d), and

Type IV flow: Abnormal flow (Fig. 1e).

Procedures of computing the backwater,  $h_1^*$ , and the total drop through the abutments,  $\Delta h$ , for each type of flow under a bridge on a rigid bed are presented in Sections 1 and 2, respectively. Section 3 considers the effect of scour on backwater. Sections 4 and 5 cover the cases of dual bridges and the superstructure partially inundated.

## 1. Computation of Backwater

a) Type I flow: Subcritical flow (Fig. 1a).

The expression for computation of backwater upstream of a bridge constriction is

$$h_1^* = K^* \alpha_2 \frac{V_{n2}^2}{2g} + \alpha_1 \left[ \left( \frac{A_{n2}}{A_{n4}} \right)^2 - \left( \frac{A_{n2}}{A_1} \right)^2 \right] \frac{V_{n2}^2}{2g}, \quad (B1)$$

where  $\alpha_2$  is the velocity head coefficient for the constriction, and  $K^*$  is the total backwater coefficient. The other symbols are defined in Chapter III and in Figure 1.

To compute backwater, it is necessary to obtain the approximate value of  $h_1^*$  by using the first part of Equation B1

$$h_1^* = K^* \alpha_2 \frac{V^2}{2g} ,$$

where  $\alpha_2$  can be found from Figure B1 with known  $M$  and  $\alpha_1$ . The value of  $A_1$  in the second part of Equation B1 can then be determined, and the total backwater can be computed from Equation B1 if the value of  $K^*$  is known.

b) Computation of  $K^*$

Figure B.2 shows the base curves for the backwater coefficient,  $K_b$ , plotted with respect to the opening ratio,  $M$ , for wingwall and spill-through abutments. In the case of a normal crossing without piers,  $K^* = K_b$ .

Backwater caused by piers in a bridge constriction may be estimated by adding an incremental backwater coefficient, designated as  $\Delta K_p$ , to the base curve coefficient,  $K_b$ , when piers are present in the waterway. For a normal crossing with piers, the total backwater coefficient becomes

$$K^* = K_b \text{ (Fig. B.2)} + \Delta K_p \text{ (Fig. B.5)} .$$

The magnitude of the incremental backwater coefficient,  $\Delta K_e$ , accounting for the effect of eccentricity, is shown in Figure B.6. The total backwater coefficient for an extremely eccentric crossing ( $e > 0.8$ ) with wingwall or spill-through abutments and piers is

$$K^* = K_b \text{ (Fig. B.2)} + \Delta K_p \text{ (Fig. B.5)} + \Delta K_e \text{ (Fig. B.6)} .$$

Figure B.7 shows the incremental backwater coefficient,  $\Delta K_s$ , for the effect of skewness of wingwall and spill-through abutments. The total backwater coefficient for a skewed crossing with piers and abutment faces aligned with the flow would be

$$K^* = K_b \text{ (Fig. B.2)} + \Delta K_p \text{ (Fig. B.5)} + \Delta K_s \text{ (Fig. B.7)} .$$

c) Type II flow: Critical flow (Figs. 1b and 1c).

The curve of Figure B.8 accounts for the contraction ratio only, which is the major factor involved. The effect of piers, eccentricity, and skew, have not been evaluated because of the tentative nature of the curve. The incremental coefficients from Figures B.5, B.6 and B.7 for piers, eccentricity, and skew, are not applicable to Type II flow problems.

The backwater for Type II flow, with no allowance for piers, eccentricity, and skew, is

$$h_1^* = \alpha_2 \frac{V_{2c}^2}{2g} (C_b + 1) - \alpha_1 \frac{V_1^2}{2g} + h_{2c} - \bar{h}_{n2} ,$$

where  $C_b$  can be found from Figure B.8 with known  $M$ ,  $\alpha_2$  can be found from Figure B.1, and the other symbols are defined in Chapter III and Figure 1.

d) Type III flow: Supercritical flow (Fig. 1d).

Theoretically, there is no backwater produced by Type III flow. No detailed information is available for supercritical flow occurring both upstream and downstream of a bridge constriction.

e) Type IV flow: Abnormal flow (Fig. 1e and Fig. B.9).

From the laboratory studies, the curves for the base backwater coefficients and the incremental backwater coefficients for Type I flow

(subcritical flow) are reasonably applicable to abnormal stage-discharge conditions. The expression for the computation of backwater for abnormal stage-discharge is

$$h_{1A}^* = K^* \alpha_2 \frac{V_{2A}^2}{2g} ,$$

where

$$K^* = K_b(\text{Fig. B.2}) + \Delta K_p(\text{Fig. B.5}) + \Delta K_e(\text{Fig. B.6}) + \Delta K_s(\text{Fig. B.7}) .$$

The subscript, A , has been added throughout to signify that this is an abnormal case. The symbols are defined in Fig. B.9.

f) Recognition of flow type

Recognition of which type of flow will occur at a proposed bridge site in the field, prior to starting the backwater computations, is difficult. As a suggestion, try the Type I flow approach for computing backwater first. Should the result appear unrealistic, repeat the backwater computation using the Type II approach. If the backwater for the Type II flow results in a lower value than for the Type I computation, the flow definitely will be Type II.

2. Computation of Total Drop Through the Abutments

a) Type I flow: Subcritical flow.

The expression for computation of total drop through the abutments is

$$\Delta h = h_1^* - h_3^* + S_o L_{1-3} ,$$

where  $h_1^*$  is the backwater computed by the method described in Section 1,  $h_3^*$  is the vertical distance from the water surface on the downstream side of the abutment to the normal water surface (Figs. 1 and B.10),  $S_o$  is

the natural slope of the stream, and  $L_{1-3}$  is the distance from Section 1 to Section 3 (Fig. 1). The methods of determining  $h_3^*$ ,  $L_{1-3}$ , and  $\Delta h$  are explained as follows:

b) Computation of  $h_3^*$

The differential level ratio,  $D_b = h_b^*/(h_b^* + h_3^*)$ , is plotted with respect to the opening ratio,  $M$ , in Figure B.10. The expression for computation of  $h_3^*$  in the case of normal crossings without piers is

$$h_3^* = h_b^* \left( \frac{1}{D_b} - 1 \right),$$

where  $h_b^*$ , which represents the backwater at a bridge for normal crossings exclusive of pier effect, can be determined by the method of computing backwater (Section 1). With a value of  $K^* = K_b$  (Fig. B.2),  $D_b$  can be found from Figure B.10.

The effect of piers on the differential level ratio,  $D_b$ , is quite small and can be neglected. The expression for computation of  $h_3^*$  is

$$h_3^* = h_1^* \left( \frac{1}{D_b} - 1 \right),$$

where  $h_1^*$  is the computed backwater, including the effect of piers, and  $D_b$  can be found from Figure B.10.

For an extremely eccentric crossing with or without piers, the total differential level ratio is

$$D^* = D_b + \Delta D_e,$$

where  $\Delta D_e$  is the incremental differential level ratio in Figure B.11, accounting for the effect of eccentricity. The expression for computation of  $h_3^*$  is

$$h_3^* = h_1^* \left( \frac{1}{D_b} - 1 \right) ,$$

where  $h_1^*$  is the computed backwater, including effects of eccentricity, with or without piers (Section 1).

The incremental differential level ratio,  $\Delta D_s$ , for the effect of skew has been plotted with respect to  $M$  in Figure B.12 for the left bank of wingwall and spill-through abutments. No detailed information is available for the difference in water level along the right bank.

c) Computation of  $L_{1-3}$  and  $\Delta h$

A trial solution is required for determining  $\Delta h$ . Enter Fig. B.13A with appropriate values of  $\Delta h/\bar{h}_{n2}$  and  $\bar{h}_{n2}$ , and obtain the corresponding value of  $L^*/b$ , where the distance  $L^*$  is defined in Figure B.13, and  $\bar{h}_{n2}$  is the mean depth of flow under the bridge, referenced to normal stage (Fig. 1).

Solving for  $L^*$  and adding the distance to Section 3 gives the distance  $L_{1-3}$  (Fig. B.13B). An estimate for  $\Delta h$  is  $h_1^* + h_3^* + S_o L_{1-3}$ . If the computed value of  $\Delta h$  differs materially from the value chosen, the above procedure is repeated until assumed and computed values agree.

For eccentric crossings with  $e > 0.7$ , multiply the  $L^*/b$  value from Figure B.13C by  $\omega$ . For example, assume that  $\Delta h/\bar{h}_{n2} = 0.2$ ,  $\bar{h}_{n2} = 10$ , and  $e = 0.88$ . The corrected value would be  $L^*/b = 0.84 \times 1.60$ , or 1.34.

To obtain the approximate distance to maximum backwater,  $L^*$ , and  $\Delta h$  for skewed crossings (Fig. B.4), the same procedure is recommended as for normal crossings except that the ordinate of Figure B.13 is read as  $L^*/b_s$ , where  $b_s$  is the distance between the skewed abutments (Fig. B.4).



d) Type IV flow: Abnormal flow.

To obtain  $\Delta h$  for abnormal stage-discharge conditions, Figure B.10 is considered approximate but applicable. The method of computation is similar to that explained in Section 2a for normal stage-discharge. The principal differences lie in the manner in which the backwater is computed for abnormal stage conditions. The expression for computation of  $h_{3A}^*$  is

$$h_{3A}^* = h_{bA}^* \left( \frac{1}{D_b} - 1 \right),$$

where

$D_b$  = differential level ratio from the base curve in Figure B.10

(no adjustment is needed for eccentricity or skew),

$h_{bA}^*$  = backwater above abnormal stage (without piers), and

$h_{3A}^*$  = vertical distance from the water surface to the abnormal stage at Section 3 (Fig. B.9 - this dimension will be the same with or without piers).

### 3. Effect of Scour on Backwater

Any means of increasing the waterway area under a bridge can be effective in reducing the backwater. To obtain backwater and related information for bridge sites where scour occurs before the flood peak, it is first necessary to compute the backwater and other quantities desired from the method outlined in Sections 1 and 2 for a rigid bed, using the original cross section of the stream at the bridge site. These values are then multiplied by a common coefficient from Figure B.15 as follows:

$$h_{1s}^* = Ch_1^*$$

$$h_{3s}^* = Ch_3^*$$

$$\psi h_s = C\psi h$$

where  $h_{1s}^*$ ,  $h_{3s}^*$ , and  $\psi h_s$  are defined in Figure B.14A, and  $A_s$  is the area of scour measured on the downstream side of the bridge (Figs. B.14B and B.14C).

#### 4. Dual Bridges

The following method for computing backwater and water surface drop through dual bridges is only applicable to Type I flow (subcritical flow).

##### a) Backwater determination.

The curve in Figure B.17 was established from tests made on normal crossings with and without piers. To determine backwater for dual bridges, it is necessary first to compute the backwater,  $h_1^*$ , for a single bridge, as previously outlined in Section 1. The backwater for the dual combination, measured upstream from the first bridge (Fig. B.17) is then

$$h_d^* = h_1^* \eta,$$

##### b) Computation of total drop through the abutments.

The water-surface level immediately downstream of the second bridge embankment at Section 3B may be obtained from Figure B.17. Compute  $h_1^*$  and  $h_3^*$  for the upstream bridge from Sections 1 and 3 and compute  $\psi h = h_1^* + h_3^*$  for the single bridge, and  $\psi h_{3B} = h_d^* + h_{3B}^*$  for the dual bridge combination. Using the ratio from Figure B.16, the value for  $h_{3B}^*$  is computed from

$$\psi h_{3B} = \xi \psi h,$$

$$\Delta h_{3B} = \psi h_{3B} + S_o L_{1-3B},$$

and

$$h_{3B}^* = \psi h_{3B} - h^*d ,$$

where all the parameters are defined in Figure B.17.

#### 5. Superstructure Partially Inundated (Type I flow only).

Cases arise in which it is desirable to compute either the backwater upstream of a bridge or the discharge under a bridge when flow is in contact with the girders.

##### a) Case I: Upstream girder in flow (Fig. B.18).

Once flow contacts the upstream girder of a bridge, orifice flow is established. Using a common expression for sluice-gate flow

$$Q = C_d b_N Z \left[ 2g \left( h_u - \frac{Z}{2} + \alpha_1 \frac{V_1^2}{2g} \right) \right]^{1/2} , \quad (B2)$$

where

$Q$  = total discharge (cfs),

$C_d$  = coefficient of discharge,

$b_N$  = net width of waterway excluding piers (ft),

$Z$  and  $h_u$  = vertical distances (see sketch in Fig. B.18).

The coefficient of discharge,  $C_d$ , is plotted with respect to the parameter  $h_u/Z$  in Figure B.18. By substituting values in Equation B2, it is possible to solve by trial and error for either the water surface upstream or the discharge under the bridge, depending on the quantities known. There is a transition zone somewhere between  $h_u/Z = 1.0$  and 1.1 where free surface flow changes to orifice flow or vice versa. The type of flow within this range is unpredictable.

The approximate depth of flow,  $h_3$ , can be obtained from Figure B.18 by entering the top scale with the proper value of  $h_u/Z$  and

reading down to the upper curve, then over horizontally to the lower curve, and finally down to the lower scale as shown by the arrows. The lower scale gives the ratio of  $h_u/h_3$ .

b) Case II: All girders in contact with flow (Fig. B.19).

To compute the water surface elevation upstream of the bridge, the water surface elevation on the downstream side and the discharge must be known. If the discharge is desired,  $\Delta h$  and the net area under the bridge are required. The experimental points in Figure B.19A, which are for both wingwall and spill-through abutments, show the coefficient of discharge to be essentially constant at 0.8 for the range of conditions tested. The equation recommended for the average bridge with two or four concrete girders is

$$Q = 0.80 b_N Z (2g\Delta h)^{1/2} .$$

Once  $\Delta h$  is computed from the above equation, the depth of flow upstream,  $h_u$ , can be obtained from Figure B.19B.

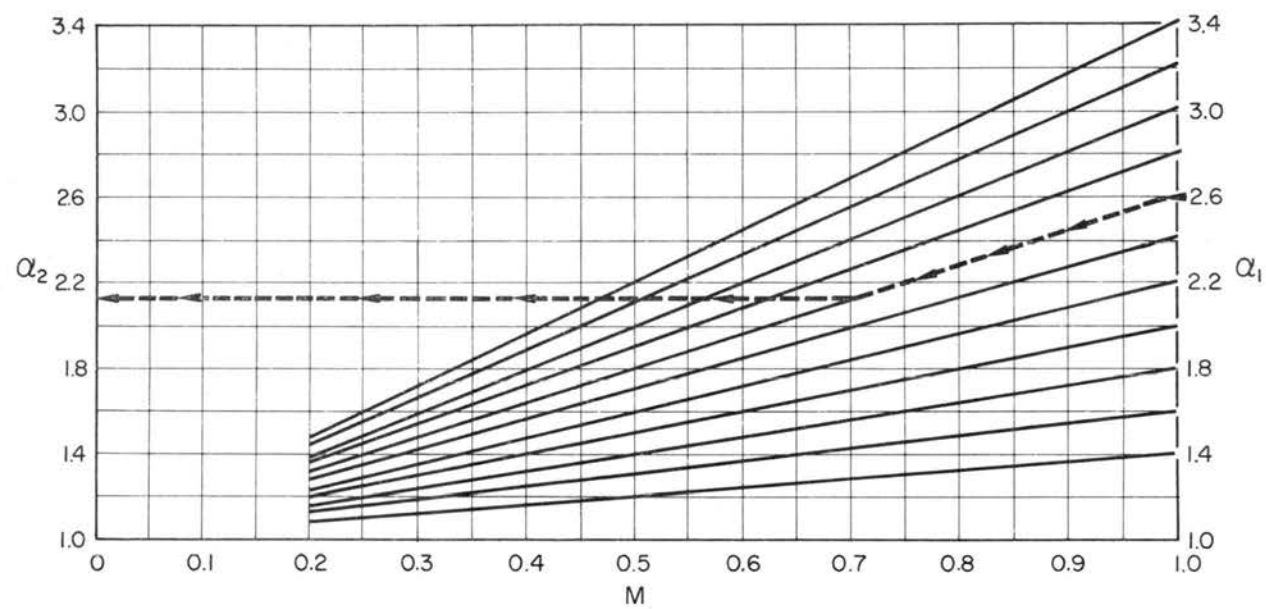


Fig. B.1 Aid for Estimating  $\alpha_2$

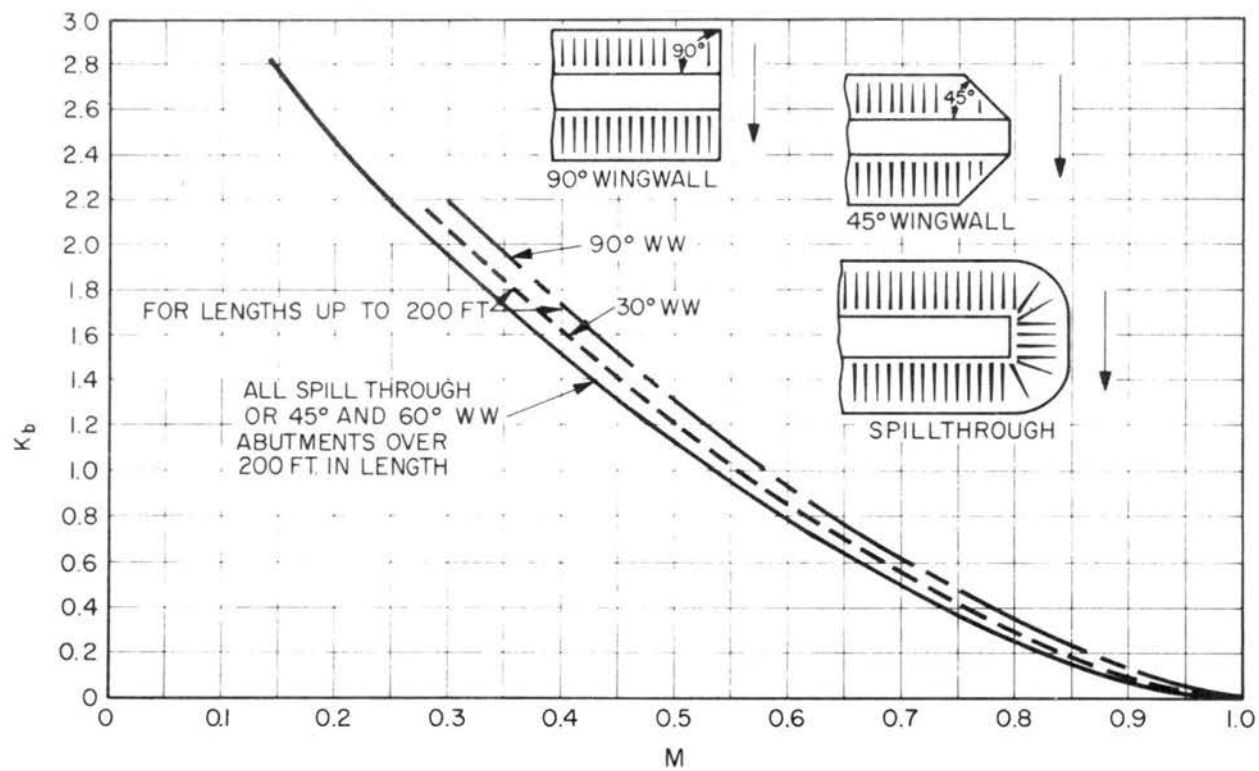


Fig. B.2 Backwater Coefficient Base Curves (Subcritical Flow)

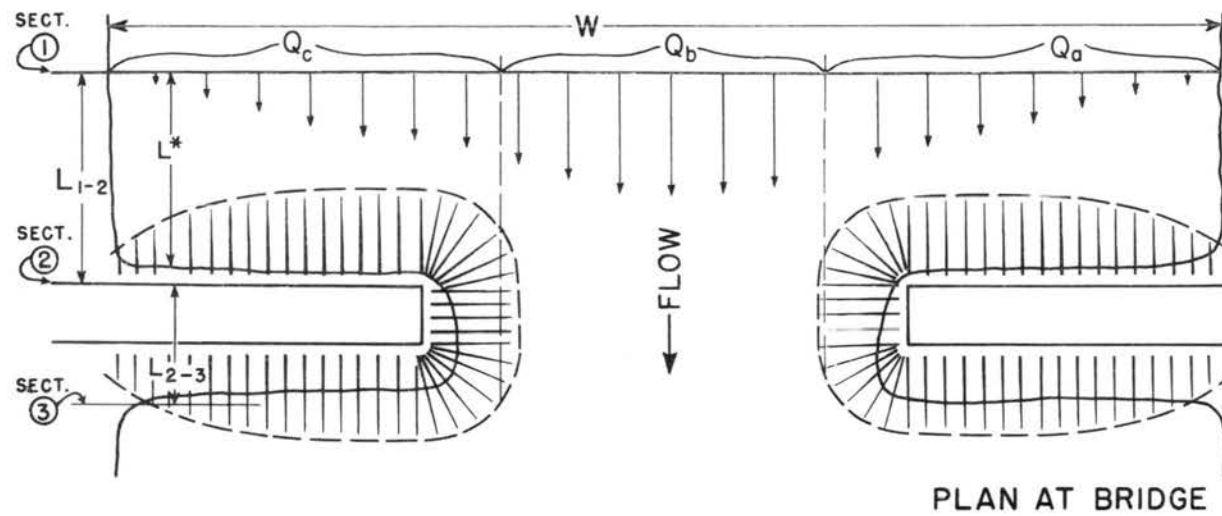


Fig. B.3 Normal Crossings: Spill-through Abutments

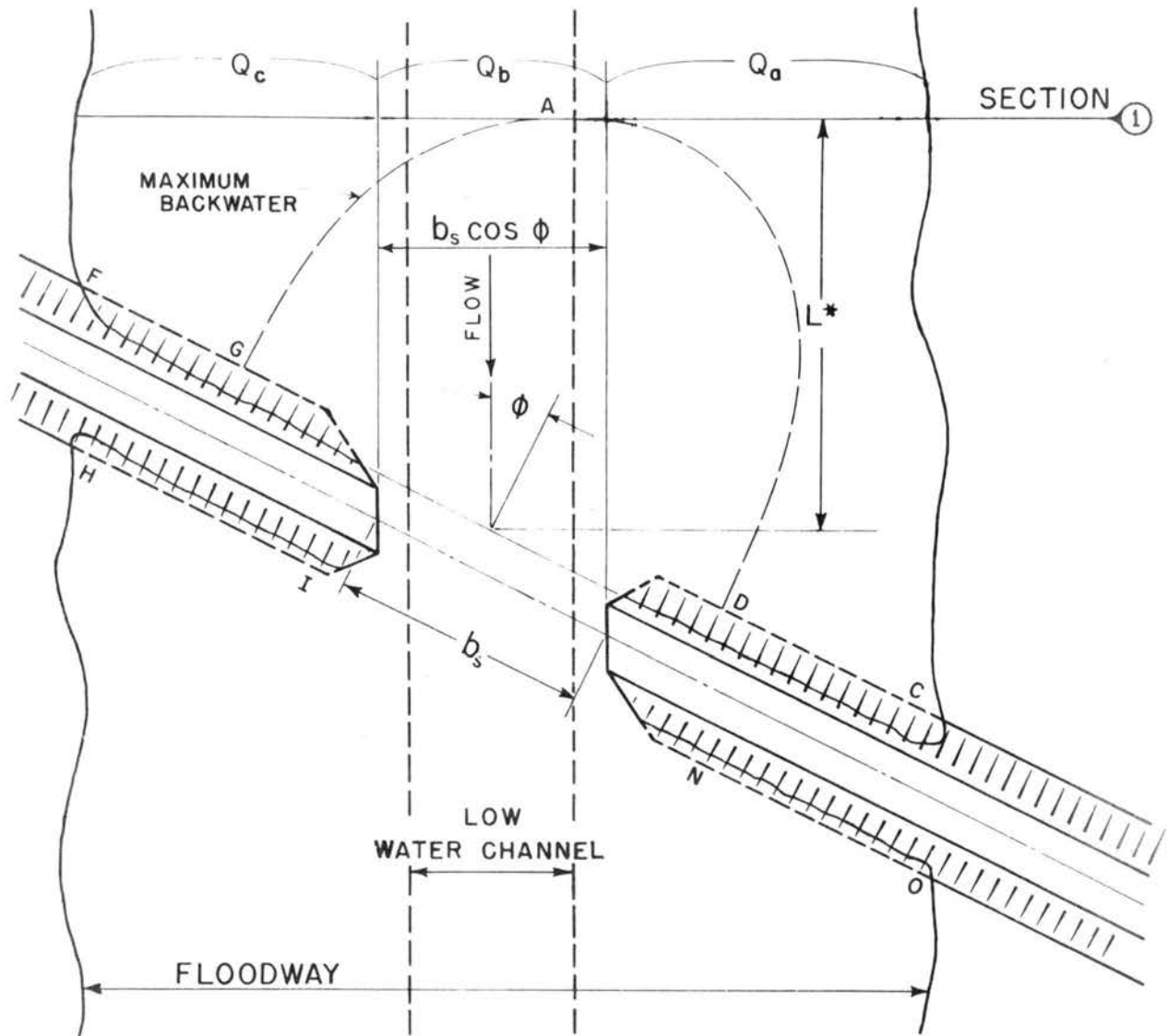


Fig. B.4 Skewed Crossings



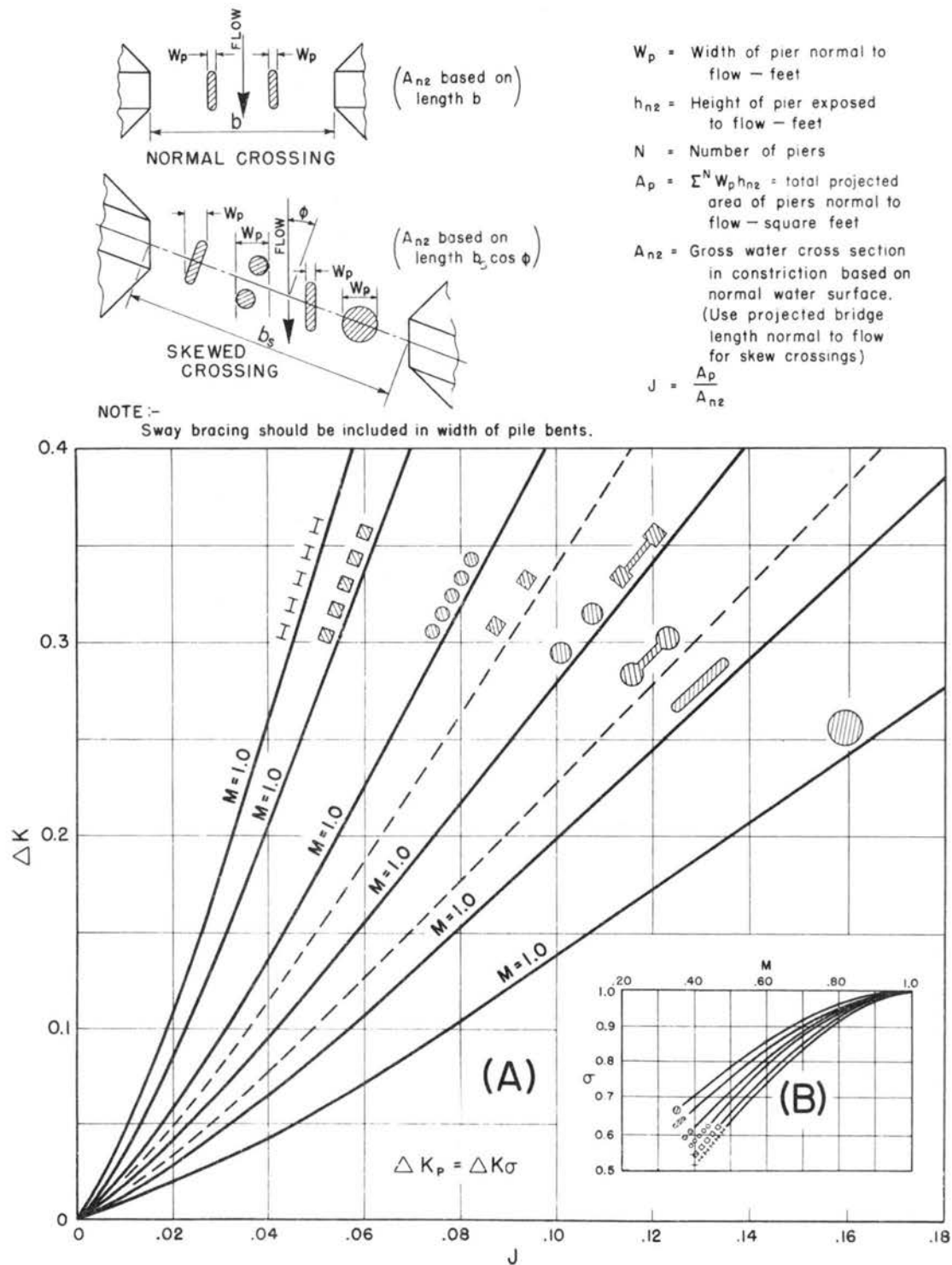


Fig. B.5 Incremental Backwater Coefficient for Piers

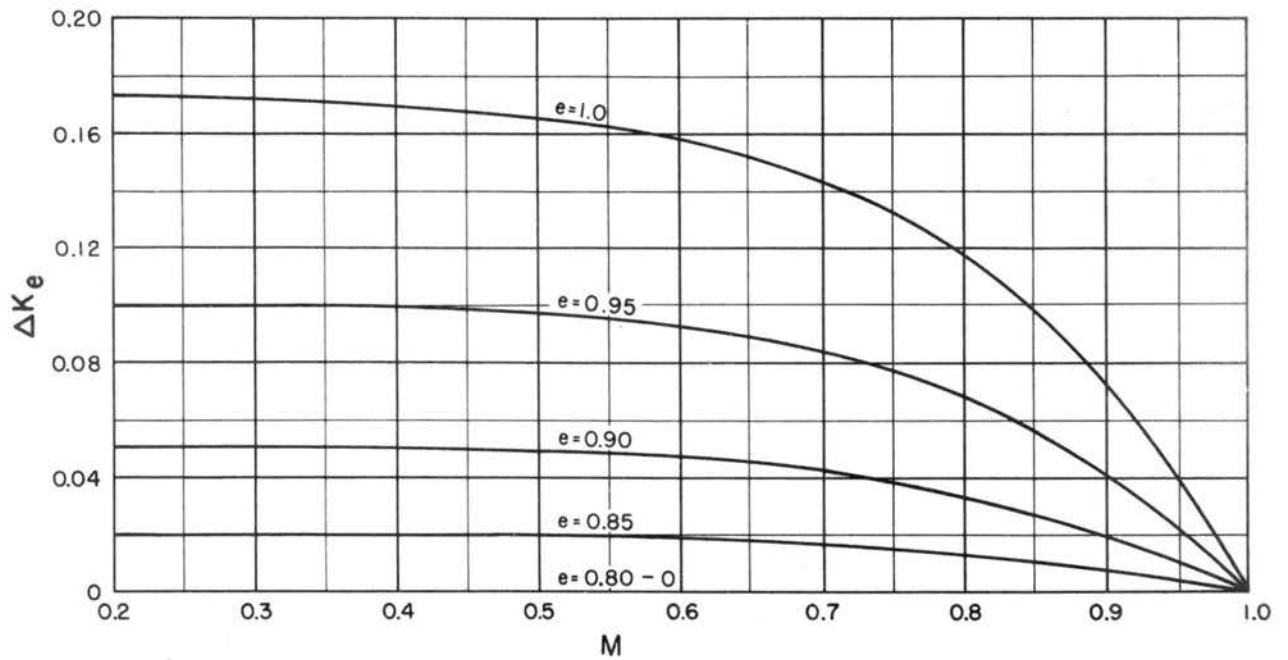
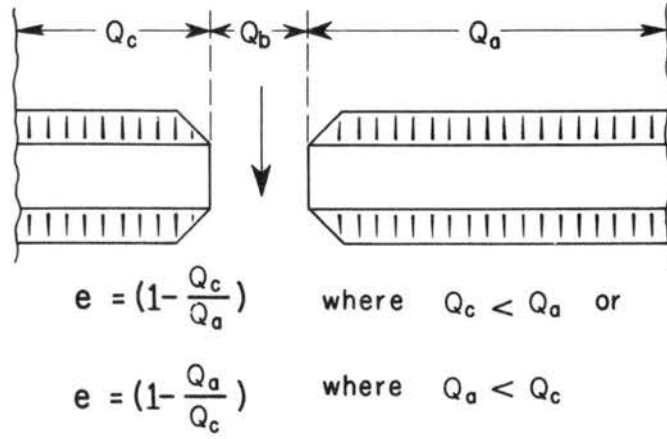


Fig. B.6 Incremental Backwater Coefficient for Eccentricity

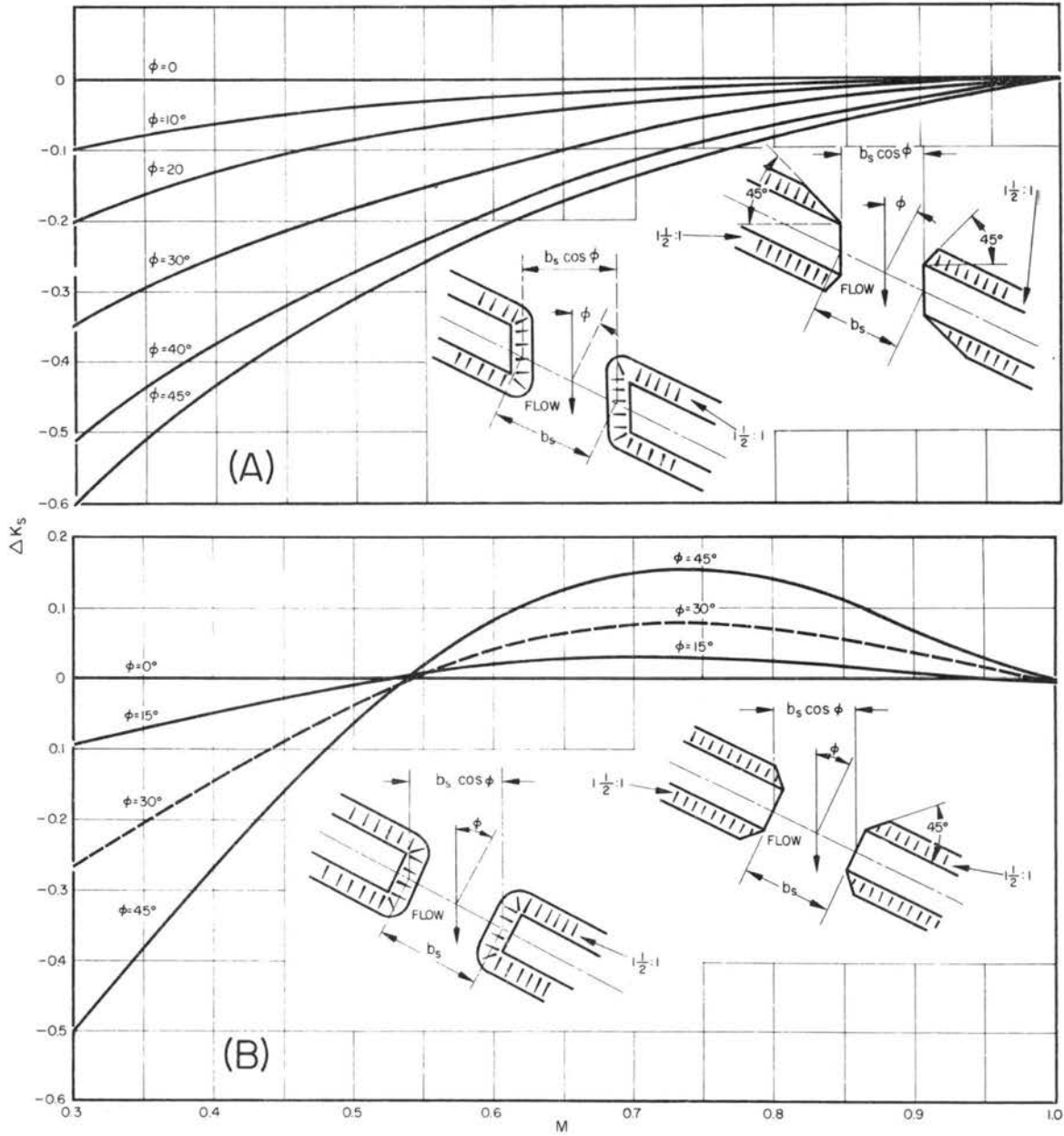


Fig. B.7 Incremental Backwater Coefficient for Skew

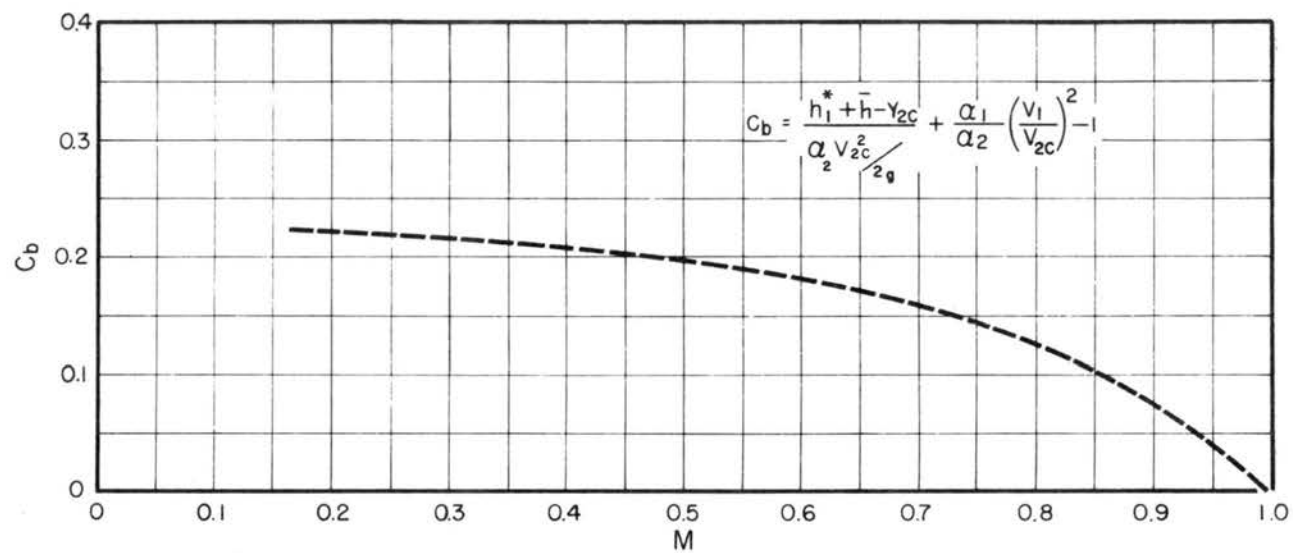


Fig. B.8 Tentative Backwater Coefficient Curve for Type II Flow

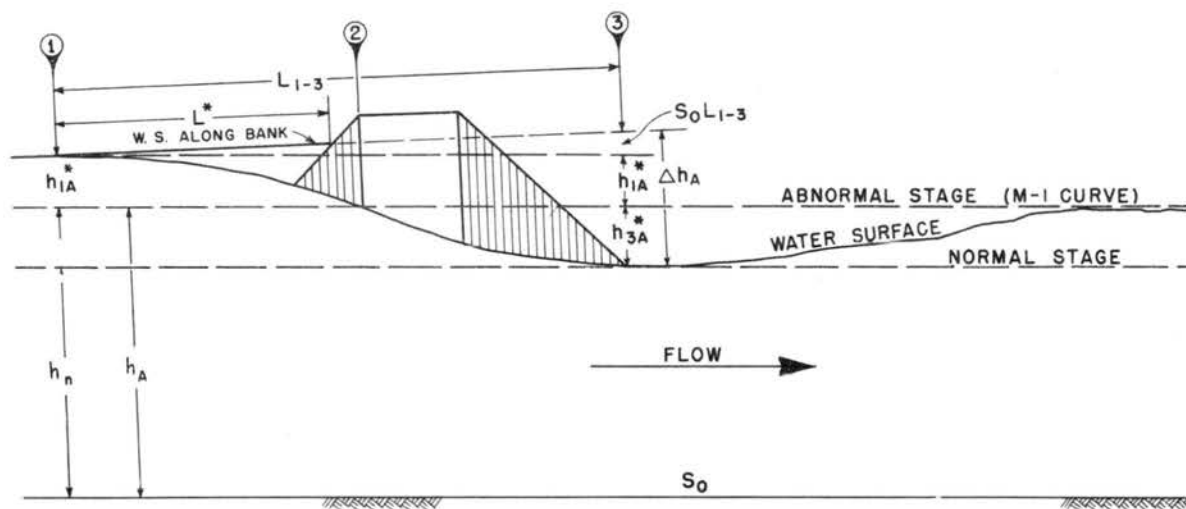


Fig. B.9 Backwater with Abnormal Stage-discharge Condition

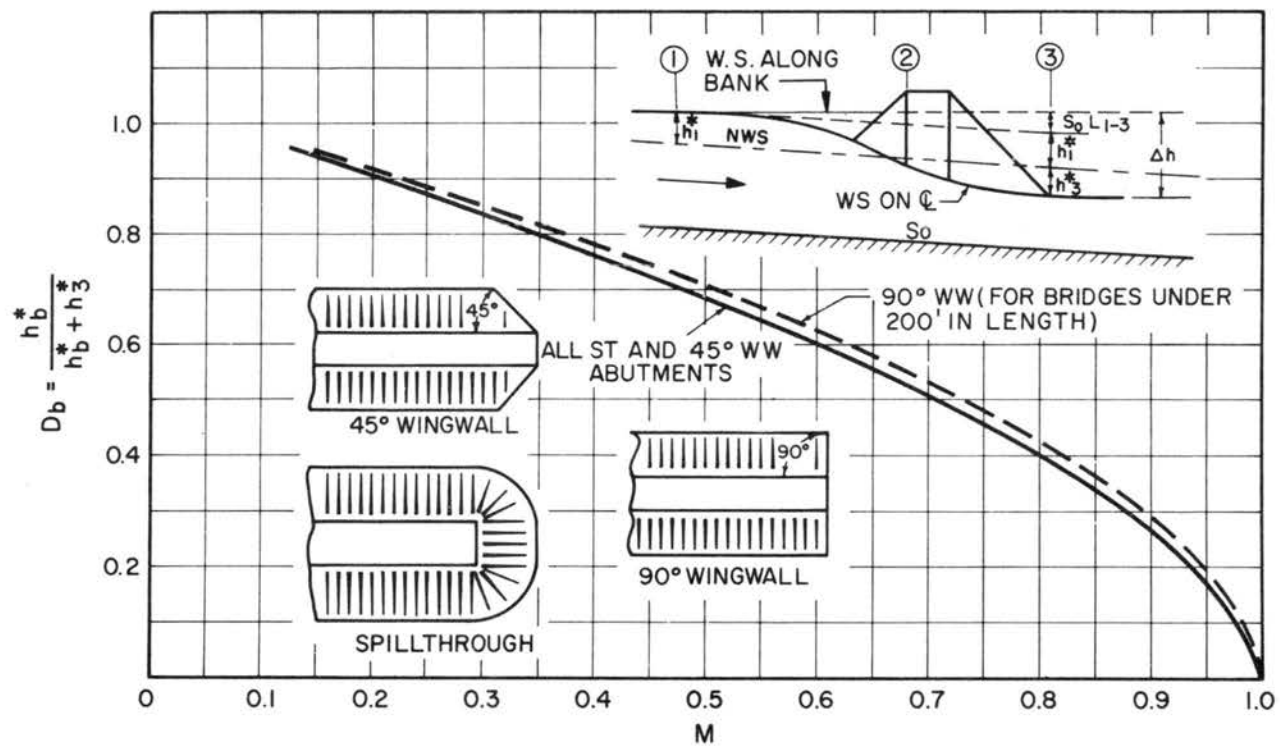


Fig. B.10 Differential Water Level Ratio Base Curves

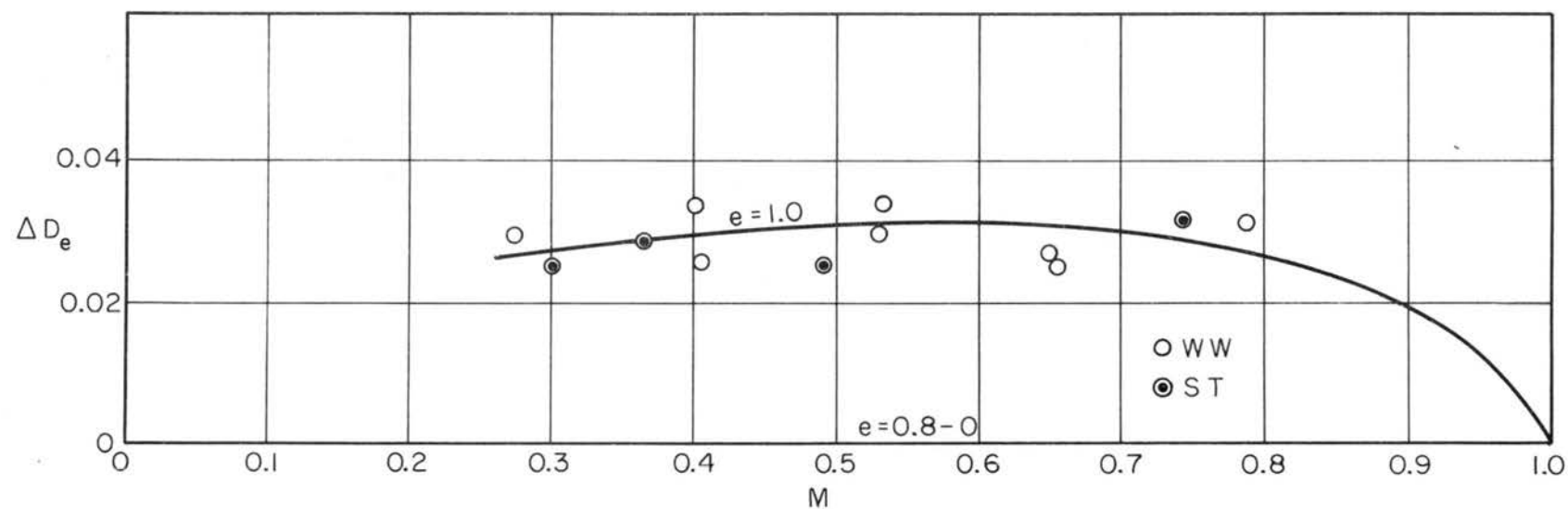


Fig. B.11 Incremental Differential Level Ratio  $\Delta D_e$  for Eccentric Crossing and Wing-wall and Spill-through Abutments

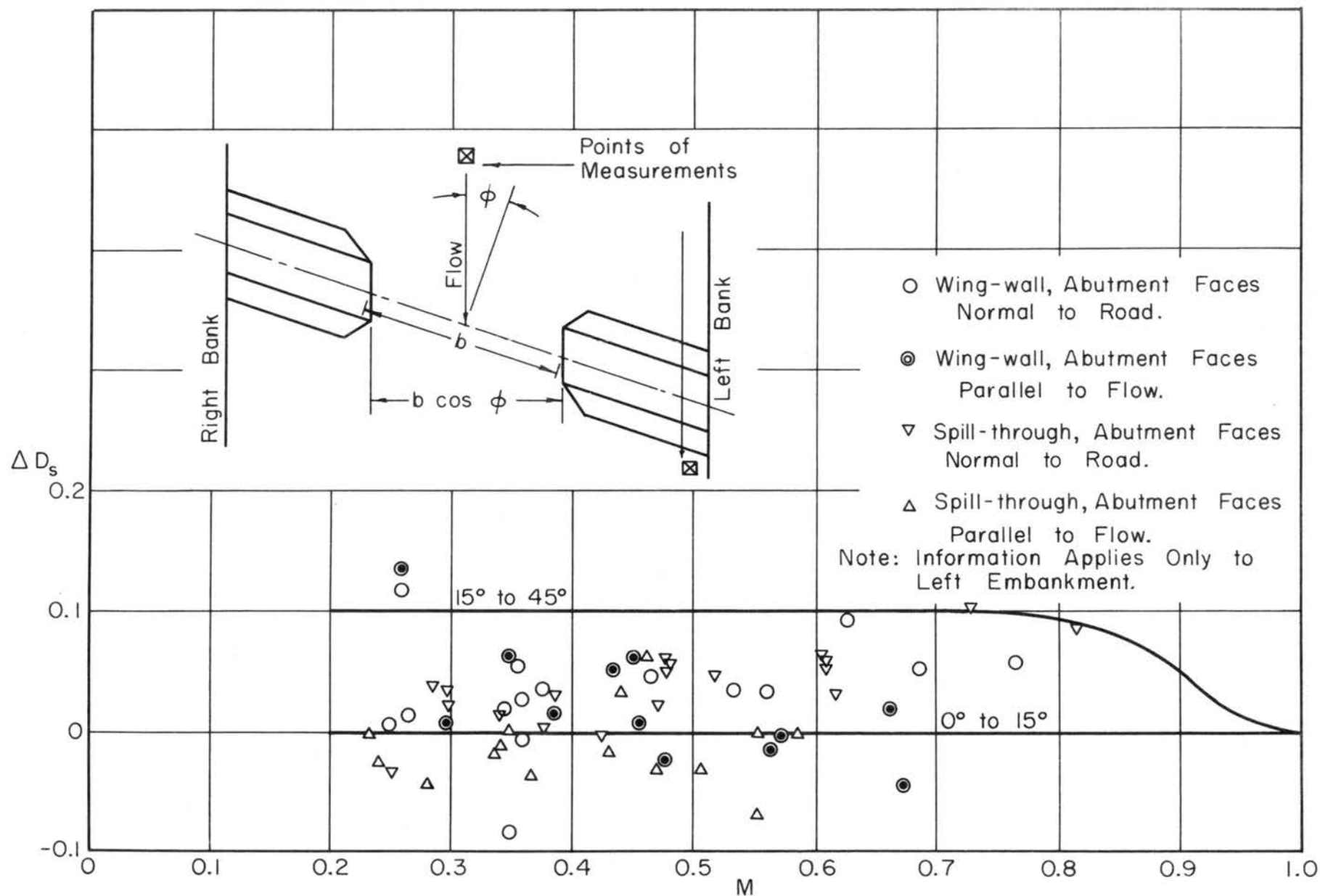


Fig. B.12 Incremental Differential Level Ratio  $\Delta D_s$  for Wing-wall and Spill-through Abutments



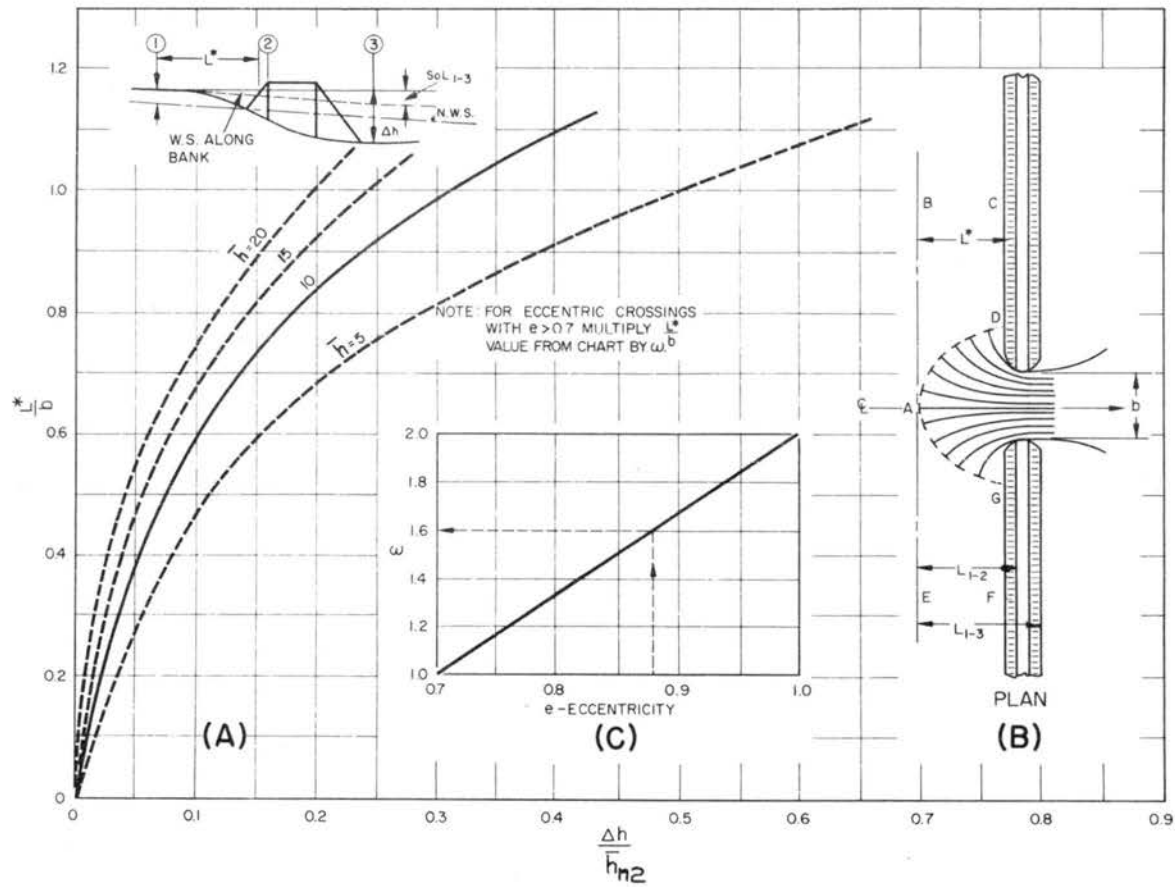


Fig. B.13 Distance to Maximum Backwater

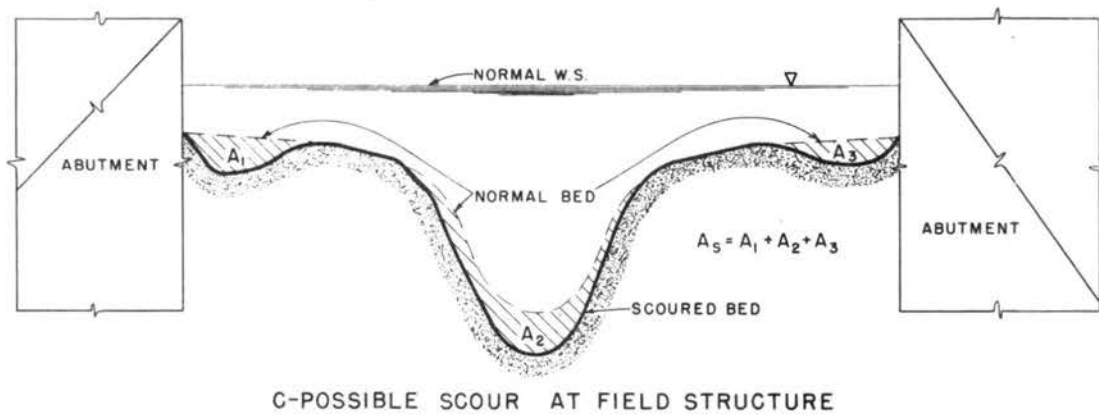
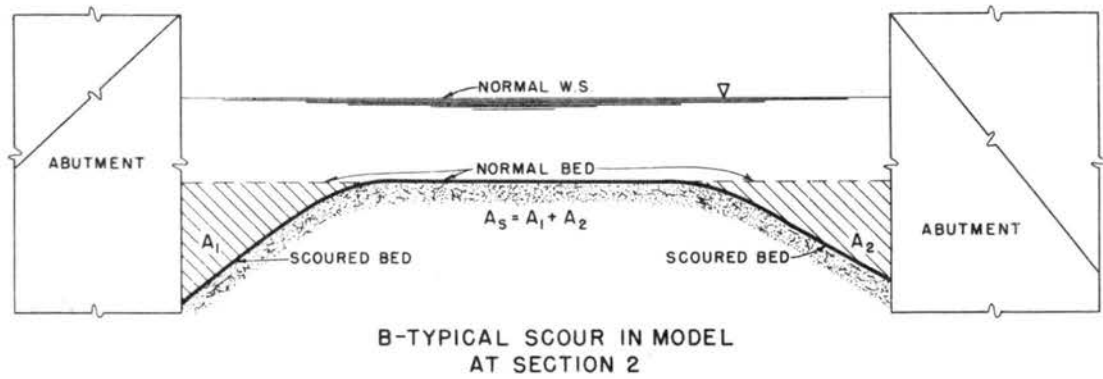
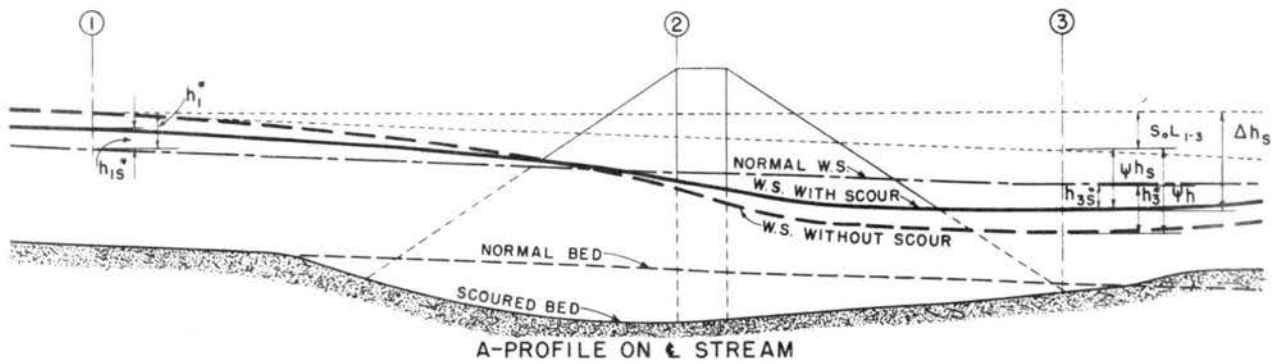


Fig. B.14 Effect of Scour on Bridge Backwater

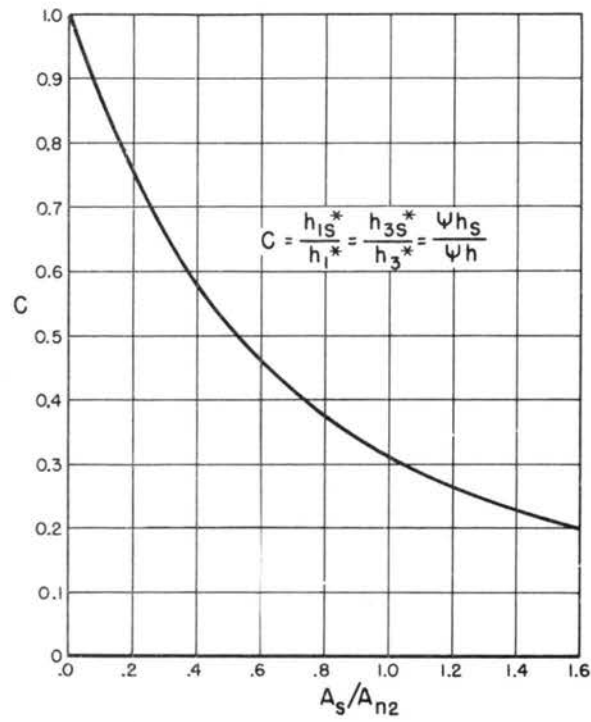


Fig. B.15 Correction Factor for Backwater with Scour

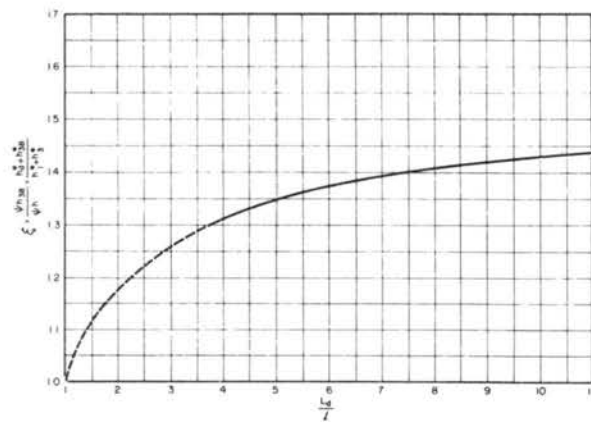


Fig. B.16 Differential Level Multiplication Factor for Dual Parallel Bridges

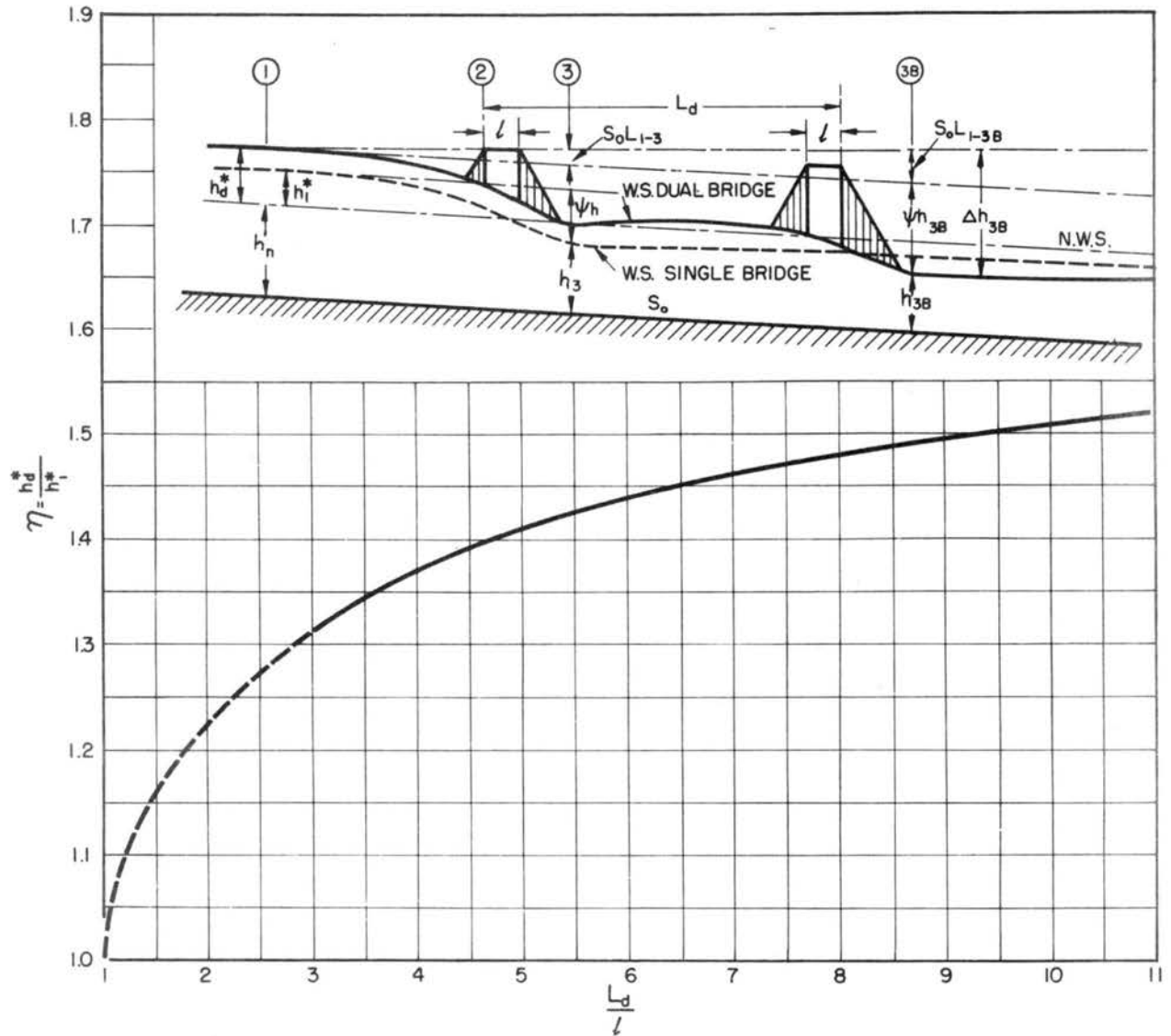


Fig. B.17 Backwater Multiplication Factor for Dual Bridges

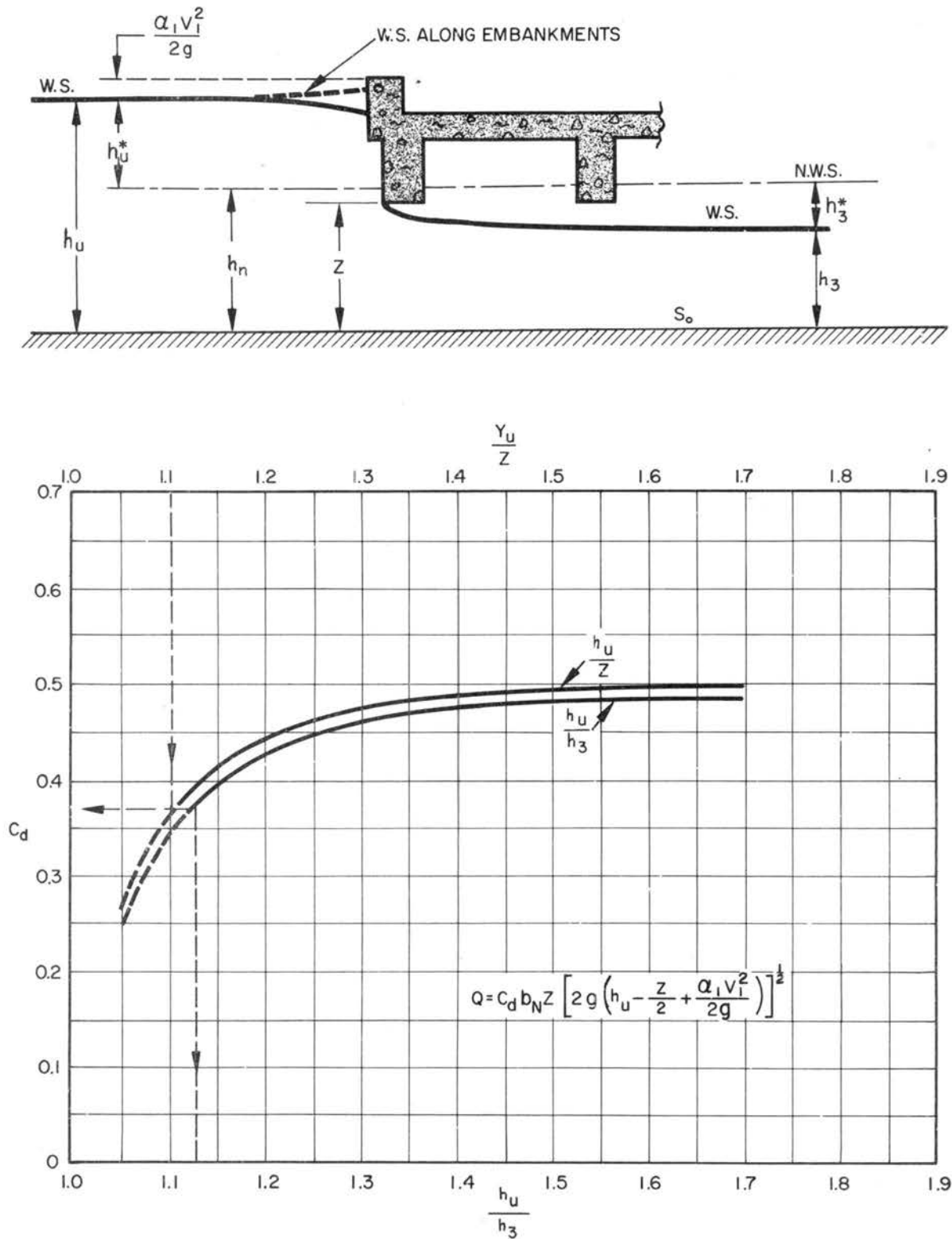


Fig. B.18 Discharge Coefficients for Upstream Girder in Flow (Case I)

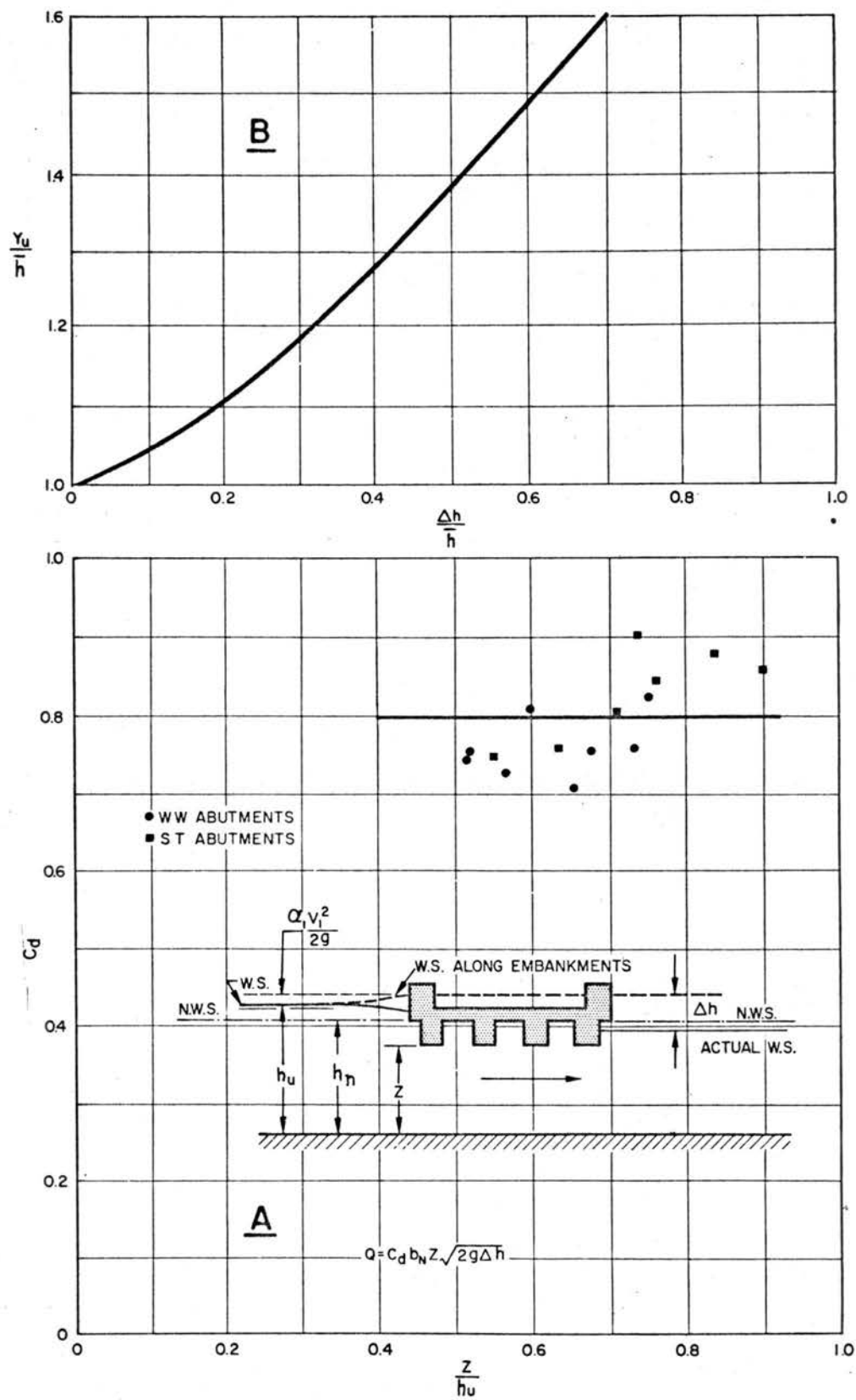


Fig. B.19 Discharge Coefficient for all Girders in Flow (Case II)

APPENDIX C  
COMPUTATION OF STABILITY COEFFICIENT

## COMPUTATION OF STABILITY COEFFICIENT

Three conditions for particle stability were listed in Chapter III. A value of  $\eta$  may be computed directly for the first condition, and iterative solutions are required for the latter two conditions.

For the stability of particles on the bed of a straight reach, Bhowmik's (8) equation is

$$\eta = \frac{1.146 (\gamma_s - \gamma_f) \tan \phi}{V_b^2 (1 + 0.85 \tan \phi)} , \quad (C1)$$

where  $\gamma_s$ ,  $\gamma_f$ ,  $V_b$ , and  $\phi$  are known.

For the spill-slope of spill-through abutments, or for the concave side slope of a bend, Bhowmik's equation is

$$K_1 = [K_2 + 1.74 V_b^2 \eta (\gamma_s - \gamma_f) \sin \lambda_1 \sin \alpha]^{\frac{1}{2}} ,$$

where

$$K_1 = [(\gamma_s - \gamma_f) \cos \alpha - 0.743 V_b^2 \eta] \tan \phi ,$$

and

$$K_2 = [0.76 V_b^4 \eta^2 + (\gamma_s - \gamma_f)^2 \sin^2 \alpha]^{\frac{1}{2}} .$$

For the sloping banks of a straight reach, the value of  $\lambda_1$  becomes zero, and the equation is

$$K_1 = K_2^{\frac{1}{2}} .$$

The latter two cases may be treated by Newton's method for the iterative solution of  $\eta$ . The equations for the spill-slopes are given, and the equations for the banks of a straight reach may be obtained by substituting  $\lambda_1 = 0$  in the following steps.



1. Compute the constants defined by

$$C_1 = (\gamma_s - \gamma_f) \cos \alpha \quad (C2)$$

$$C_2 = [(\gamma_s - \gamma_f) \sin \alpha]^2 \quad (C3)$$

$$C_3 = 0.743 V_b^2 \quad (C4)$$

$$C_4 = 0.76 V_b^4 \quad (C5)$$

$$C_5 = 1.74 V_b^2 (\gamma_s - \gamma_f) \sin \lambda_1 \sin \alpha \quad (C6)$$

2. Using equation C1 for an estimate of  $\eta$ , compute the following values

$$K_1 = (C_1 - C_3 \eta) \tan \phi$$

$$K_2 = (C_4 \eta^2 + C_2)^{1/2}$$

$$K_3 = (K_2 + C_5 \eta)^{1/2}$$

$$K_1' = -C_3 \tan \phi \quad (C7)$$

$$K_2' = C_4 \eta / K_2$$

$$K_3' = 0.5 (K_2' + C_5) / K_3 \quad .$$

3. Compute the values of

$$f(\eta) = K_1 - K_3$$

$$f'(\eta) = K_1' - K_3'$$

$$\eta_1 = \eta - f(\eta) / f'(\eta) \quad .$$

4. If the value of  $\eta_1$  approximately equals  $\eta$ , the iteration process is finished. If  $\eta_1$  is not equal to  $\eta$ , steps 2, 3, and 4 must be

repeated using the value of  $\eta_1$  as  $\eta$  . No more than four iterations are usually required.

Table C1 is an example of the computations for the stability coefficient on the spill-slope of a spill-through abutment. Data for the example were:

$$V_b = 2.77 \text{ fps}$$

$$\gamma_s = 165 \text{ lb/cu ft}$$

$$\gamma_f = 62.4 \text{ lb/cu ft}$$

$$\lambda_1 = 66 \text{ deg}$$

$$\alpha = 26.5 \text{ deg}$$

$$\phi = 33 \text{ deg .}$$

Table C1. Computational Example for the Solution of the Stability Coefficient  $\eta$  on a Spill-Through Abutment Spill-Slope

Compute:

$$\begin{aligned} \eta_{\text{trial}}(\text{eqn C1}) &= 6.39 & C_1(C2) &= 91.8 & C_2(C3) &= 2,100 \\ C_3(C4) &= 5.71 & C_4(C5) &= 44.9 & C_5(C6) &= 558 \\ K_1'(C7) &= -3.71 \end{aligned}$$

Iteration =	1	2	3	4	5
Trial $\eta =$	$\eta_{\text{trial}} = 6.39$	3.45	3.68		
$K_1 = (C_1 - C_3\eta) \tan \phi =$	35.8	46.7	46.0		
$K_2 = (C_4\eta^2 + C_2)^{1/2} =$	62.6	52.6	52.1		
$K_3 = (K_2 + C_5\eta)^{1/2} =$	60.2	44.4	45.9		
$K_2' = C_4\eta / K_2 =$	4.57	2.94	3.16		
$K_3' = 0.5(K_2' + C_5) / K_3 =$	4.56	6.33	6.10		
$f(\eta) = K_1 - K_3 =$	-24.4	2.3	0.1		
$f'(\eta) = K_1' - K_3' =$	-8.27	-10.04	-9.81		
$\eta_1 = \eta - f(\eta) / f'(\eta) =$	3.45	3.68	3.69		
Trial $\eta = \eta_1?$	No	No	Yes		